UNIVERSITEIT VAN PRETORIA
UNIVERSITY OF PRETORIA
YUNIBESITHI YA PRETORIA
Faculty of Engineering, Built Environment and Information Technology

Titanium metal particle growth through autocatalytic electroless deposition in a molten salt slurry reactor

by

Jaco Johannes Swanepoel

A thesis submitted in partial fulfilment of the requirements for the degree

Doctor of Philosophy in Engineering

in the

Department of Chemical Engineering
Faculty of Engineering, Built Environment & Information Technology
University of Pretoria
Pretoria

September 2020

Titanium metal particle growth through autocatalytic electroless deposition in a molten salt slurry reactor

Student: *Jaco Johannes Swanepoel*
Supervisor: *Professor Mike D. Heydenrych*
Department: *Chemical Engineering*
University: *University of Pretoria*
Degree: *Doctor of Philosophy in Engineering*

SYNOPSIS

Near-net-shape manufacturing of titanium metal components through powder metallurgy confers various cost-saving benefits, from improved material utilisation to reduced energy consumption. Further savings can be realised by reducing the cost of the titanium metal powder that is used as feed material in powder metallurgy.

Titanium metal-powder production costs can be reduced by removing the steps currently needed (i.e. milling, vacuum arc re-melting and atomisation) to convert titanium Kroll sponge into a powder product that is suitable for use in powder metallurgy. This can be potentially achieved through a controlled metallothermic reduction of titanium tetrachloride to produce a titanium metal powder product that can be used directly in powder metallurgy.

Consequently, this thesis divides titanium metal-powder into two main categories, namely primary and secondary metal powder products.

Titanium metal-powder is classified as a primary product when it can be used directly as feed material in powder metallurgy. In contrast, a secondary metal-powder product requires extra processing steps after chemical reduction before it can be used in powder metallurgy.

To illustrate, titanium metal powder produced through plasma spheroidization is an example of a secondary metal powder product.

The metallothermic reduction reaction is known to have two dominant reaction mechanisms. These mechanisms have a characteristic product morphology that forms under specific reaction conditions. The first mechanism is responsible for the sponge-like morphology obtained from the Kroll process, while the second mechanism results in an ultrafine precipitate that has a surface area to volume ratio large enough to oxidise in air to the extent that it cannot be regarded as commercially pure.

Consequently, a primary titanium metal-powder product has to date not been realised as efforts to achieve particle growth on this ultrafine precipitate have been unsuccessful.

This thesis's main objective was to demonstrate that metal particle growth on suspended metal particles is indeed possible through a controlled metallothermic reduction in a molten salt reaction medium.

Subsequent efforts resulted in the postulation of a third reaction mechanism that would enable titanium metal particle growth. The postulated growth mechanism is electrochemical and referred to as “autocatalytic electroless deposition on suspended titanium metal particles”.

Theory development and modelling efforts indicated that the postulated growth mechanism is possible, but only in a particular and low concentration range where both reagents are present in a meta-stable equilibrium with each other in the molten chloride reaction medium. The concentration range is estimated to be in the range of parts per million for each reagent.

It was further shown that more than one product morphology is inherent in the conditions where the postulated mechanism is possible as there is no dominant reaction mechanism at such low reagent concentrations. Therefore, the metallothermic reduction reaction should be regarded as a system of reaction mechanisms at these conditions.

Experimental results substantiated the postulated growth mechanism's existence to the extent where β-titanium metal was deposited on the surface of metallised ilmenite particles.

The deposited layer was distinguishable from the substrate particle as ilmenite contains α-titanium (i.e. a hexagonally closed packed crystal system).

Therefore, controlled titanium metal particle growth is hypothetically possible through a mechanism known as “autocatalytic electroless deposition”.

However, further effort is still needed to demonstrate whether a viable primary titanium metal powder product can be produced.

KEYWORDS: Titanium metal powder, metallothermic reduction, molten salt, autocatalytic electroless deposition, titanium tetrachloride, titanium metal crystals

ACKNOWLEDGEMENTS

I would like to express my sincere gratitude to the following people and institutions:

- The Department of Science and Technology and the Titanium Centre of Competence for funding
- The Council for Scientific and Industrial Research (CSIR) for the use of their facilities
- Dr Shahed Fazzluddin for his role as CSIR supervisor
- CSIR colleagues for their support. Honourable mentions include:
    - Eugene Swanepoel
    - Dr Shaan Oosthuizen
    - Danie Wilkins
    - Martin Williams
- Harold Coetzee as an instructor to everything LabVIEW related
- Prof Dawie van Vuuren for his mentorship and introduction to titanium metal powder production
- Prof Mike Heydenrych for his guidance and support as academic supervisor
- My loving parents Johan and Magdalena for always believing in me
- My beautiful wife Lyndal-Lee for her unwavering love, support and understanding
- My son, Noak – I dedicate this work to you.

TABLE OF CONTENTS

LIST OF FIGURES

LIST OF TABLES

LIST OF ABBREVIATIONS

bcc	Body-centred cubic
BEC	Back-scattered electron composition
C.P.	Commercially pure
CSIR	Council for Scientific and Industrial Research
CSTR	Continuous stirred-tank reactor
DST	Department of Science and Technology
EBSD	Electron backscatter diffraction
EDS	Energy-dispersive X-ray spectroscopy
hcp	Hexagonal close-packed
HMI	Human-machine interface
IP	Intellectual property
LR-EMR	Long-range electronically mediated reaction
PM	Powder metallurgy
PSD	Particle size distribution
SEM	Scanning electron micrograph/microscopy
SFM	Segregated feed model
SR-EMR	Short-range electronically mediated reaction
XRD	Powder X-ray diffraction

CHAPTER 1 – INTRODUCTION

1.1 – Background and motivation

Titanium metal offers a unique combination of properties. It is strong, lightweight, corrosion-resistant and biocompatible. It outperforms other structural metals up to 500 °C by having one of the highest strength-to-density ratios in this temperature range. It is not surprising then that titanium is listed as one of the most important structural metals globally, ranked 6th after iron, aluminium, copper, zinc, and magnesium (Cardarelli, 2008).

Titanium's biocompatibility and stability in corrosive environments conceal that it is in fact, a highly reactive substance that can burn in pure nitrogen (Cardarelli, 2008: 275). The product of corrosion is, however, thermodynamically very stable. This combination of reactivity and stability provides the basis for titanium's corrosion resistance in that corrosion resistance is created as a result of oxidation itself. The resulting oxide layer that forms between the bulk metal and atmosphere protects the base metal from further oxidation.

The properties inherent in titanium metal make it ideal for use in everyday life, but its reactivity towards the atmosphere and other elements increases production and fabrication cost. The result is that titanium metal is about four to five times more expensive than stainless steel (Fang *et al.*, 2017: 2). The difficulty of producing pure titanium metal can be illustrated by the fact that large-scale production was only first successfully demonstrated in the early 1950s (Housley, 2007). Research and development have been ongoing since then trying to make low-cost titanium metal a reality.

In this regard, significant progress has been made, as near-net-shape manufacturing of titanium metal components through powder metallurgy confers various cost-saving benefits, from optimum material usage to reduced energy consumption.

However, inherent to powder metallurgy is the need for high-quality powder as starting material. Titanium metal powder is currently produced predominantly through techniques such as the plasma rotating electrode process (PREP) or gas atomisation of metal ingots or

billets (Oosthuizen *et al.*, 2011, Yolton & Froes, 2015). It is important to emphasize that these techniques all require a pure metal as feed material.

Producing a pure titanium metal is an expensive process with various intermediary steps, each of which adds to the final cost. For example, the Kroll process (which is the most well-known and established chemical method for titanium metal production) produces a sponge-like metal product that must be crushed, milled and double vacuum arc re-melted before it is regarded as commercially pure. These post-processing steps typically account for up to half of the total production cost (Roskill, 2013: 43).

Using pre-reduced titanium metal as feed material for powder production means that the already expensive titanium metal is processed into an even more expensive product. This price increase can be up to 30 times the original metal price (Withers, 2015).

Therefore, the current titanium metal value chain is not optimally aligned to benefit fully from powder metallurgy. This situation can be positively altered by reducing feed material costs. It is not surprising then that various institutions worldwide are actively trying to find alternative low-cost titanium metal powder production processes (Qian & Froes, 2015).

A theme common to some of the process options considered is to enforce control over the metallothermic reduction of titanium tetrachloride to result in a metal powder product that can be used directly as feed material in powder metallurgy (Van Vuuren, 2009a, 2009b & 2010; Oosthuizen *et al.*, 2011 & Oosthuizen, 2016).

Direct production of a viable titanium metal powder product would eliminate the need for metal ingot production in applications that use powder metallurgy to produce components. Each process step eliminated during powder production will directly improve downstream titanium powder metallurgy's economic viability.

From this point forward, titanium metal powder produced through direct metallothermic reduction is classified as a primary metal powder product when no other post-production steps are needed before it can be used in powder metallurgy. In turn, a titanium metal powder produced from an existing titanium metal source (billet or ingot) is classified as a secondary titanium metal powder product.

The Department of Science and Technology (DST) contracted the Council for Scientific and Industrial Research (CSIR) in South Africa to develop a process that can produce a primary titanium metal powder product (CSIR, 2018).

The CSIR's research and development efforts resulted in what is called the CSIR-Ti process. The CSIR-Ti process aims to produce a primary titanium metal powder product through a two-stage metallothermic reduction of titanium tetrachloride in a molten chloride salt as a reaction medium (Oosthuizen, van Vuuren & Swanepoel, 2015). Intellectual property relating to the CSIR-Ti process has been secured internationally via three different patents (Oosthuizen & van Vuuren, 2011; Oosthuizen *et al.*, 2015; Oosthuizen, Swanepoel *et al.*, 2017).

However, the current understanding of metallothermic reduction is that this extremely spontaneous reaction will produce either a sponge-like product that deposits electrochemically on the reactor internals or an ultrafine precipitate that oxidise as soon as it comes in contact with the atmosphere (van Vuuren, 2015: 84). Crystallisation theory defines reactive crystallisation as precipitation (Demopoulos, 2009: 199). Therefore, the current understanding of reactive crystallisation predicts an ultrafine precipitate's formation rather than particle growth due to the metal's insolubility in the molten salt reaction medium.

Ultrafine powder has a particle size between 0.1 µm and 1 µm (Neikov, 2009: 4). A spherical titanium particle size of at least 5 µm is needed to prevent oxygen contamination exceeding the allowable limits (Hansen & Gerdemann, 1998: 58). This contamination will occur through surface oxidation in a normal atmosphere.

Therefore, controlled titanium metal particle growth is an essential prerequisite needed to make primary metal powder production a reality.

1.2 – Research objectives

This thesis's main objective is to demonstrate that titanium metal particle growth is possible through controlled metallothermic reduction on metal particles suspended in a molten chloride salt.

The following objectives are in support of the main objective:

1. Propose a titanium metal particle growth mechanism.
2. Build a theoretical foundation describing the system of reaction mechanisms (i.e. known and postulated).
3. Estimate the experimental conditions required where the postulated growth mechanism is most likely to occur.
4. Compare the different reaction mechanisms (known and postulated) with each other to estimate the selectivity of each.
5. Conduct an experiment to demonstrate titanium metal particle growth.

1.3 – Scope of work

Work presented in this thesis is multi-disciplinary. Relevant subject matter includes thermodynamics, electrochemistry, reaction kinetics, crystallisation, and colloidal and surface chemistry, to name but a few. To complete the project within a reasonable time and budget, defining the scope and limitations of work was necessary. This dissertation will focus strictly on the research objectives in Section 1.2, as listed below:

1. Literature review
    a. Conduct a literature review of non-ferrous metal powder production techniques.
    b. Conduct a literature review of titanium metal powder production via metallothermic reduction.
    c. Propose a growth mechanism based on the literature reviewed.
    d. Find and review literature applicable to the proposed mechanism.
2. Theory building
    a. Estimate a concentration range where Ti^{2+} cations and Na^{0} co-exist in meta-stable equilibrium with each other.
    b. Build a theoretical foundation in which all possible reaction mechanisms (i.e. known and postulated) can be compared in order to estimate selectivity for each mechanism.
3. Modelling and simulation
    a. Develop an algorithm that models the frequency of collisions in a simulated three-dimensional sample space representing the reaction environment.

   b. Apply the algorithm in a Monte Carlo simulation to estimate selectivity between postulated and known reaction mechanisms.
4. Use the model outputs to guide experimental work to enable a demonstration of titanium metal particle growth via the postulated autocatalytic electroless deposition mechanism.

1.4 – Limitations

The following limitations are applicable:

- The commercialisation of the CSIR-Ti process is of strategic importance to the South African government, and thus confidentiality must be considered. Therefore, the work presented in this thesis is strictly limited to that already in the public domain, i.e. patents, journal articles, conference presentations, and book chapters.
- Reaction kinetics will not be determined in this study.
- Crystallisation kinetics will not be determined in this study.
- Colloidal particle-particle interactions and their effect on the hypothetical crystal growth will not be considered in this study.
- The suitability of experimentally produced powders for powder metallurgy will not be evaluated in this study.

The limitations listed above can be used as a starting point for future investigations.

1.5 – Definition of terms

Various terms are used throughout this thesis. This section defines and describes each term to prevent ambiguity.

The following definitions and terms are used:

- *Primary metal powder product:* Titanium metal powder produced through direct metallothermic reduction can be classified as being a “primary metal powder product”

when no post-production steps are required before the powder can be used in powder metallurgy.

- *Secondary metal powder product:* Titanium metal powder produced from an existing titanium metal source (billet or ingot) is classified as a “secondary titanium metal powder”.
- *Autocatalytic electroless deposition:* Autocatalytic electroless deposition (or autocatalytic plating) is a form of electroless plating where the substrate surface allows for electron exchange between two physically separated redox half-cell reactions.
- *SR-EMR:* The term SR-EMR is used to describe the mechanism when both electron and ion transfer occur via the molten salt, i.e. when no external electrical conductor present. An ultrafine precipitate is a typical product when the SR-EMR mechanism is dominant during metallothermic reduction.
- *LR-EMR:* The term LR-EMR is used to describe electron transfer via a conducting intermediary or any other electronically conductive substrate. Kroll sponge is a typical product when LR-EMR is the dominant reaction mechanism during metallothermic reduction.

CHAPTER 2 – LITERATURE REVIEW

2.1 – Chapter overview

This chapter reviews the literature to propose a mechanism for titanium metal growth on suspended titanium particles in a molten salt medium. The proposed mechanism is then used as a foundation for theory-building and experimental work.

The literature review is divided into three subsections. These are:

1. A literature review of titanium metal powder production for use in powder metallurgy (Section 2.2)
2. A literature review of the metallothermic reduction reactions (Section 2.3)
3. A literature review on electroless deposition (Section 2.4)

2.2 – Titanium metal powder production

2.2.1 – Primary vs secondary metal powder production

Powder metallurgy is a broad field that typically consists of the following steps:

1. Production of metal powders
2. Compaction and shaping of powders
3. Sintering processes
4. Post-sintering processes

These processing steps follow sequentially from each other, meaning that each processing step depends (with regard to the techniques and equipment selected to achieve the required outcome) on the outputs of the preceding step (Sanderow, 1998). Table 1 summarises the various categories of titanium metal powder metallurgy (Froes, Eylon & Bomberger, 2015: 177).

Table 1: Categories of titanium powder metallurgy
(Adapted from Froes, Eylon & Bomberger, 2015: 177)

Category	Features
Additive manufacturing	Powder feed melted with a laser or other heat source
Powder injection moulding	Use of a binder to produce complex, small parts
Spraying	Solid or potentially liquid
Near-net shapes	Pre-alloyed and blended elemental
Far-from-equilibrium process	Rapid solidification, mechanical alloying and vapour deposition
Thermo-hydrogen processing	Use of hydrogen as a temporary alloying element
Porous materials	Less than 100% dense materials

In the powder metallurgy value chain, powder production is the first step contributing to production costs and defines the number of downstream processing steps needed to result in a high-quality metal component. This is because each powder production technique results in a unique powder product that requires further post-processing before the powder is suitable for downstream use. Therefore, efficient powder production is crucial for the powder metallurgy value chain.

There are numerous techniques available to produce non-ferrous metal powder products. These powder production techniques are generally categorised as either mechanical or chemical (Trudel, 1998). The main techniques available for non-ferrous metal powder production are shown in Figure 1.

Each technique shown in Figure 1 produces a product with characteristic physical and chemical properties (Neikov, 2009: 2). Selecting a powder production method is not a trivial activity. Consideration is required as to how the powder produced will influence the downstream processing steps and, ultimately, the final metal component's material properties.

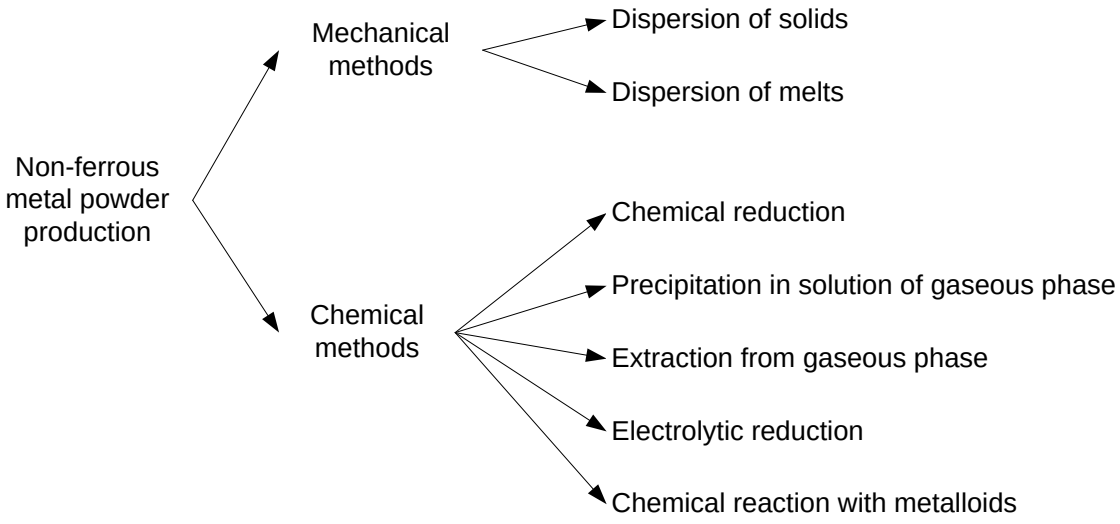

Figure 1: Techniques used to produce non-ferrous metal powders (Adapted from Trudel, 1998)

Table 2 provides several considerations to keep in mind when selecting a non-ferrous metal powder production technique.

Table 2: Considerations for selecting a metal powder production technique

Operational	Powder quality
Powder production rate Production costs etc.*	Chemical composition (purity) Particle size (and size distribution) Particle morphology Surface roughness Porosity (surface area) Compressibility etc.*

*This is not a comprehensive list

Table 2 simplifies the number of considerations into two categories, i.e. operational considerations and powder quality. Operational considerations relate mostly to production economics, while powder quality relates to product specifications and usability in downstream processing. Therefore, a high-quality metal powder product is not a qualitative statement, but rather a parameter defined by many other quantifiable properties.

The three most important properties that determine powder product quality are (Neikov, 2009: 3):

- Chemical composition
- Particle morphology
- Particle size distribution

Chemical composition quantifies the number of chemical elements that make up the powder.

Particle morphology is used to describe particle shape and directly impact downstream materials handling requirements. The British Standards Institute has defined the following particle morphologies (Kaye, 1998):

1. Acicular: Needle shaped
2. Angular: Sharp-edged or roughly polyhedral shaped
3. Dendritic: A branched crystalline shape
4. Fibrous: Regularly or irregularly threadlike
5. Flaky: No formal definition in the British Standard
6. Granular: Approximately equidimensional but irregularly shaped
7. Irregular: Lacking any symmetry
8. Modular: Rounded, irregularly shaped
9. Spherical: Globular shaped

Particle morphology depends mostly on the production method used. The various particle morphologies are shown in Figure 2.

Powder particle size is a fundamental characteristic of powder metallurgy (Neikov, 2009: 3). Typical particle size ranges required for use in different powder applications are illustrated in Figure 3.

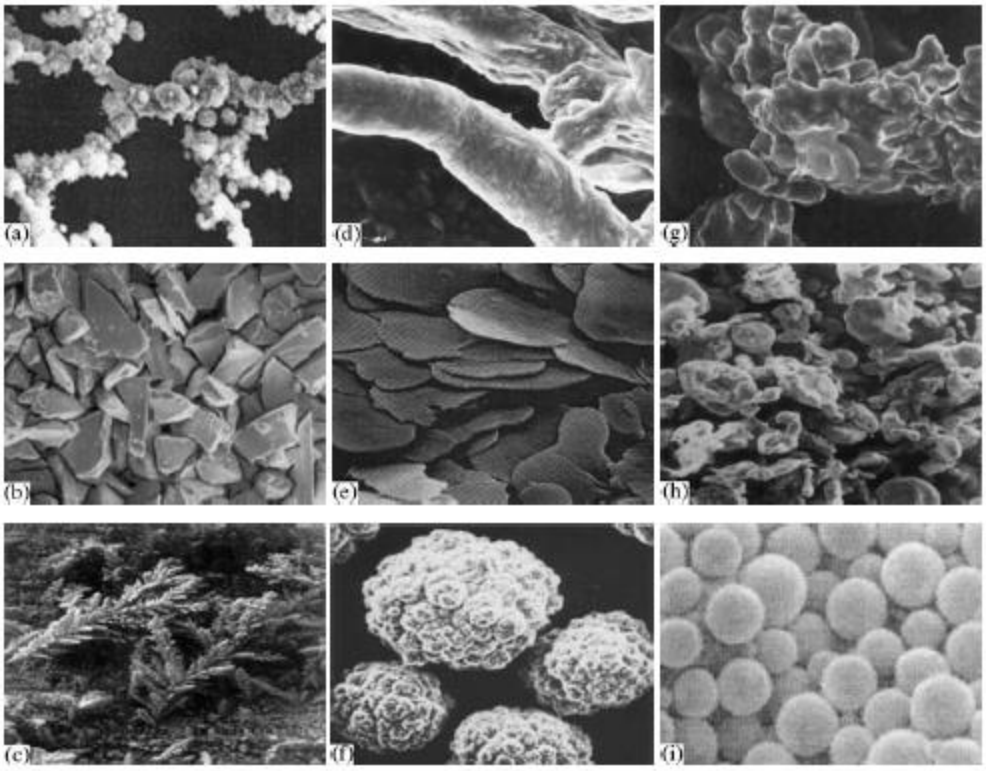

Figure 2: Characteristic particle shapes
(a) Acicular; (b) angular; (c) dendritic; (d) fibrous; (e) flaky; (f) granular; (g) irregular; (h) modular & (i) spherical powder particles (Source: Neikov, 2009: 3)

Not all metal powder products are, therefore equal. A high-quality metal powder product can only be classified as such when it complies with *all* the required specifications, not just one.

Metal powders frequently require further processing in order to meet the specifications required for use in powder metallurgy. Each post-processing step added has a direct cost implication for the final metal product.

Producing a titanium metal powder product with limited or no post-reduction processing steps can be of significant value to the titanium powder metallurgy value chain.

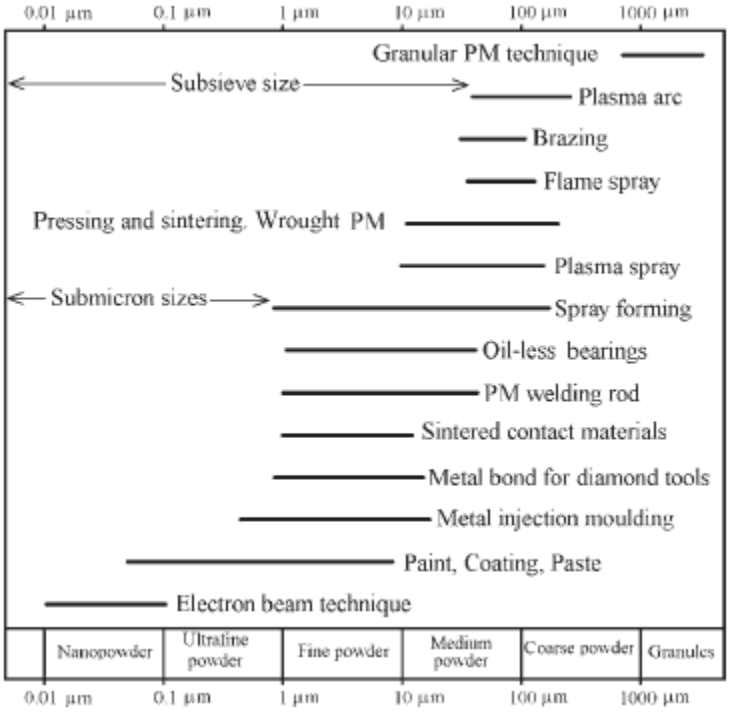

Figure 3: Ranges of a particle size suitable for different applications of non-ferrous metal powders (Source: Neikov, 2009: 4)

A titanium metal powder product can, therefore, be grouped into two categories. The first is where titanium metal powder produced through metallothermic reduction can be used directly as feed material in powder metallurgy. The second category is where a useable titanium metal powder product is obtained only after multiple post-reduction processing steps.

These two product categories were defined in Section 1.1 as either primary and secondary metal powder products.

In summary, powder production is not a “one size fits all” solution. Various considerations are required for downstream application.

2.2.2 – Titanium metal powder production

Chemical composition, particle morphology and particle size were highlighted in Section 2.2.1 as the three most important properties determining the quality of a metal powder product.

Chemical composition, or purity, is essential for any component made from titanium metal. Impurities must not exceed the ranges listed in Table 3 for a metal component to benefit from titanium's unique characteristics.

Table 3: Chemical composition (wt.%) of commercially pure titanium metal grades

	N	C	H	Fe	O
Gr. 1	0.03	0.08	0.015	0.2	0.18
Gr. 2	0.03	0.08	0.015	0.3	0.25
Gr. 3	0.05	0.08	0.015	0.3	0.35
Gr. 4	0.05	0.08	0.015	0.5	0.40

(Source: Cardarelli, 2008: 301)

However, producing chemically pure titanium metal is a complicated undertaking due to its reactivity with atmosphere and other elements. Industrial-scale production of pure titanium metal was only successfully achieved in the early 1950s (Housley, 2007).

The high reactivity of titanium metal towards atmospheric gases and other metals effectively prescribes that a chemical method be used (as illustrated in Figure 1) to produce a chemically pure product (Neikov, 2009: 1).

Numerous chemical routes can be used to produce titanium metal. Figure 4 illustrates some of the methods considered during the 1960s.

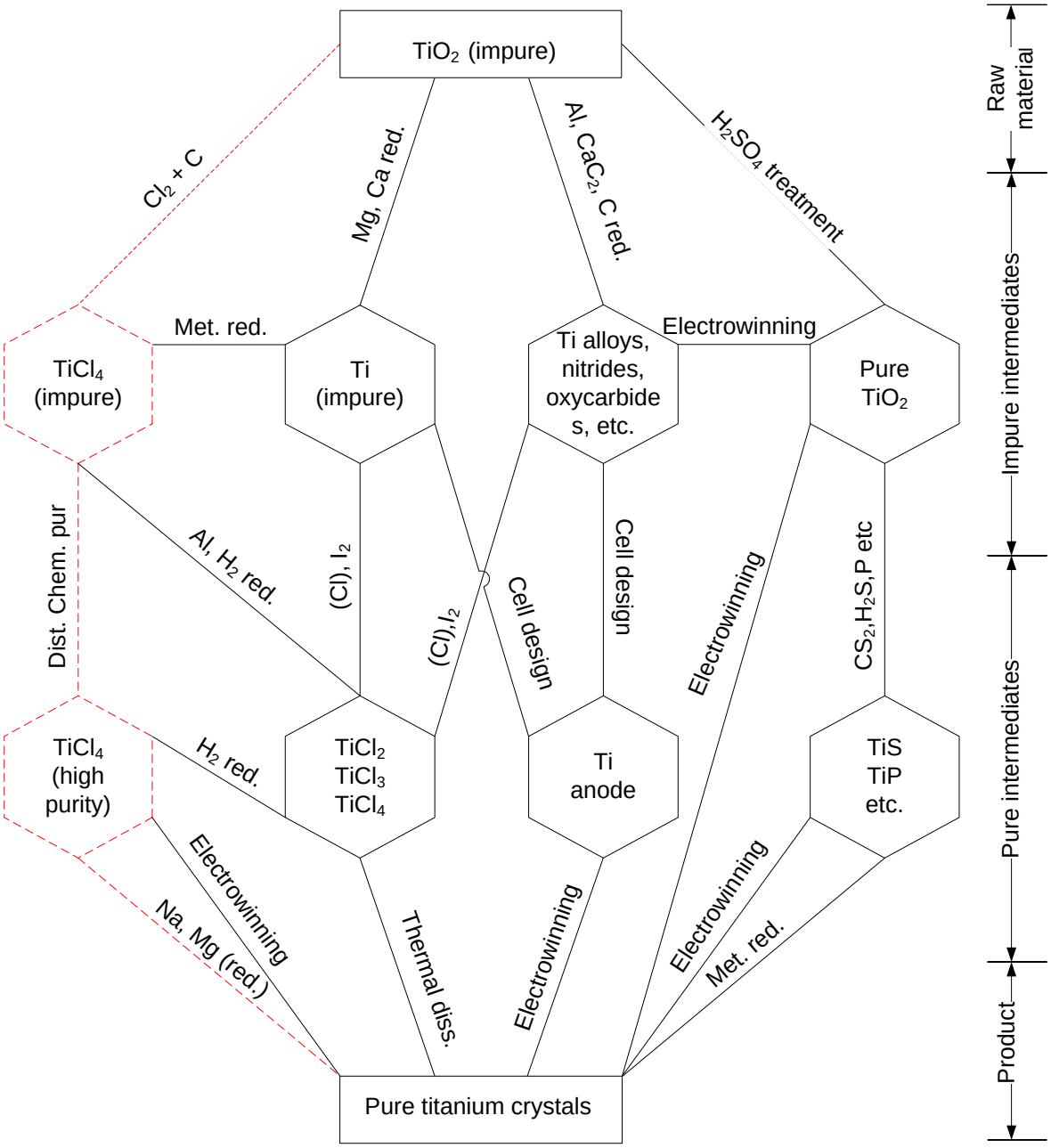

Figure 4: Possible chemical paths from titanium mineral to titanium metal (Adapted from Henrie, 1965)

Since the conception of Figure 4, many more options, conceptually possible and demonstrated, have been developed. Table 4 summarises recent technologies that focus on titanium metal production.

Table 4: Alternative process routes for titanium metal production

Name / Organisation	Process / Products / Comments
FFC	Oxide, electrolytic molten $CaCl_2$
MER	Oxide, electrolytic
SRI	Fluidised bed H_2 reduction of $TiCl_4$
BHP (Billiton), Australia	Oxide electrolytic, pre-pilot plant
Idaho Ti	Plasma quench, chloride
Ginatta, Italy	Electrolytic, chloride
OS, Ono, Japan	Electrolytic/calciothermic oxide
MIR, Germany	Iodide reduction
CSIR, South Africa	Electrolysis of oxide
Okabe-I, Tokyo, Japan	Oxide, reduction by Ca
Okabe-II, Tokyo, Japan	Oxide, Ca vapour reduction
Vartec, Idaho	Oxide, Ca vapour reduction
Northwest Institute for Non-ferrous Metal Research, China	Innovative hydride-dehydride
CSIRO, Australia	Chloride, fluidised bed, Na
Armstrong/ITP	Chloride, continuous reduction with Na
DMR	Aluminothermic rutile feedstock
MIT	Oxide, electrolysis
QIT/Rio Tinto	Slag, electrolysis
Tresis	Argon plasma, chloride
Dynamet Technology	Low-cost feedstock

(Source: Froes, 2015: 17)

Even though significant progress has been made to improve titanium metal production, nearly all industrial processes still use the Kroll process (Roskill, 2013: 20). The reader is referred to the significant body of literature available regarding alternative titanium metal production methods (van Vuuren, 2009a & 2009b; Froes, 2012; EHK Technologies, 2004; Turner *et al.*, 2001; Fang *et al.*, 2017).

The Kroll process (reaction path highlighted in Figure 4 with a dashed red line) uses Reaction 1 for titanium metal production:

$$TiCl_4 + 2Mg \rightarrow Ti + 2MgCl_2$$ Reaction 1

Reaction 1 is generally known as a metallothermic reduction reaction. The metallothermic reduction reaction is further discussed in Section 2.3.

The Kroll process produces titanium metal in batches using the following general sequence (Turner *et al.*, 2001):

1. The complete inventory of required magnesium (Mg) is loaded into a sealed batch reactor with an inert (Ar(g)) atmosphere.
2. The reactor is then heated to between 800 and 900 °C.
3. Titanium tetrachloride ($TiCl_4$) is slowly fed into the reactor over several days to prevent heat accumulation inside the reactor.
4. Molten magnesium chloride ($MgCl_2$) salt is tapped from the reactor during production to provide more useable volume for further reaction. This step is repeated several times.
5. Vacuum distillation is applied to remove un-reacted Mg and $MgCl_2$ after reaction completion.
6. The titanium product is then pressed, or jackhammered out of the reduction vessel.

The product morphology obtained using the Kroll process is known as titanium sponge due to its sponge-like appearance and porous structure.

The sponge-like metal product typically adheres to reactor internals. This adhesion causes the outer layers of the product to be contaminated with metals in the reactor's construction material. Iron contamination is especially prevalent when the reactor is operated above 1 000 °C.

A two-ton block of titanium sponge is shown in Figure 5 as an example.

Figure 5: Two-ton block of titanium sponge
(Source: Subramanyam, 1993: 446)

Section 2.2.1 highlighted that not all powder products are equal. The Kroll sponge shown in Figure 5 is an example of a product that cannot be classified as a primary metal powder. Substantial effort is required to produce a viable metal powder product from this bulk metal product.

The following post-processing steps are typically used in sequence to produce a viable metal powder product from titanium metal sponge (EHK Technologies, 2004: 2):

- Sponge purification
- Comminution
- Blend sponge, scrap, alloy
- Compact
- Weld electrode
- Vacuum arc re-melting
- Ingot conditioning

The titanium metal ingots are then used as the starting material to produce spherical titanium metal powder using mechanical methods such as gas atomisation.

In summary, titanium metal powder obtained via the Kroll process is classified as a secondary metal powder product because it is produced using a combination of chemical and mechanical methods (shown in Figure 1).

2.2.3 – Concluding remarks

Not all metal powder products are equal. This is especially true when the powder is intended for powder metallurgy.

A distinction is therefore made between so-called primary and secondary metal powder products.

Titanium metal powder produced through direct metallothermic reduction can be regarded as a primary metal powder product when no other post-production steps are needed. In contrast, a titanium metal powder produced from an existing titanium metal source (billet or ingot) is classified as a secondary titanium metal powder product. Therefore, titanium metal powder produced from Kroll sponge is classified as a secondary metal powder product. Significant effort is required to transform the sponge-like product into one in which the chemical composition, particle morphology, and particle size fall within allowable limits for powder metallurgy.

The Kroll process is still the predominantly used commercial titanium metal production method. There are other methods available, but none that can produce a primary titanium metal powder product. For such a process to exist, it is critical that control over chemical composition, particle size and morphology is realised. Emphasis is, however, currently mostly on chemical composition alone.

Titanium metal purity is directly related to how “clean” the reaction is kept during production, i.e. regarding foreign dissolved metal cations, contamination from product deposition on reactor internals and inert reaction atmosphere.

A process producing a free-flowing primary titanium metal powder product will require controlled deposition, i.e. on the particle and not the reactor internals and control over particle morphology (shape and size).

Producing a free-flowing titanium powder product with sufficiently large titanium particles is a significant challenge. According to Demopoulos (2009:199), crystallisation theory defines reactive crystallisation as precipitation. Therefore, the current understanding of reactive crystallisation predicts the formation of an ultrafine precipitate rather than particle growth due to the metal's insolubility in the molten salt reaction medium.

For reactive metals like titanium, a minimum spherical particle diameter of at least 5 µm is needed to prevent oxygen contamination (through surface oxidation) from exceeding the allowable limits (Hansen & Gerdemann, 1998: 58). Table 5 provides an estimated oxygen content of several particle sizes based on an oxide monolayer's presence.

Table 5: An estimation of oxygen content in several sizes of powder based on a monolayer of oxide

Particle size (µm)	**Oxygen** (wt.%)
149	0.0006
44	0.0019
5	0.0168
1	0.0838
0.5	0.1676

(Source: Hansen & Gerdemann, 1998: 58)

Therefore, a review of the metallothermic reduction reaction is needed to hypothesize a mechanism that can be used to increase the size of suspended titanium metal particles.

2.3 – Metallothermic reduction of Ti^{4+}

2.3.1 – Redox reaction

The Kroll process produces titanium metal (Ti^0) via metallothermic reduction of $TiCl_4$. The following chemical equation is applicable:

$$TiCl_4 + 2Mg \rightarrow Ti_{(s)} + 2MgCl_2 \qquad \text{Reaction 2}$$

Reaction 2 is a spontaneous exothermic reaction with ΔG = -403 kJ/mol at 900 °C. Both magnesium and magnesium chloride are liquid at this temperature, while titanium tetrachloride a gas.

Magnesium (Mg^0) provide the electrons required to reduce the Ti^{4+} oxidation state in $TiCl_4$ to elemental titanium, Ti^0. In this instance, Mg^0 is referred to as the reductant.

A reaction is known as a redox reaction when electrons are transferred from one species to another (Kotz & Treichel, 2003: 835). Reaction 2 can therefore be rewritten as two separate half-reactions:

$$Ti^{4+} + 4e^- \rightarrow Ti_{(s)} \qquad \text{Reaction 3}$$

$$2Mg \rightarrow 2Mg^{2+} + 4e^- \qquad \text{Reaction 4}$$

Reactions 3 and 4 each represent one-half of an electrochemical cell.

Therefore, the metallothermic reduction can be regarded as a galvanic electrochemical cell when the reaction is allowed to proceed in a reductant's molten chloride salt.

A simplified galvanic (spontaneous) electrochemical cell is illustrated in Figure 6 to show that the overall reaction can continue even when the half-cell reactions are physically separated from each other.

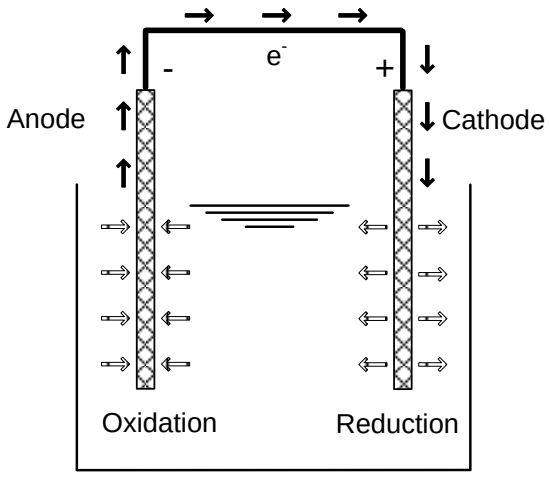

Figure 6: Illustration of a simplified galvanic cell
(Adapted from Atkins & de Paula, 2002: 265)

Electrons are withdrawn from one electrode (site of oxidation) and collected at the other electrode (site of reduction). A solid arrow in Figure 6 represents the electrons. Electron transfer may be accompanied by other events, such as an atom or ion transfer, but the net effect is electron transfer and hence a change in the oxidation number of an element (Atkins & de Paula, 2002: 263). The transparent arrows in Figure 6 represent the flow of anions.

In a metallothermic reduction reaction, the reductant (site of oxidation in Figure 6) can be any alkali or alkali earth metal thermodynamically favouring reaction completion. More generally, Reaction 2 can be written as follows:

$$Ti^{n+} + {}^{n}/_{m}\,B^{0} \rightarrow Ti^{0}_{(s)} + {}^{n}/_{m}\,B^{m+} \qquad \text{Reaction 5}$$

In Reaction 5, Ti^{n+} is a titanium cation with oxidation number n (n = 2, 3 or 4 as titanium has three oxidation states), and B^{0} is the reductant with an oxidation number m ($m = 1$ for alkali metals and $m = 2$ for alkali earth metals).

Sub-stoichiometric reduction of Ti^{4+} will result in either Ti^{3+} or Ti^{2+} cations. The following half-reactions are possible:

$$Ti^{3+} \rightarrow Ti^{4+} + e^{-} \quad \text{Reaction 6}$$

$$Ti^{2+} \rightarrow Ti^{3+} + e^{-} \quad \text{Reaction 7}$$

$$Ti^{2+} \rightarrow Ti^{4+} + 2e^{-} \quad \text{Reaction 8}$$

Stepwise reduction of Ti^{4+} is utilised in the Hunter process to enforce more control during Ti^{0} production. The Hunter process uses Na^{0} as the reductant in the following two reactions:

$$Ti^{4+} + 2Na^{0} \rightarrow Ti^{2+} + 2Na^{2+} \quad \text{Reaction 9}$$

$$Ti^{2+} + 2Na^{0} \rightarrow Ti^{0}{}_{(s)} + 2Na^{2+} \quad \text{Reaction 10}$$

A benefit of Ti^{4+} sub-stoichiometric reduction is that $TiCl_2$ is soluble in molten chloride salts as Ti^{2+} cations. The thermodynamic driving force for reaction can be reduced by diluting the Ti^{2+} cation concentration in the molten salt.

The metallothermic reduction reaction is somewhat unique in that the molten salt reaction medium is both a pure ionic liquid and forms as a by-product of the reaction itself. Another benefit of this system is that the number of chemical species present during the reaction can be limited to only three (i.e. Ti^{n}, Na^{n}, and Cl^{-} anions, with n variable on the oxidation level).

The mobility of ions in molten salt, as reflected in their electrical conductivity, can be an order of magnitude higher (greater than 1 $S.cm^{-1}$) than that of aqueous electrolytes (Dryfe, 2007: 875; Alcock, 2001: 318). The conditions for electrochemical reaction in a molten salt medium are therefore very favourable.

Like Figure 6, a metallothermic reduction reaction can proceed without any physical contact between reactants when provision is made for electron and ion transfer between half-cell reactions (Henrie & Baker, 1960: 30). These prerequisites are usually met as the reactor is constructed from metal (i.e. electron conductor). This typically results in the deposition of Ti^{0} on reactor internals. This problematic deposition on reactor internals is one reason why a Kroll reactor is forced into a batch operation mode.

2.3.2 – Overview of known reaction mechanisms resulting in titanium metal

2.3.2.1 – Galvanic reaction at the interfacial region

Henrie & Baker (1960) studied the Ti^{4+} metallothermic reduction with Na^0 and postulated that reduction occurs by two stepwise reactions.

The first stage reaction is a sub-stoichiometric reduction of Ti^{4+} to produce soluble titanium sub-chlorides, predominantly Ti^{2+}, as shown in Reaction 9.

The second stage reduction occurs in the molten NaCl between Na^0 and $TiCl_2$ (Reaction 10). This is a heterogeneous reaction between two separate regions. The alpha (α) region consists of dissolved Na^0 in molten NaCl, and the beta (β) region consists of $TiCl_2$ dissolved in molten NaCl. The interfacial zone between the $\alpha - \beta$ regions are separated by distance γ and is referred to as the σ-zone. These regions are illustrated in Figure 7.

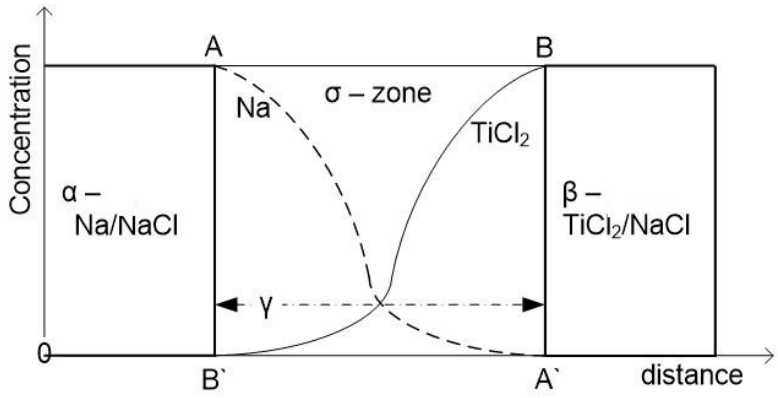

Figure 7: Concentration gradient of Na^0 and $TiCl_2$ in the interfacial region (Adapted from Henrie & Baker, 1960: 25)

Figure 7 illustrates the variation in concentrations of reacting species across the interfacial region (σ-zone). The Na^0 and $TiCl_2$ concentrations in the transition zone can be estimated using the equilibrium constant (K_a) for Reaction 10.

Henrie and Baker (1960: 16) estimated the equilibrium constant for Reaction 10 to be equal to 2.38×10^{12} at 850 °C. The equilibrium constant and its relation to Reaction 10 are provided in Equation 1. This extremely large value shows just how thermodynamically favourable the metallothermic reduction reaction is in forming Ti^0.

$$K_a = \frac{\alpha^2_{NaCl}}{\alpha^2_{Na} \cdot \alpha_{TiCl_2}} = 2.38\ x\ 10^{12}$$ Equation 1

In Equation 1, α denotes the activity of each component.

Henrie and Baker (1960: 30) used Figure 8 to explain their postulated growth mechanism. Figure 8 is a rework of Figure 7 but without the concentration gradients shown in the interfacial region. Instead, a titanium crystal is superimposed on the diagram and bridges the interfacial region to connect the α and β zones with each other.

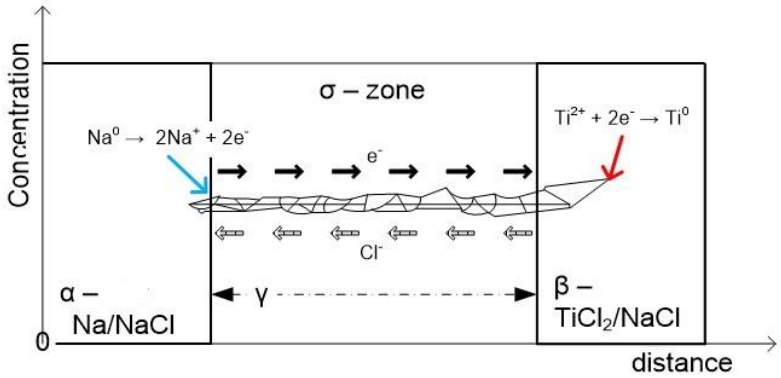

Figure 8: Condition for deposition of Ti^0 through the interfacial region (Adapted from Henrie & Baker, 1960: 30)

Figure 8 is analogous to the electronic conductor of Figure 6 in that the metallic Ti^0 allows for electron transfer (solid arrow) from the α-zone, through the interfacial region, to the β-zone where Ti^0 deposition and growth occurs. In turn, the Cl^- anions (empty arrows) are released in the β-zone and transferred via the pure ionic liquid to the site of dissolved Na^0 oxidation.

In summary, Henrie & Baker (1960) postulated that the mechanism is a heterogeneous reaction between these two zones and that the reaction is electrochemical. The model proposed is a galvanic reaction at the interfacial region.

2.3.2.2 – Electronically mediated reaction (EMR)

Okabe & Sadoway (1998) dubbed the metallothermic reaction mechanism in molten salt as an “electronically mediated reaction” (EMR). They postulated that the overall reaction was rate-limited by electron transport between the reactants.

The EMR mechanism was further subdivided into either “short-range” EMR (SR-EMR) or “long-range” EMR (LR-EMR).

Table 6 summarises a comparison made between the SR- and LR-EMR mechanisms (Okabe & Waseda, 1997:29).

The SR-EMR term is used to describe the mechanism when both electron and ion transfer occur via the molten salt, i.e. there is no external electrical conductor present. Okabe and Sadoway (1998) mentioned that physical contact between the two reagents is required for the SR-EMR mechanism to proceed. Furthermore, Okabe and Waseda (1997: 29) postulated that electron transfer might also occur via electronically conducting molten salt, especially when using Na^0 dissolved in molten NaCl. Therefore, the product obtained from the SR-EMR mechanism is considered to form by homogeneous nucleation. The SR-EMR mechanism seems similar to precipitation, cementation or contact displacement reactions, especially concerning the product’s insolubility in the molten salt (Demopoulos, 2009: 199).

The LR-EMR term is used to describe electron transfer via a conducting intermediary or any other electronically conductive substrate. Therefore, the LR-EMR mechanism is virtually the same as that of a galvanic cell. Okabe & Sadoway (1998) suggested that LR-EMR is the dominant mechanism during Kroll sponge production. The sponge-like product obtained results from heterogeneous nucleation on the intermediary substrate, followed by the growth of sponge-like product on the product itself because the metallic product is also an electron conductor.

Table 6: Comparison between short-range and long-range EMR

	Short-range EMR	Long-range EMR
The nominal distance of electron transfer	Short	Long
Major electron pathway	Electronically conducted molten salt	Metal (e.g. reaction container, metal deposit)
Major reaction	Homogeneous	Heterogeneous
Major morphology of the deposit	Powder	Highly connected deposits (bulk form, dendritic form, sponge)
Location of deposit	Dispersed in molten salt	Controllable
Features	Fast reaction, possible to produce very fine powder	Controllable reaction speed, no direct physical contact between feed and reductant, choice of salt is restricted, and large variation of reductant

(Source: Okabe & Waseda, 1997: 29)

Different product morphologies are produced when a specific mechanism is dominant. The SR-EMR mechanism favours powder production, while the LR-EMR mechanism favours a sponge-like product (Okabe & Sadoway, 1998). Therefore, sponge-like growth may be a direct consequence of producing an electronically conductive material like Ti^0.

2.3.3 – Concluding remarks

Section 2.3.1 discussed how the Ti^{4+} metallothermic reduction-reaction system is comparable to a galvanic electrochemical cell when the reaction is allowed to proceed in a molten chloride salt of the reductant.

Section 2.3.2 presents evidence from the literature supporting this view in that both sources (Henrie & Baker, 1960; Okabe & Sadoway, 1998) described the reaction mechanism as being electrochemical in nature.

Okabe and Waseda (1997: 29) distinguished between two dominant reaction mechanisms, each with a unique product morphology and formation site. The SR-EMR mechanism results in a precipitate forming in the bulk of the molten salt solution. The LR-EMR mechanism is used to explain the deposition on reactor internals and subsequent further growth on the deposit to result in what is referred to as a sponge-like product.

The illustration sourced from Henrie and Baker (1960) in Figure 8 explains why titanium growth is observed when the interfacial region between two separate zones (each of which contains a reagent) is bridged with an electron conductor such as Ti^0.

With Figure 8 as a reference, the following hypothesis is postulated:

> *Titanium metal particle growth is possible through electrochemical titanium metal deposition when titanium metal particles are suspended and maintained in a molten chloride salt with both titanium dichloride and reductant present in a meta-stable equilibrium.*

The postulated growth mechanism requires reaction conditions like those inside the interfacial region (σ-zone) described in Figure 8, but with suspended Ti^0 particles present.

Figure 9 illustrates the postulated scenario with a Ti^0 particle suspended in the interfacial region illustrated in Figure 8.

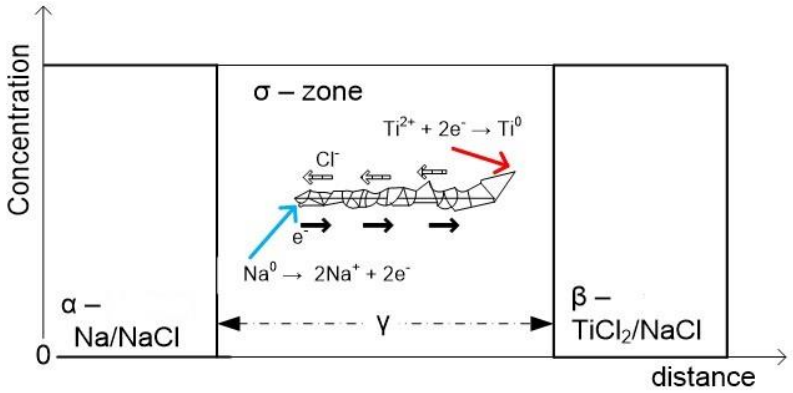

Figure 9: The postulated scenario for Ti^0 deposition on suspended Ti^0 particles

Figure 9 shows that the reacting species do not interact directly with each other, but via the suspended Ti^0 particles. Electrochemical deposition conditions are favourable as the Ti^0 product is electronically conductive and surrounded by a pure ionic liquid. The two half-cell reactions can then proceed on the suspended Ti^0 particles, like LR-EMR via the reactor internals (Okabe & Waseda, 1997).

However, the postulated growth mechanism is potentially impractical with an equilibrium constant equal to 2.38×10^{12} as only trace amounts of both reagents can be present. A deviation from this concentration range will result in either precipitation or deposition on reactor internals.

The postulated growth mechanism is similar to a method known as “electroless deposition”. In the electroless deposition, both reductant and metal cations are simultaneously dissolved in a solution containing a substrate surface. The reductant and metal cations react with each other via the substrate surface but can still react with each other in solution to result in a condition referred to as “bath instability” (discussed in Section 2.4.4).

2.4 – Electroless deposition

2.4.1 – Overview of electroless deposition

Electroless plating describes metal deposition methods through electrochemical reaction but without electric current supplied from an external source (Mallory & Hajdu, 1990: vii). Therefore, electroless deposition is characterised by selective reduction of metal ions in

solution, but only on the substrate's surface submerged in a solution containing the metal cations.

Electroless deposition is frequently referred to as “chemical deposition” (Popov *et al.*, 2016: 329). Electroless deposition can be further subdivided into two groups, these being (Djokić & Cavallotti, 2010: 253):

- Heterogeneous processes: galvanic displacement deposition
- Combined homogeneous and heterogeneous processes: autocatalytic electroless deposition

Essentially, these electroless plating processes differ in how and where they obtain the electrons needed for reduction. Both are discussed in the following paragraphs.

Galvanic displacement deposition is the simplest form of electroless plating (Mallory & Hajdu, 1990: 1). Galvanic displacement deposition is also known as contact displacement, immersion plating or cementation. An example of contact displacement is when copper cations in solution are reduced and deposited as metallic copper (Cu^0) on metallic zinc (Zn^0) when Zn^0 is submerged in a copper sulphate solution. The following two half-cell reactions are applicable:

$$Zn^0 \rightarrow Zn^{2+} + 2e^- \qquad \text{Reaction 11}$$

$$Cu^{2+} + 2e^- \rightarrow Cu^0 \qquad \text{Reaction 12}$$

However, the reaction stops immediately as soon as the surface is covered with Cu^0. The less noble substrate's surface acts as a reducing agent for the metallic cations of a more noble metal (Djokić & Cavallotti, 2010: 254). Therefore, the overall redox reaction can not continue without an electron source strong enough to reduce the Cu^{2+} cation in the example mentioned. Limited deposition thickness is therefore inherent to galvanic displacement.

Autocatalytic electroless deposition (or autocatalytic plating) is a form of electroless plating where a chemical reaction proceeds continuously on the electron-conducting substrate surface. In this instance of electroless plating, the substrate performs a catalytic function in

that selective reduction of metal cations in solution occurs on the substrate surface (Mallory & Hajdu, 1990: 2).

The electrons needed for autocatalytic electroless deposition are provided by a reducing agent dissolved in the homogeneous solution, containing the dissolved metal cations that are to be deposited. As noted above, this makes autocatalytic electroless deposition a combined homogeneous and heterogeneous process.

Various reducing agents can be used. Some of those reported in the literature include (Djokić & Cavallotti, 2010: 257):

- Formaldehyde
- Hydrazine
- Hypophosphite
- Ascorbic Acid
- Hydrogen

However, the reducing agent and metal cation concentrations must be maintained so that the homogeneous reaction between these two reagents is suppressed in the bulk solutions (Paunovic & Schlesinger, 2006: 139).

An autocatalytic electroless deposition allows continued metal deposition on the substrate for as long as the reagents are present in the electrolyte at the correct concentrations. Figure 10 illustrates the difference in deposition thickness achievable between autocatalytic electroless deposition and contact displacement deposition.

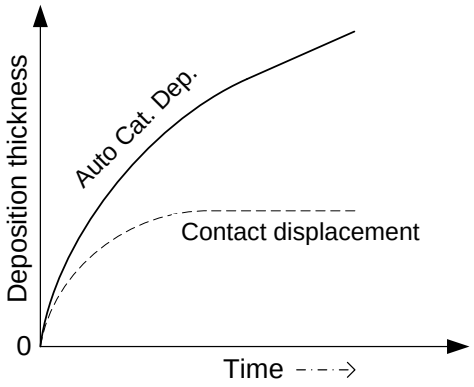

Figure 10: Thickness vs time comparison between autocatalytic electroless deposition and contact displacement deposition
(Adapted from Mallory & Hajdu, 1990: 2)

The substrate surface plays an essential role in autocatalytic electroless deposition and therefore must be prepared before metallisation in many cases, especially for deposition on ceramics, polymers and other non-metals (Popov *et al.*, 2016: 352). The deposit itself catalyses further metal cation reduction once the initial metallic layer has been deposited on the prepared substrate surface.

In the electrochemical mechanism for autocatalytic electroless deposition, the substrate is considered as a shared electrode on which both half-cell reactions occur (Paunovic & Schlesinger, 2006: 140).

2.4.2 – Mechanisms of electroless deposition

Five different mechanisms have been proposed for electroless deposition. These are (Popov *et al.*, 2016: 356):

- Atomic hydrogen mechanism
- Hydride ion mechanism
- Electrochemical mechanism
- Metal hydroxide mechanism
- Universal mechanism

The reader is referred to Djokić (2002: 87-107) for a more in-depth discussion of each mechanism.

These mechanisms can generally be divided into two main categories (Djokić & Cavallotti, 2010: 262). The first category involves mechanisms in which intermediate species, such as hydroxides, hydroxyl complexes, hydride ions or hydrogen react with the reducing agent. The second category deals with mechanisms where autocatalytic electroless deposition is explained using the mixed-potential theory, with independent anodic and cathodic processes.

Popov *et al.* (2016: 357) strongly recommended, however, that each autocatalytic electroless deposition reaction be evaluated as having a unique mechanism. Generalisation should, therefore, be avoided.

2.4.3 – Mixed-potential theory

The postulated growth mechanism is a combination of both homogeneous and heterogeneous processes. Also, independent anodic and cathodic processes occur on the suspended Ti^0 particle surface. The postulated growth mechanism is, therefore defined as autocatalytic electroless deposition.

Mixed-potential theory can be used to explain the autocatalytic electroless deposition mechanism. The theory is therefore briefly reviewed here.

Assume the overall reaction of an autocatalytic electroless deposition reaction is:

$$M^{z+}_{solution} + Red_{solution} \xrightarrow{catalytic\ surface} M_{lattice} + Ox_{solution} \qquad \text{Reaction 13}$$

where

Ox is the oxidation product of the reducing agent Red

The catalytic surface may be a substrate S or catalytic nuclei of the metal M dispersed on a non-catalytic surface S (Paunovic & Schlesinger, 2006: 139).

Reaction 13 can be decomposed into two half-cell reactions, cathodic (Reaction 14) and anodic (Reaction 15).

$$M^{z+}_{solution} + ze^- \xrightarrow{catalytic\ surface} M_{lattice} \quad \text{Reaction 14}$$

$$Red_{solution} \xrightarrow{catalytic\ surface} Ox_{solution} + me^- \quad \text{Reaction 15}$$

The reducing agent's equilibrium potential must be more negative than that of the metal electrode so that the reducing agent can function as an electron donor and the dissolved metal cations as an electron acceptor.

In the electrochemical model for autocatalytic electroless deposition, Reactions 14 and 15 occur on the same electrode and at the same electrode-electrolyte interface (Paunovic & Schlesinger, 2006: 139).

When a catalytic surface is submerged in a solution containing both M^{z+} cations and a reducing agent, the two half-cell reactions occur on two different sites on the catalytic surface, with a flow of electrons between these sites (Paunovic & Schlesinger, 2006: 140).

Each of these half-reactions strives to establish equilibrium but, because both occur on the same electrode, the result is a new steady-state mixed potential (E_M).

The mixed potential, illustrated in Figure 11, is where the partial cathodic and anodic polarisation curves intersect. The rate of autocatalytic electroless deposition (i_{dep}) can also be obtained from this diagram.

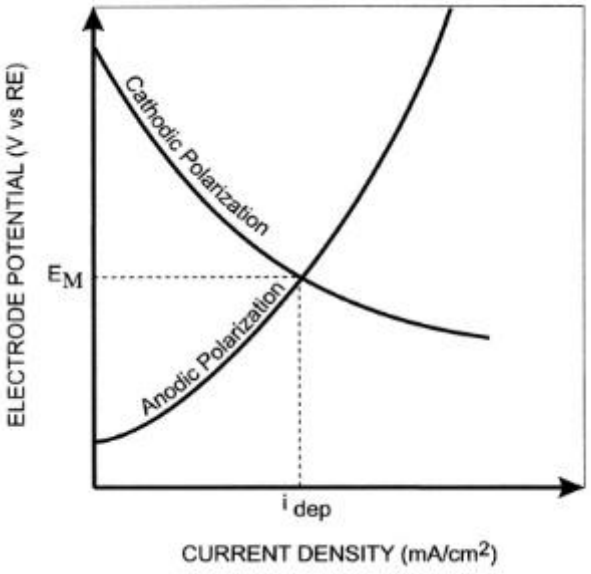

Figure 11: Schematic diagram of partial cathodic and partial anodic polarisation curves in terms of mixed-potential theory
(Source: Djokić, 2002: 94)

2.4.4 – Bath instability

The term “bath instability” is used in the literature to describe the conditions where deposition quality is significantly diminished, combined with the deposition of metal powders in the bulk solution (Popov *et al.*, 2016: 354; Djokić & Cavallotti, 2010: 258).

The following observations regarding bath instability were made while studying metal cation concentration, reductant concentration and temperature (Popov *et al.*, 2016: 355):

- With temperature and reductant concentration held constant:
  - A small increase in metal cation concentration leads to a slight increase in deposition rate combined with insignificant surface roughening.
  - A significant increase in metal cation concentration may not influence the deposition rate.
- With temperature and metal cation concentration held constant:
  - An increase in the reductant concentration usually leads to a significant increase in metal cation reduction. This typically leads to bath instability and subsequent powder deposition in the bulk.
- With reductant and metal cation concentration held constant:

- An increase in temperature leads to an increased rate of metal cation reduction; this condition also typically leads to bath instability.

2.4.5 – Concluding remarks

Ti^0 particle growth is an essential prerequisite needed to make primary metal powder production a reality.

The literature review in Section 2.3.2 resulted in a postulated Ti^0 particle growth mechanism. The postulated growth mechanism is illustrated and discussed in Figure 9 and Section 2.3.3.

Section 2.3.3 further explained that the postulated growth mechanism is similar to electroless deposition. Section 2.4 subsequently reviewed the different methods and mechanisms of electroless deposition.

The postulated growth mechanism is a combination of both homogeneous and heterogeneous processes. Also, independent anodic and cathodic processes occur on the suspended Ti^0 particle surface. Section 2.4.3, therefore defined the postulated growth mechanism as electrochemical autocatalytic electroless deposition.

With autocatalytic electroless deposition as the foundation, Section 2.4.3 showed that a suspended Ti^0 particle, as illustrated in Figure 9, could be referred to as a “mixed electrode” when applying the mixed-potential theory.

Section 2.4 concluded by discussing the term “bath instability”. This unwanted condition is similar to that described in Section 2.3.3, where a deviation from the meta-stable equilibrium concentration will result in either precipitation or deposition on reactor internals.

CHAPTER 3 – THEORY BUILDING

3.1 – Chapter overview

The aim of this chapter is twofold. The first objective is to estimate a concentration range where Ti^{2+} cations and Na^0 atoms co-exist in meta-stable equilibrium.

The second objective is to build a theoretical foundation in which all possible reaction mechanisms (i.e. known and postulated) can be compared to estimate each mechanism's selectivity.

Chapter 3 contains the following sections:

1. The metallothermic reduction reaction used as a case study in Chapters 3 and 4 are defined in Section 3.2.
2. The reagent concentrations present in equilibrium with each other are estimated in Section 3.3.
3. The system of possible reaction mechanisms at low reagent concentrations is defined in Section 3.4.
4. Collision theory is briefly reviewed in Section 3.5.
5. The chapter concludes with Section 3.6 in which it is proposed that the different reaction mechanisms can be compared with each other using a parameter similar to the frequency factor in collision theory.

3.2 – The Na-$TiCl_2$-NaCl reaction system

The reaction between $TiCl_2$ and Na^0 (Reaction 10) dissolved in molten NaCl salt is the metallothermic reduction reaction selected as a case study.

$$TiCl_2 + 2Na^0 \rightarrow Ti^0 + 2NaCl \qquad \text{Reaction 10}$$

$TiCl_2$ can be produced either through sub-stoichiometric Ti^{4+} reduction (Reaction 9) or by the reaction between Ti^{4+} and Ti^0. The Hunter process uses a stepwise reduction of $TiCl_4$ for Ti^0 production. Reaction 10 represents the second reduction step of the Hunter process.

The two half-cell reactions for Reaction 10 are:

$$Ti^{2+} + 2e^- \rightarrow Ti^0 \qquad \text{Reaction 16}$$

$$2Na^0 \rightarrow 2Na^+ + 2e^- \qquad \text{Reaction 17}$$

Henrie and Baker (1960) and Boozenny (1962) both studied Reaction 10 at 850 °C. Reaction 10 is selected as the case study because both sources estimated values for the activity coefficients, which are required to quantify reagent concentrations for non-ideal equilibrium conditions. Table 7 lists the activity coefficients obtained by each study.

Table 7: Reported activity coefficients for Na^0-Ti^{2+} equilibrium in molten NaCl at 850 °C

Activity coefficient (γ)	**Henrie & Baker (1960: 19) Upper range**	**Henrie & Baker (1960: 19) Lower range**	**Boozenny (1962: 955)**
Ti^{2+}	0.04	0.18	0.66
Na^0	5	12.3	25

3.3 – Na^0 and Ti^{2+} meta-stable equilibrium

Meta-stable equilibrium between Ti^{2+} cations and dissolved Na^0 in molten NaCl is a fundamental prerequisite for the postulated growth mechanism illustrated in Figure 9, Section 2.3.3.

Henrie & Baker (1960: 16) estimated the equilibrium constant for Reaction 10 (at 850 °C) using the free energy of formation equal to 2.38 x 1012.

The equilibrium constant and its relation to Reaction 10 are provided in Equation 1.

$$K_a = \frac{\alpha_{NaCl}^2}{\alpha_{Na}^2 \cdot \alpha_{TiCl_2}} = 2.38\ x\ 10^{12} \qquad \text{Equation 1}$$

In Equation 1, α_j^i denotes the activity of reactant *j* in solution, and *i* is the order of reactant in the overall reaction equation. For elemental species such as Ti^0, the activity is equal to one ($\alpha_{Ti} = 1$).

The activity can, in turn, be related to the reagent concentrations by using the activity coefficient (γ_j^i). The relationship between activity and activity coefficients is shown in Equation 2 (Fogler, 2006: 83):

$$\alpha_j^i = \gamma_j^i \cdot x_j^i \qquad \text{Equation 2}$$

The equilibrium constant for a reaction can subsequently be written as (Fogler, 2006: 1022):

$$K_a = K_\gamma K_x \qquad \text{Equation 3}$$

where

$$K_x = \frac{x_{NaCl}^2}{x_{Na}^2 \cdot x_{TiCl_2}} \qquad \text{Equation 4}$$

Rearranging Equation 3 gives

$$\frac{1}{K_x} = \frac{K_\gamma}{K_a} = \frac{x_{Na}^2 \cdot x_{TiCl_2}}{x_{NaCl}^2} \qquad \text{Equation 5}$$

Therefore,

$$x_{Na} = \left(\frac{K_\gamma \cdot x_{NaCl}^2}{K_a \cdot x_{TiCl_2}}\right)^{1/2} \quad \text{Equation 6}$$

As first approximation ($\gamma_{NaCl} \approx 1$), the quotient of activity coefficient (K_γ) equals

$$K_\gamma = \frac{1}{\gamma_{Na}^2 \cdot \gamma_{TiCl_2}} \quad \text{Equation 7}$$

Substituting Equation 7 into Equation 6 gives

$$x_{Na} = \left(\frac{x_{NaCl}^2}{K_a \cdot \gamma_{Na}^2 \cdot \gamma_{TiCl_2} \cdot x_{TiCl_2}}\right)^{1/2} \quad \text{Equation 8}$$

Equation 8 can then be used to calculate the Na^0 concentration in equilibrium with Ti^{2+} cations as a function of different $TiCl_2$ concentrations. Microsoft Excel Solver can be used to solve Equation 8 by varying the NaCl mol fraction, with the constraint that the sum of all mol fractions ($TiCl_2$, NaCl and Na^0) must be equal to one.

The results illustrated in Figure 12 were calculated assuming a reaction medium composed of 1 000 000 atoms in total.

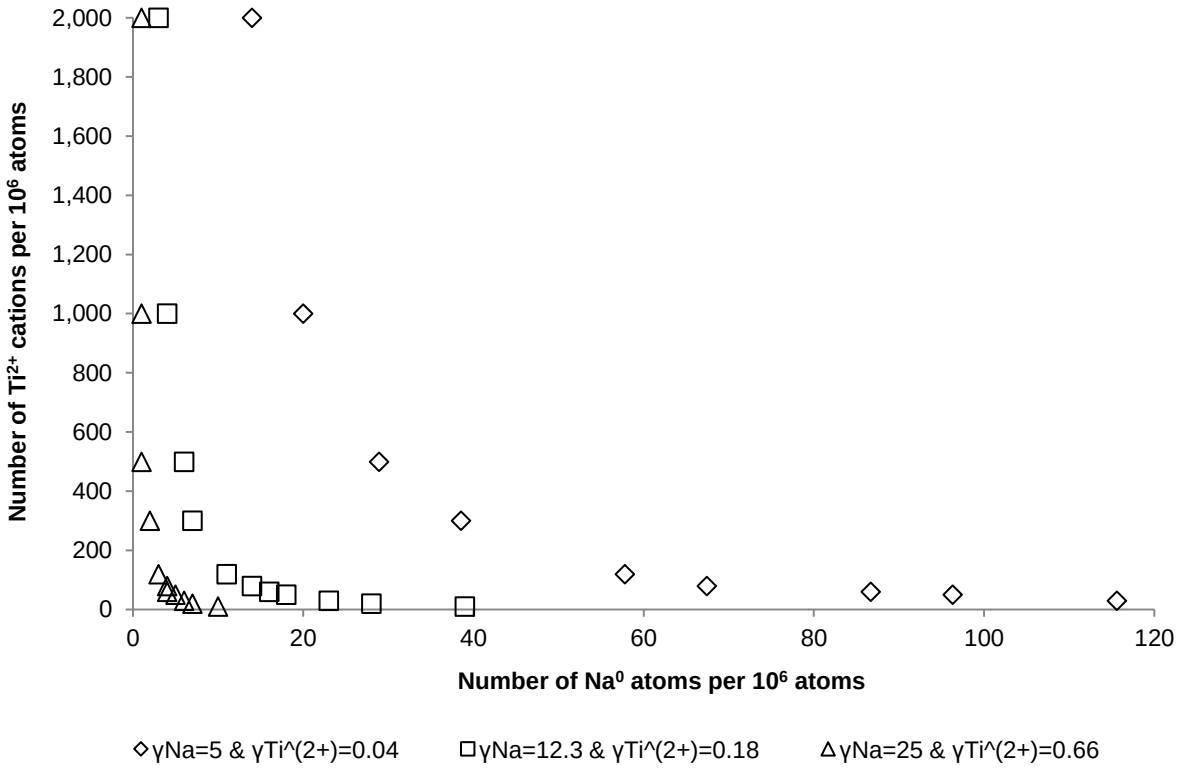

Figure 12: Ti^{2+} and Na^0 equilibrium in molten NaCl at 850 °C for different activity coefficients

Section 2.3.3 mentioned that the postulated growth mechanism is potentially impractical due to the low concentrations where $TiCl_2$ and Na^0 are in equilibrium.

Figure 12 shows that the $TiCl_2$ and Na^0 equilibrium concentrations are almost insignificant when using the lower range of both Henrie & Baker's (1960) and Boozenny's (1962) estimates of activity coefficients. The postulated growth mechanism might still be theoretically possible but is very likely to be impractical for beneficial use at these low concentrations.

The upper range activity coefficients estimated by Henrie & Baker (1960) suggest that there might be a narrow concentration range in which the postulated growth mechanism is possible.

Figure 12, therefore, highlights the importance of accurate and representative activity coefficients for reactions with an equilibrium constant like that of Reaction 10.

The two Henrie and Baker (1960:19) estimates of activity coefficients were obtained by superimposing an activity plot of Na^0 on the phase diagram of Na^0-NaCl at 850 °C. Boozenny (1962), in turn, obtained his estimates of activity coefficients by extrapolating data that were obtained from electrochemical studies.

It is important to emphasize that both sources *estimated* the activity coefficients. The *actual* activity coefficients are unknown, but these estimates provide insight into whether or not the postulated growth mechanism is possible for a reaction with such a large equilibrium constant.

The equilibrium concentrations predicted by the upper range activity coefficients of Henrie & Baker (1960) are repeated in Figure 13, but this time with a secondary vertical axis illustrating the percentage of Na^0 atoms in stoichiometric excess for a given Ti^{2+} cation concentration.

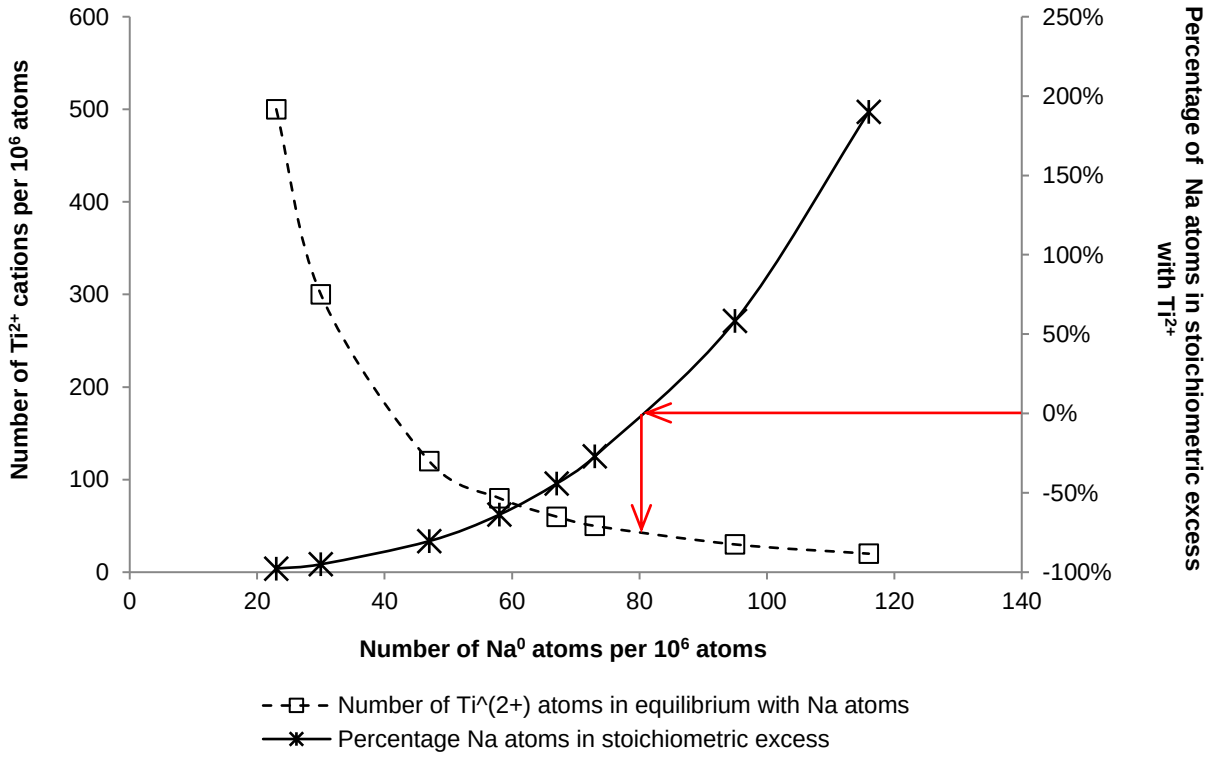

Figure 13: Percentage Na^0 atoms in stoichiometric excess with Ti^{2+} cations at 850 °C

$\gamma_{TiCl_2} = 0.04$ & $\gamma_{Na} = 5$

In Figure 13, approximately 80 Na^0 atoms are in stoichiometric equilibrium with 40 Ti^{2+} cations in a reaction medium consisting of 1 000 000 atoms in total.

Only the upper range activity coefficients of Henrie & Baker (1960) are used from this point onward.

The results shown in Figure 13 do not include any Ti^0 particles dispersed in the reaction medium. This is not representative in a reaction system in which Ti^0 particles accumulate. The Ti^0 particles will occupy space previously available to Na^+ and Cl^- ions to result in less volume for Ti^{2+} cations and Na^0 atoms to dissolve in.

The equilibrium concentrations for three Ti^0 mol concentrations are illustrated in Figure 14.

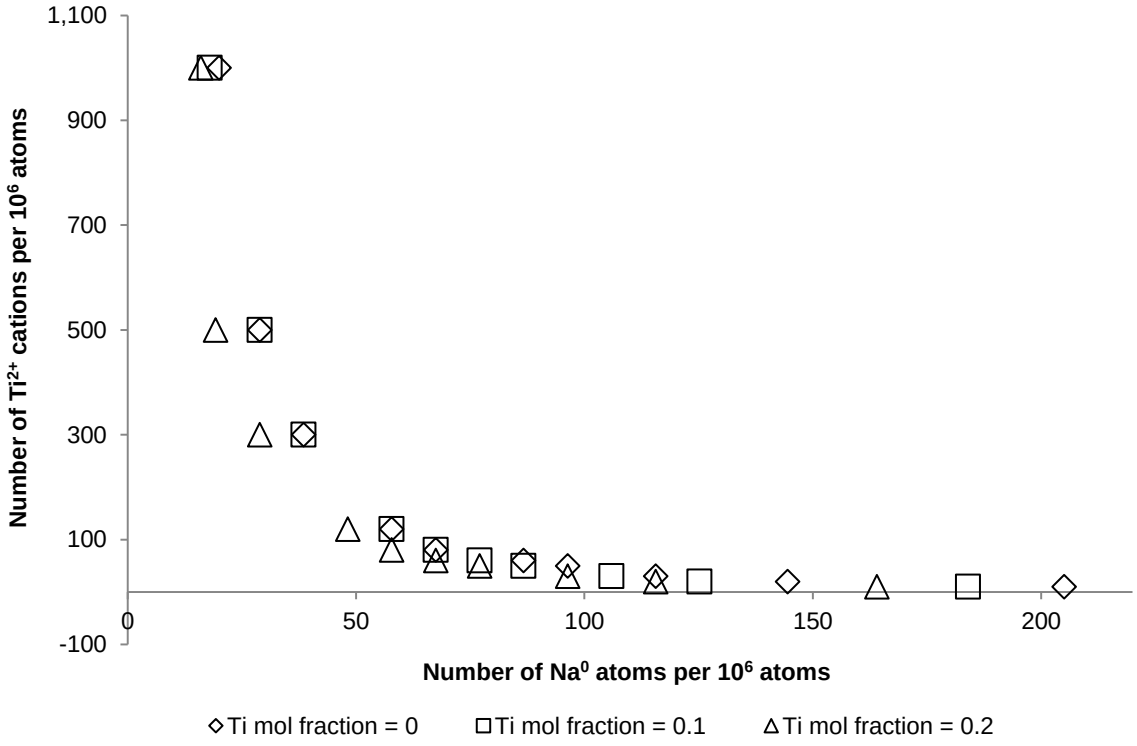

Figure 14: Ti^{2+} and Na^0 equilibrium in molten NaCl at 850 °C for different Ti^0 mol fractions

$\gamma_{TiCl_2} = 0.04$ & $\gamma_{Na} = 5$

3.4 – System of reaction mechanisms

In Chapter 2, Section 2.3.2, it was stated that Okabe & Sadoway (1998) defined two dominant reaction mechanisms, SR-EMR and LR-EMR and that different morphologies are formed when either of these mechanisms is dominant.

Furthermore, each reaction mechanism has a specific site of formation (Okabe & Waseda, 1997: 29). The SR-EMR mechanism results in a precipitate which forms in the bulk of the molten salt reaction medium, while the LR-EMR mechanism results in deposition on reactor internals and subsequent growth on the deposit, leading to what is known as sponge-like product.

The postulated growth mechanism is dependent on the presence of a suspended substrate surface (i.e. particle) with which both dissolved reagents can electrochemically interact to result in Ti^0 particle growth.

There are, therefore, three possible reaction mechanisms. These are:

- SR-EMR (precipitation reaction)
- LR-EMR (deposition on reactor internals)
- Postulated autocatalytic electroless deposition on suspended Ti^0 particles

The most fundamental prerequisite needed for any reaction is that the stoichiometric requirements between reagents are satisfied.

A prerequisite for precipitation (i.e. the SR-EMR mechanism) is that a minimum number of metal cations is needed to form a cluster before nucleation into a solid phase can occur. This minimum number of atoms is referred to as the critical nuclei size. The critical nuclei size depends mainly on the solubility (or supersaturation) of the solid in the specific solution (Paunovic & Schlesinger, 2006: 113). For simplicity, assume that the critical nuclei size for a Ti^0 nucleus is equal to two Ti^0 atoms in molten NaCl.

A metallic substrate surface is a prerequisite for both LR-EMR and the postulated metal particle growth mechanisms. For the LR-EMR mechanism, the metallic substrate surface is any part of the reactor in contact with the molten chloride salt reaction medium. A suspended

Ti^0 particle is, in turn, the required metallic substrate surface needed for the postulated particle growth mechanism.

Each reaction mechanism has a set of prerequisites that must be complied with before a reaction can proceed through that mechanism. The prerequisites described above all relate to different interactions between different components. On this premise, the selectivity for a successful reaction through one mechanism in a system of possible mechanisms can be estimated, to an extent, by evaluating when the prerequisites are met in Monte Carlo simulation.

Figure 15 is a schematic illustration of a reaction system (for Reaction 10) with concentrations similar to those shown in Figure 13 where LR-EMR, SR-EMR and the postulated particle growth mechanisms are all possible. The distances between various components and surfaces within this system are represented by λ_i. The applicable prerequisites (i.e. physical contact when λ_i = 0) for each reaction mechanism are summarised in Table 8.

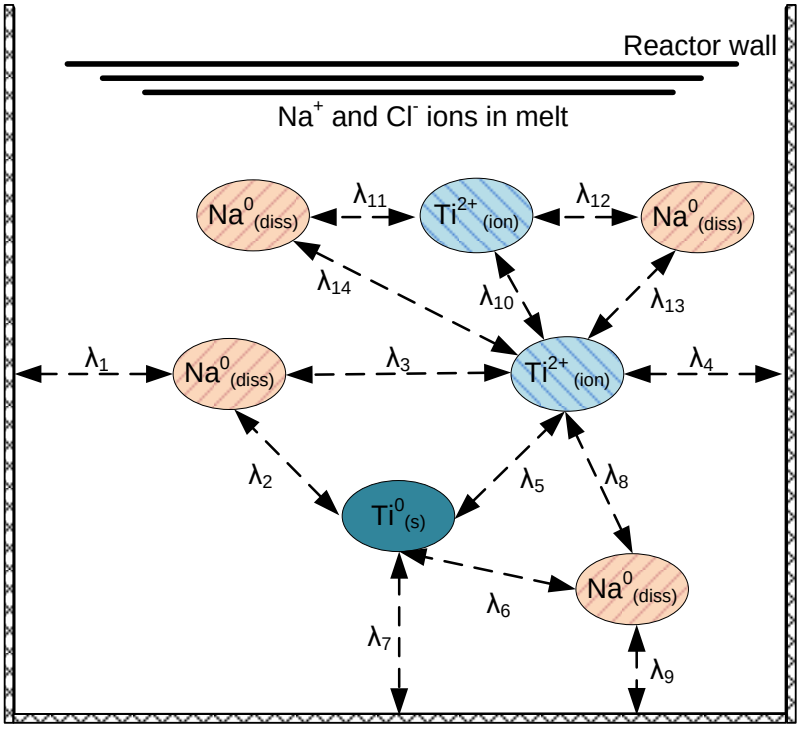

Figure 15: Possible interactions as a function of relative distances between components (Refer to Table 8)

Table 8: Relative distances between components for different reaction mechanisms

Mechanism	λ_1	λ_2	λ_3	λ_4	λ_5	λ_6	λ_7	λ_8	λ_9	λ_{10}	λ_{11}	λ_{12}	λ_{13}	λ_{14}
LR-EMR (deposition)	0			0					0					
LR-EMR (growth)	0				0		0		0					
SR-EMR (precipitation)			0					0		0	0	0	0	0
Autocatalytic electroless deposition (particle growth)		0			0	0								

(Refer to Figure 15)

As an example, Figure 15 and Table 8 show the conditions required for sponge growth via the LR-EMR mechanism. When λ_1 and λ_9 are both "touching" the reactor wall (i.e. $\lambda = 0$) and Ti^0 has already been deposited on the reactor ($\lambda_7 = 0$), all that is needed for sponge growth is that a dissolved Ti^{2+} cation make contact ($\lambda_5 = 0$) with the previously deposited Ti^0.

Each interaction can be further defined regarding the rate-controlling steps. Possible rate-limiting steps include (Paunovic & Schlesinger, 2006: 77):

- Charge transfer
- Diffusion
- Chemical reaction
- Crystallisation

The number of prerequisites listed in Table 8, combined with the low concentrations illustrated in Figure 13, suggests that all reaction mechanisms are possible. A distribution of different product morphologies is therefore likely under these conditions.

The postulated growth mechanism's selectivity relative to competing reaction mechanisms' selectivity is vital for practical use.

3.5 – Collision theory

The basis of collision theory is that reacting molecules are required to collide with each other at adequate speeds before a reaction can proceed. Collision theory is arguably the simplest quantitative way to account for reaction rates in homogeneous gas-phase reactions (Atkins & de Paula, 2002: 944).

To illustrate, assume the following homogeneous reaction:

$$A + \frac{b}{a}B \rightarrow \frac{c}{a}C + \frac{d}{a}D \qquad \text{Reaction 18}$$

The rate of reaction concerning the consumption of reagent A in Reaction 18 is written as (Fogler, 2006: 83):

$$-r_A = k_A C_A^{\propto} C_B^{\beta} \qquad \text{Equation 9}$$

where

k_A = the rate constant at a specific temperature
$C_A^{\propto}$ = the concentration of A with order $\propto$

The rate of a homogeneous gas-phase reaction is intuitively proportional to the concentrations of reagents present. Analogous to Section 3.4, a reaction can only proceed when reagents interact with each other. The likelihood of interactions is directly proportional to the number of components that can interact.

However, not all collisions lead to a reaction, hence the need for the rate constant in Equation 9. The rate constant gives the rate of successful collisions (Atkins & de Paula, 2002: 881).

The Arrhenius equation is used to quantify the rate constant as a function of temperature (Fogler, 2006: 83).

The Arrhenius equation is shown in Equation 10.

$$k_A(T) = Ae^{-E/RT}$$ Equation 10

where

A = frequency factor or pre-exponential factor

E = the activation energy, J/mol

R = gas constant, 8.314 J/mol

T = absolute temperature, K

Equation 10 consists of two terms: the exponential and frequency factors.

The exponential factor can be interpreted as the fraction of collisions that have sufficient kinetic energy to lead to a reaction, while the frequency factor is a measure of the rate at which collisions occur irrespective of energy. The product of these two factors provides an estimate of successful collisions that lead to a reaction (Atkins & de Paula, 2002: 881).

Equation 11 can be used to estimate the frequency factor. The reader is referred to the literature for further information on its application (Fogler, 2006: 128, Atkins & de Paula, 2002: 945).

$$A = \pi\sigma_{AB}^2 \left[\frac{8\pi k_B T}{\mu\pi}\right]^{1/2} N_{Avo}$$ Equation 11

The system of reaction mechanisms described in Section 3.4 is relatively complex. The postulated growth mechanism's selectivity relative to the selectivity of competing reaction mechanisms is of considerable significance to this thesis.

As a first attempt, selectivity towards each reaction mechanism can be estimated using the frequency factor concept for homogeneous gas-phase reactions, combined with the minimum prerequisites listed in Table 8.

3.6 – Concluding remarks

Meta-stable equilibrium between Ti^{2+} cations and Na^0 atoms dissolved in molten NaCl (Reaction 10) is a fundamental prerequisite needed for the postulated growth mechanism illustrated in Figure 9, Section 2.3.3.

Meta-stable equilibrium concentrations were calculated with three sets of estimated activity coefficients. Only one of these sets indicated the existence of a concentration range where the postulated growth mechanism is possible; the other two sets indicated the postulated mechanism to be unlikely or impractical. According to the results illustrated in Figure 13, approximately 80 Na^0 atoms are in stoichiometric equilibrium with 40 Ti^{2+} cation pairs in a reaction medium consisting of 1 000 000 atoms in total.

It is conceivable that more than one product morphology will be obtained at such low concentrations. Therefore, the metallothermic reduction reaction should be regarded as a system of reaction mechanisms at these low reagent concentrations.

Therefore, the selectivity of the postulated growth mechanism relative to the selectivity of competing reaction mechanisms is of paramount importance in determining its practical application.

Section 3.4 indicated that a reaction mechanism could only proceed once all the defined prerequisites have been satisfied. For simplicity, the following prerequisites were listed to determine whether a specific reaction mechanism is successful:

- The relative distances between reagents and substrate surfaces (reactor internals and suspended Ti^0 particles)
- The stoichiometric requirements for the reaction
- The number of Ti^{2+} cations required to form a stable Ti^0 nuclei

Section 3.4 subsequently defined this system of reaction mechanisms as a function of distances between the different components in the closed system.

Section 3.5 shows how the rate of homogeneous gas-phase reactions is related to the frequency of successful collisions between reagents. A successful collision occurs when the reagents collide with sufficient energy and at an appropriate angle.

The collision theory is, however, applicable only to homogeneous gas-phase reactions. Interactions between reactants in solutions are very different. Reactant molecules need to move through a solution that adds resistance to movement, with the result that the frequency of interactions is significantly lower (Atkins & de Paula, 2002: 951).

Interactions between reagents are even further complicated for heterogeneous mechanisms such as the LR-EMR and the postulated autocatalytic electroless deposition reactions.

The metallothermic reduction-reaction mechanisms described in Section 3.4 are therefore relatively complex.

The metallothermic reduction reaction is known to be kinetically very fast. Fast kinetics combined with a considerable equilibrium constant suggest that a reaction is very likely to proceed as soon as the minimum prerequisites of stoichiometry, critical nuclei size and the presence of a substrate surface are met.

Therefore, as a first attempt to quantify this system of reaction mechanisms, each reaction mechanism will be evaluated with regard to the frequency of collisions (i.e. frequency factor) where the minimum prerequisites are met.

This analysis will provide insight into the selectivity of competing reaction mechanisms.

CHAPTER 4 – MODELLING & SIMULATION

4.1 – Chapter overview

Section 3.6 proposed using the minimum prerequisites listed in Table 8 and the concept of the frequency of successful collisions in Section 3.5 to estimate each reaction mechanism's selectivity in a system of possible reaction mechanisms.

Results can be generated by repeatedly randomising component positions (Ti^0, Ti^{2+}, Na^0, Na^+ and Cl^-) in the molten NaCl reaction medium and then determining the number of valid interactions where all prerequisites are met. (Refer to Figure 15 and Table 8 in Section 3.4.)

This chapter reports on the modelling and simulation work conducted to estimate each reaction mechanism's selectivity as described above.

Chapter 4 contains the following sections:

1. Section 4.2 provides the scope of work for the modelling and simulation objectives.
2. Section 4.3 is a brief overview of the algorithm used for modelling and simulation.
3. Section 4.4 lists the assumptions and limitations applicable to the algorithm.
4. Section 4.5 provides the results obtained from modelling in a Monte Carlo study.
5. Section 4.6 presents concluding remarks.

4.2 – Modelling and simulation: scope of work

The scope of work required for modelling and simulation included:

1. Develop a rule-based algorithm:
    - For the metallothermic reduction-reaction based on half-cell Reactions 16 and 17:

$$Ti^{2+} + 2e^- \rightarrow Ti^0 \quad \text{Reaction 16}$$

$$2Na^0 \rightarrow 2Na^+ + 2e^- \quad \text{Reaction 17}$$

- Simulate an ideally mixed, randomised three-dimensional metallothermic reduction-reaction system consisting of variable reagent and suspended Ti^0 particle concentrations.
- Analyse for different interactions in the three-dimensional system described above. The interactions of interest include:
  i. Interactions that meet the required reaction stoichiometry
  ii. Reagent-reactor surface interactions
  iii. Reagent-suspended Ti^0 particle surface interactions
  iv. Interactions that require a defined number of Ti^{2+} cations or Na^0 atoms before a phase-change reaction can occur.

2. Conduct a Monte Carlo simulation using the algorithm to determine the number of valid interactions where all prerequisites are met for each reaction mechanism at different reagent and Ti^0 particle concentrations.
3. Use the results obtained to:
   - Evaluate whether the postulated growth mechanism (i.e. autocatalytic electroless deposition) is indeed possible
   - Estimate the selectivity between the three different reaction mechanisms.

4.3 – Algorithm overview

Assume that a metallothermic reduction-reaction system with a fixed number of components (Ti^0, Ti^{2+}, Na^0, Na^+ and Cl^-) is contained within a defined three-dimensional sample-space at a specific moment in time (i.e. $\Delta t = 0$).

Furthermore, assume that a three-dimensional Cartesian coordinate system can be used to relate the positions of all components within this three-dimensional sample-space. Each component's position within the three-dimensional sample-space is therefore fixed by three independent variables, the (x,y,z) coordinates. The three-dimensional sample-space is assumed to be cubic, i.e. $x_{max} = y_{max} = z_{max}$.

Figure 16 is a schematic illustration of a single atom or ion (black dot) surrounded by 26 other components in a three-dimensional Cartesian coordinate system with a sample-space size equal to 27 (3 x 3 x 3) positions.

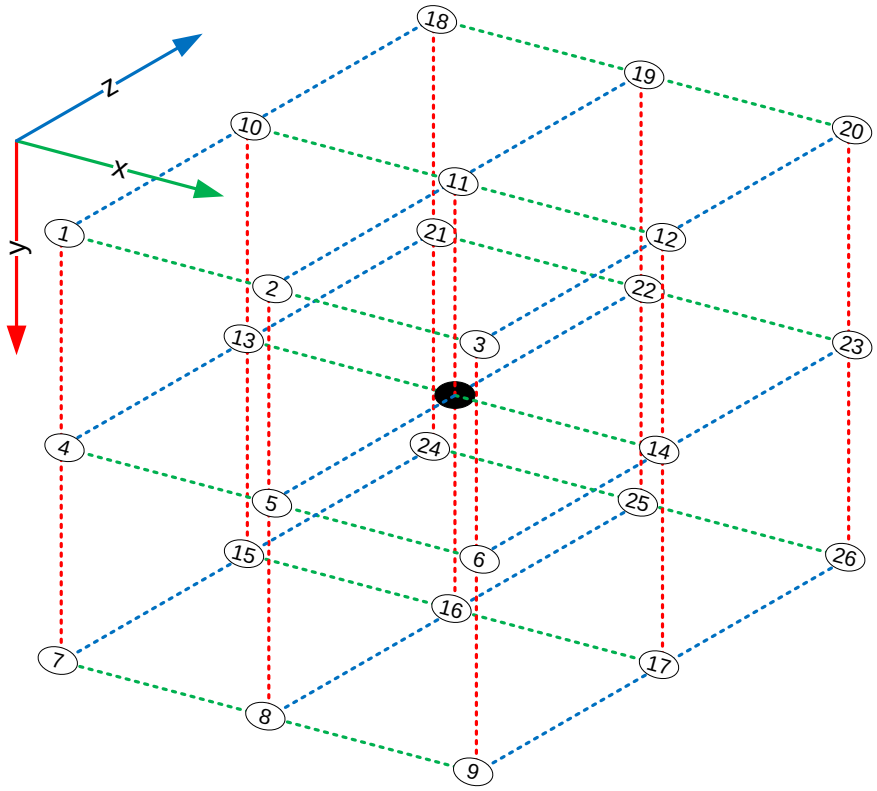

Figure 16: Three-dimensional sample-space around a single component

The positions of all components in Figure 16 can be related to the core component's position, as indicated in Table 9.

Essentially, the (x,y,z) coordinates in a cubic three-dimensional Cartesian coordinate system can be used as an “accounting system” where all the components are connected but also unique. For example, this approach allows for randomising component positions (Ti^0, Ti^{2+}, Na^0, Na^+ and Cl^-) or “build” Ti^0 particles using a defined number of Ti^0 atoms into a sample-space that represents the reaction environment.

Table 9: Three-dimensional Cartesian coordinates for the 26 positions relative to one component

Position ID#	Coordinates relative to one component (black dot in Figure 19)		
	X	**y**	**z**
Core component	**0**	**0**	**0**
1	-1	-1	-1
2	0	-1	-1
3	+1	-1	-1
4	-1	0	-1
5	0	0	-1
6	+1	0	-1
7	-1	+1	-1
8	0	+1	-1
9	+1	+1	-1
10	-1	-1	0
11	0	-1	0
12	+1	-1	0
13	-1	0	0
14	+1	0	0
15	-1	+1	0
16	0	+1	0
17	+1	+1	0
18	-1	-1	+1
19	0	-1	+1
20	+1	-1	+1
21	-1	0	+1
22	0	0	+1
23	+1	0	+1
24	-1	+1	+1
25	0	+1	+1
26	+1	+1	+1

Figure 17 is a block flow diagram illustrating the algorithm's sequence and main steps. As a whole, the algorithm consists of seven main phases.

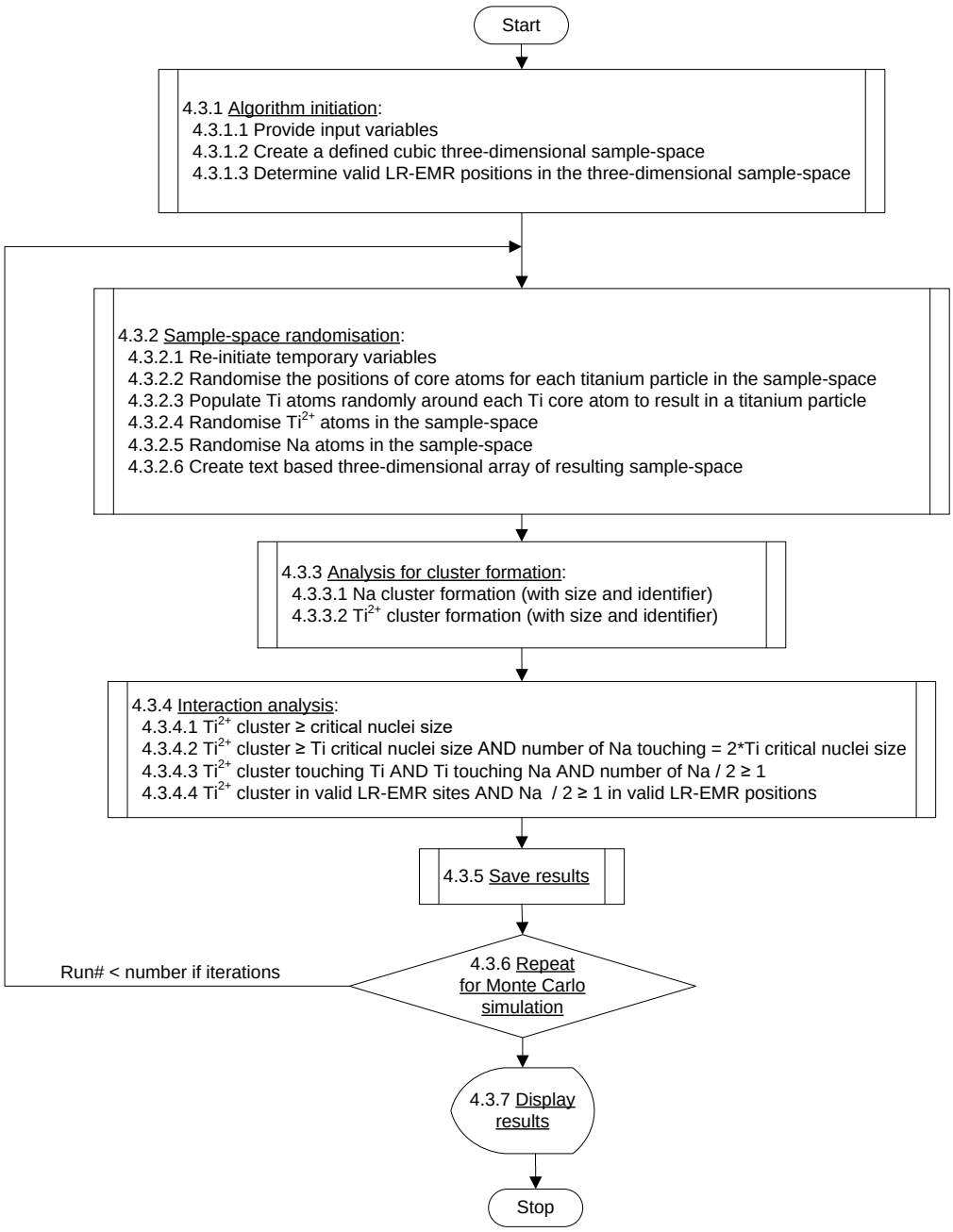

Figure 17: Block flow diagram illustrating the different steps in the algorithm

The numbering used for each step in Figure 17 refers to the sections below in which that particular step is discussed.

4.3.1 – Algorithm initiation

The algorithm starts with an initiation sequence where input variables are declared, and once-off tasks are completed that do not need to be repeated during iteration.

Pseudo-code is used to illustrate the logic applied. Words written in ***italic bold*** represent variables and arrays, while pseudo-code is represented by words in UPPERCASE.

Pseudo-code is used to discuss only steps 4.3.1 and 4.3.2 of the algorithm. Only a brief overview of the other steps is provided.

LabVIEW 2014™ was used for software development. LabVIEW, a dataflow programming language, was preferred as the algorithm design is based on three-dimensional data structures, i.e. arrays.

4.3.1.1 – Provide input variables

The following input variables must be declared:

- *The* ***number of positions in the sample-space:*** The value assigned to this variable represents the total sample-space size. This algorithm is specific to cubic sample-spaces. Only values that return an integer for the cube root of the value can be assigned to this variable. In pseudo-code, this variable is subsequently used to calculate the ***positions per dimension axis*** variable:

  ASSIGN
  Positions per dimension axis = (***number of positions in the sample-space***)$^{1/3}$

  The smallest number of positions available in the sample-space for this algorithm is 27.
- The ***number of iterations:*** The value assigned to this variable represents the number of iterations needed for the Monte Carlo study. The algorithm is repeated for each iteration.
- The ***number of Ti^0 particles in sample-space:*** The value assigned to this variable represents the total number of Ti^0 particles present in the sample-space. Each particle, in turn, consists of several Ti^0 atoms.

- The ***number of Ti^0 atoms per particle:*** Each Ti^0 particle consists of a number of Ti^0 atoms. The maximum number of atoms per Ti^0 particle in this algorithm is limited to 27.
- The ***number of Ti^{2+} cations in sample-space:*** The value assigned to this variable represents the number of Ti^{2+} cations present in the sample-space.
- The ***number of Na^0 atoms in sample-space:*** The value assigned to this variable represents the number of Na^0 atoms present in the sample-space.
- ***Ti^0 critical nuclei size:*** Minimum number of Ti^{2+} cations required in a cluster for a chemical reaction to produce a Ti^0 nucleus.

4.3.1.2 – Create a defined cubic three-dimensional sample-space

This sequence starts by assigning a unique integer value (***position ID***) to each element in a three-dimensional array (***defined 3D sample-space* [ ][ ][ ]**). The ***position ID*** variable represents a specific position in the ***defined 3D sample-space* [ ][ ][ ]** that a component can occupy. The size of each dimension in the array is equal to the ***positions per dimension axis*** variable.

The ***position ID*** variable serves three essential purposes. These are:

- To keep a record of all the positions available in the three-dimensional sample-space.
- To find the (x,y,z) coordinates from the ***defined 3D sample-space* [ ][ ][ ]**.
- To randomise various reagents and Ti^0 atoms into the ***randomised 3D sample-space* [ ][ ][ ]**.

ASSIGN ***position ID*** = ***1***
FOR z = 0 to ***positions per dimension axis***
  FOR y = 0 to ***positions per dimension axis***
    FOR x = 0 to ***positions per dimension axis***
      ASSIGN ***Defined 3D sample-space* [z][y][x] = *position ID***
      INCREMENT ***position ID***
      INCREMENT x
    END
    INCREMENT y

END
INCREMENT z
END

Figure 18 is an illustration of how this pseudo-code is executed in LabVIEW.

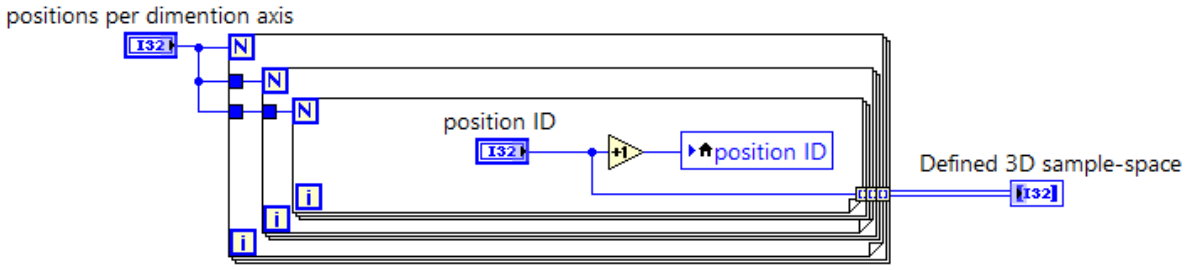

Figure 18: LabVIEW dataflow sequence that creates a three-dimensional array with position ID values assigned to each element

All ***position ID*** values are added to a one-dimensional array (***1D for unused positions*** **[ ]**) for use in sample-space randomisation (Section 4.3.2), analysis for cluster formation (Section 4.3.3) and interaction analysis (Section 4.3.4).

ASSIGN ***position ID = 1***
FOR index = 0 to ***Number of positions in the sample-space***
ASSIGN ***1D for unused positions*** **[**index**]** =***position ID***
INCREMENT ***position ID***
INCREMENT index
END

4.3.1.3 – Determine valid LR-EMR positions in the three-dimensional sample-space

This algorithm evaluates three different scenarios. These are:

- Case 1: One flat surface is available for the LR-EMR mechanism. The (x,y,0) plane represents the surface evaluated in this algorithm. Case 1 is illustrated in Figure 19.

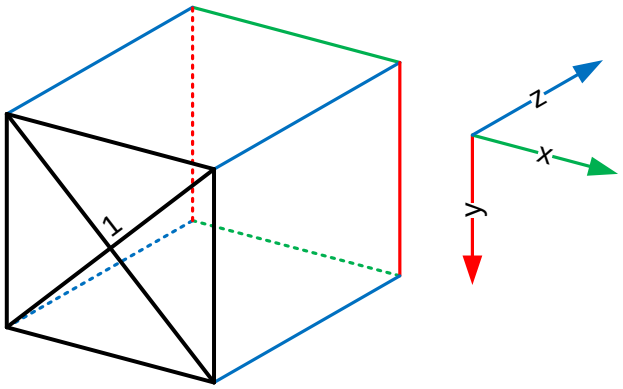

Figure 19: Case 1: one flat surface available for the LR-EMR mechanism

- Case 2: Two perpendicular flat surfaces are available for the LR-EMR mechanism. The (x, y, 0) and (x, 0, z) planes are the surfaces evaluated in the algorithm. Case 2 is illustrated in Figure 20.

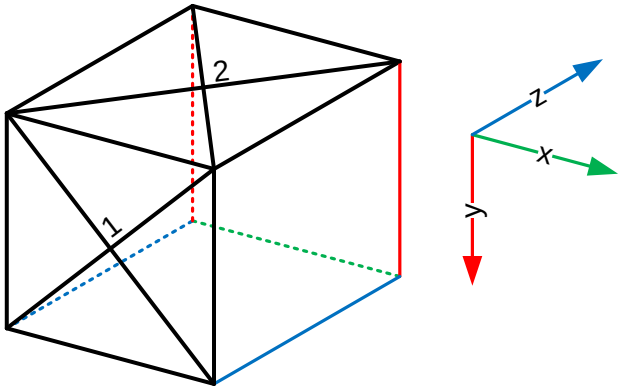

Figure 20: Case 2: two perpendicular flat surfaces available for the LR-EMR mechanism

- Case 3: Three flat surfaces are available for the LR-EMR mechanism. The (x, y, 0), (x, 0, z) and (0, y, z) planes are the surfaces evaluated in the algorithm. Case 3 is illustrated in Figure 21.

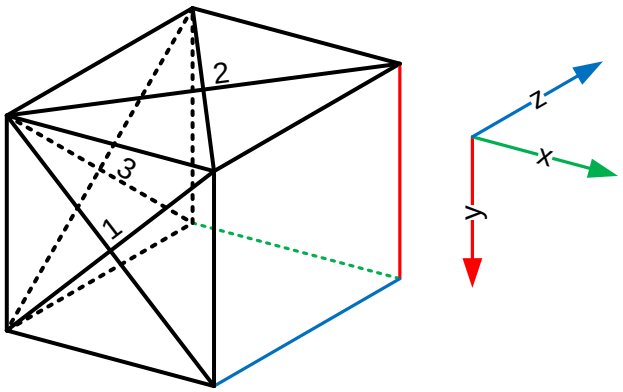

Figure 21: Case 3: three flat surfaces available for the LR-EMR mechanism

The ***position ID*** values of positions on the planes described above are stored in a one-dimensional array called ***1D for valid LR-EMR positions*** **[ ]**. This array is used in the interaction analysis (Section 4.3.4) sequence. The pseudo-code for Case 3 is as follows:

```
ASSIGN index = 0
FOR y = 0 to positions per dimension axis
    FOR x = 0 to positions per dimension axis
        1D for valid LR-EMR positions [index] = Defined 3D sample-space [0][y][x]
        INCREMENT index
        INCREMENT x
    END
INCREMENT y
END

FOR z = 0 to positions per dimension axis
    IF z = 0, then
        INCREMENT z
    ELSE
        FOR x = 0 to positions per dimension axis
            1D for valid LR-EMR positions [index] = Defined 3D sample-space [z][0][x]
            INCREMENT index
            INCREMENT x
        END
```

END
INCREMENT z
END

FOR z = 0 to ***positions per dimension axis***
IF z = 0, then
INCREMENT z
ELSE
FOR y = 0 to ***positions per dimension axis***
IF y = 0, then
INCREMENT y
ELSE
1D for valid LR-EMR positions **[**index**]** = ***Defined 3D sample-space*** **[**z**][**y**][**0**]**
INCREMENT index
INCREMENT y
END
END
END
INCREMENT z
END

Figure 22 illustrates how the last FOR loop ((0, y, z) plane) is implemented in LabVIEW.

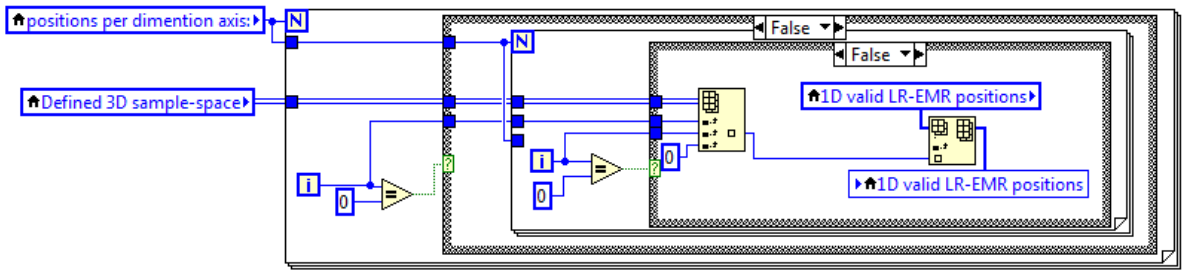

Figure 22: LabVIEW dataflow sequence that extracts position IDs on the (0, y, z) plane

4.3.2 – Sample-space randomisation

This phase in the algorithm can be regarded as the "engine" used to simulate an ideally mixed, randomised three-dimensional metallothermic reduction-reaction system consisting of variable reagent and suspended Ti^0 particle concentrations.

4.3.2.1 – Re-initiate temporary variables

The following temporary variables are used in each iteration:

- ***Working 1D for unused positions* [ ]*:*** This is a one-dimensional array containing all unoccupied (or unused) positions still available in the three-dimensional sample-space. This variable is re-initiated as follows:

  ASSIGN
  ***Working 1D for unused positions* [ ]**= ***1D for unused positions* [ ]**

- ***2D for Ti^0 particles* [ ][ ]*:*** This is a two-dimensional array with three columns. Each row represents one titanium atom. The columns are used to record the following:
  - The first column (x = 0) shows the ***position ID*** for this Ti^0 atom in the three-dimensional sample-space.
  - The second column (x = 1) is a unique number that represents the ***Ti^0 particle ID*** that this Ti^0 atom belongs to. The maximum particle ID number is equal to the ***Number of Ti^0 particles in the sample-space***.
  - The third column (x = 2) represents the atom number of this specific Ti^0 atom in a Ti^0 particle with this specific ***Ti^0 particle ID***. Other Ti^0 atoms with the same ***Ti^0 particle ID*** will have a different atom number. The maximum atom number is equal to the ***Number of Ti^0 atoms per particle***.
- ***1D for reserved positions* [ ]*:*** This temporary one-dimensional array keeps a record of all positions used in the three-dimensional sample-space.
- ***2D xyz split 1* [ ][ ]*:*** This is a temporary two-dimensional array with three columns. Each row represents one Ti^0 atom. The columns are used to record the following:
  - First column (x = 0) shows the x-coordinate for this Ti^0 atom in the three-dimensional sample-space.
  - The second column (x = 1) shows the y-coordinate for this Ti^0 atom in the three-dimensional sample-space.

- The third column (x = 2) shows the z-coordinate for this Ti^0 atom in the three-dimensional sample-space.

- ***2D with xyz coordinates for each Ti^0 reserved position* [ ][ ]*:*** This is a two-dimensional array with three columns. Each row represents one Ti^0 atom. The columns are used to record the following:
  - First column (x = 0) shows the x-coordinate for this Ti^0 atom in the three-dimensional sample-space.
  - The second column (x = 1) shows the y-coordinate for this Ti^0 atom in the three-dimensional sample-space.
  - The third column (x = 2) shows the z-coordinate for this Ti^0 atom in the three-dimensional sample-space.

4.3.2.2 – Randomise the positions of core atoms for each Ti^0 particle in the sample-space

This sequence consists of two main steps. First, random ***position ID***s are obtained for each Ti^0 core atom and, secondly the corresponding (x,y,z) coordinates are extracted for each of these positions from the ***Defined 3D sample-space* [ ][ ][ ]**.

The pseudo-code for the randomisation is as follows:

ASSIGN size = 0
ASSIGN random-index = 0
FOR ***Ti^0 particle ID*** = 0 ***Number of Ti^0 particles in sample-space***
  COMPUTE size = ARRAY SIZE (***working 1D for unused positions* [ ]**) - 1
  COMPUTE random-index = size * random value generator
  COMPUTE random-index = ROUND DOWN (random-index)
  APPEND
  working 1D for unused positions* [**random-index**]** TO ***1D for Ti^0
  ***reserved positions* [ ]**
  DELETE ***working 1D for unused positions* [**random-index**]**
  ASSIGN size = 0
  ASSIGN random-index = 0
INCREMENT ***Ti^0 particle ID***
END

Figure 23 is an illustration of how this pseudo-code is executed in LabVIEW.

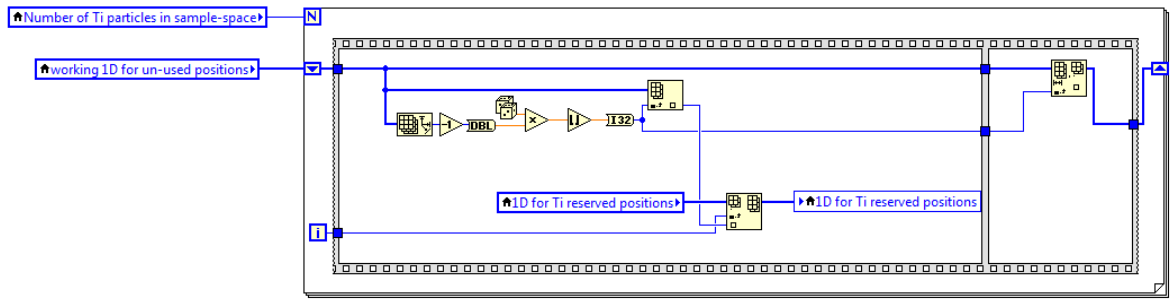

Figure 23: LabVIEW dataflow sequence using position IDs to randomise the position of the first atom in each Ti^0 particle

Extracting the (x,y,z) coordinates for each Ti^0 core atom is time-intensive at high Ti^0 particle concentrations. Performance can be improved by splitting the workload into four different sequences that run in parallel.

The pseudo-code for splitting is as follows:

COMPUTE split index = ARRAY SIZE (***1D for Ti^0 reserved positions*** **[ ]**) ⁄ 2
SPLIT ***1D for Ti^0 reserved positions*** **[**split index**]**
    OUTPUT 1D top half [ ] AND 1D bottom half [ ]
COMPUTE split index 2 = ARRAY SIZE (1D top half [ ]) ⁄ 2
SPLIT 1D top half [split index 2]
    OUTPUT ***1D for multi-thread split 1*** **[ ]** AND ***1D for multi-thread split 2*** **[ ]**
COMPUTE split index 3 = ARRAY SIZE (1D bottom half [ ]) ⁄ 2
SPLIT 1D bottom half [split index 3]
    OUTPUT ***1D for multi-thread split 3*** **[ ]** AND ***1D for multi-thread split 4*** **[ ]**

Figure 24 is an illustration of the LabVIEW dataflow sequence diagram.

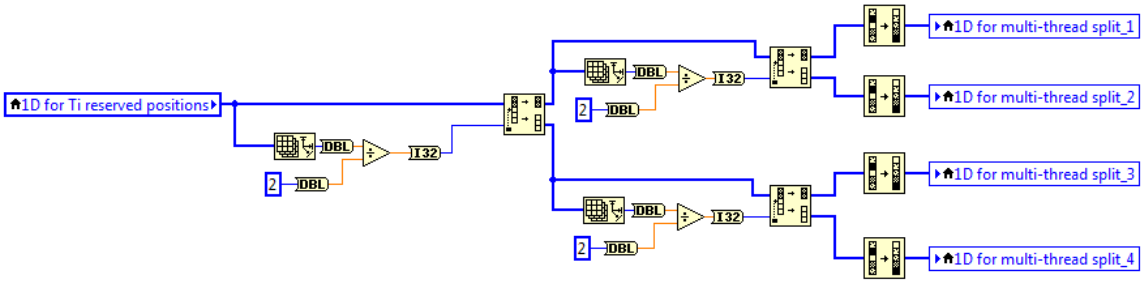

Figure 24: LabVIEW dataflow sequence to split an array for multi-thread processing

Each of these one-dimensional arrays (***1D for multi-thread spread* 1-4 [ ]**) can then be used to find the unique (x,y,z) coordinates for each of the positions identified as the core of a titanium particle.

The pseudo-code for the ***1D for multi-thread split 1* [ ]** is as follows:

FOR position = 0 to ARRAY SIZE (***1D for multi-thread split 1* [ ]**)
    For z = 0 to ***positions per dimension axis***
        For y = 0 to ***positions per dimension axis***
            FOR x = to ***positions per dimension axis***
                IF***1D for multi-thread split 1*** **[**position**] = *Defined 3D sample-space*** **[**z**][**y**][**x**]**
                THEN APPEND ***2D xyz split 1*** **[**x,y,z**][**x**]**
                ELSE END
            INCREMENT x
            END
        INCREMENT y
        END
    INCREMENT z
    END
INCREMENT position
END

Figure 25 is an illustration of the LabVIEW dataflow sequence.

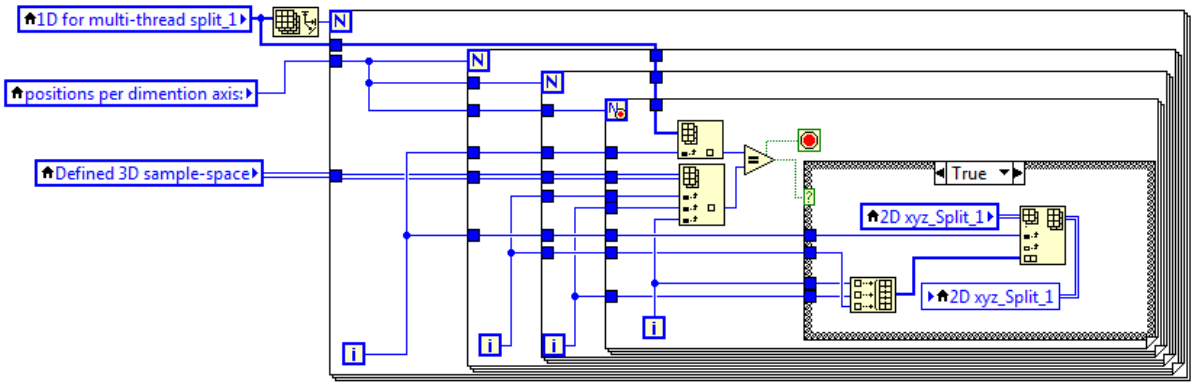

Figure 25: LabVIEW dataflow sequence to extract (x,y,z) coordinates for the position ID of the core atom in each Ti^0 particle

The different threads are then recombined into one two-dimensional array that contains the (x,y,z) coordinates for all core Ti^0 particle atoms. The LabVIEW dataflow sequence diagram for reassembly is shown in Figure 26.

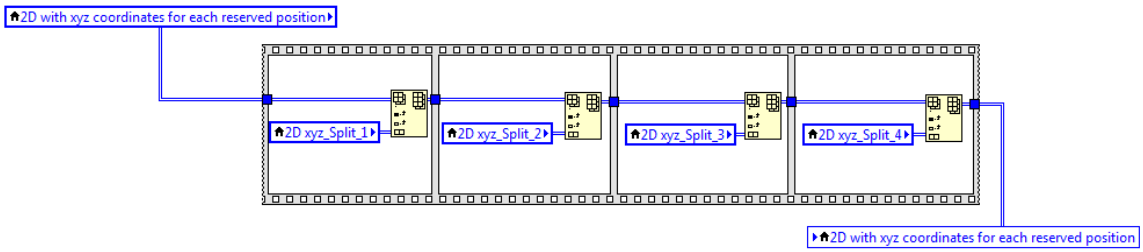

Figure 26: LabVIEW dataflow sequence to recombine different arrays containing the (x,y,z) coordinates of reserved positions

4.3.2.3 – Populate Ti^0 atoms randomly around the core Ti^0 atom to result in a Ti^0 particle

The pseudo-code applicable to this section is as follows:

FOR ***Ti^0 particle ID*** = 0 to ***Number of Ti^0 particles in sample-space***

ASSIGN ***1D for multi-thread split 1*** **[ ]** = 0

ASSIGN ***1D for multi-thread split 2*** **[ ]** = 0

ASSIGN ***1D for multi-thread split 3*** **[ ]** = 0

ASSIGN ***1D for multi-thread split 4*** **[ ]** = 0

ASSIGN x = ***2D with (x,y,z) coordinates for each Ti^0 reserved position*** **[*Ti^0 particle ID*] [**0**]**

ASSIGN y = ***2D with (x,y,z) coordinates for each Ti^0 reserved position*** **[*Ti^0 particle ID*] [**1**]**

ASSIGN z = ***2D with (x,y,z) coordinates for each Ti^0 reserved position*** **[*Ti^0 particle ID*] [**2**]**

ASSIGN ***position ID***= ***Defined 3D sample-space*** **[**z**][**y**][**x**]**

APPEND ***2D for Ti^0 particles*** **[*position ID*] [*Ti^0 particle ID* +1,1]**

*## obtain **position ID**s for positions around the **position ID** for the core Ti^0 atom ##*
The [-1, 1, -1] position relative to the core atom is illustrated in Figure 27
To prevent repetition, the pseudo-code:
*## **1D for Ti^0 positions around Ti^0 core atom** **[*Defined 3D sample-space*** **[**z**][**y**][**x**]]** ##*
*## is replaced with **X_temporary*** **[**z**][**y**][**x**]** with x, y, z variables ##

```
FOR i = 0 to 25
    IF i = 0 THEN
        APPEND
        X_temporary [z-1][y+1][x-1]
    ELSE IF i = 1 THEN
        APPEND
        X_temporary [z][y+1][x-1]
    ELSE IF i = 2 THEN
        APPEND
        X_temporary [z+1][y+1][x-1]
    ELSE IF i = 3 THEN
        APPEND
        X_temporary [z-1][y][x-1]
    ELSE IF i = 4 THEN
        APPEND
        X_temporary [z][y][x-1]
    ELSE IF i = 5 THEN
        APPEND
        X_temporary [z+1][y][x-1]
    ELSE IF i = 6 THEN
```

```
    APPEND
    X_temporary [z-1][y-1][x-1]
ELSE IF i = 7 THEN
    APPEND
    X_temporary [z-1][y][x-1]
ELSE IF i = 8 THEN
    APPEND
    X_temporary [z+1][y-1][x-1]
ELSE IF i = 9 THEN
    APPEND
    X_temporary [z-1][y+1][x]
ELSE IF i = 10 THEN
    APPEND
    X_temporary [z][y+1][x]
ELSE IF i = 11 THEN
    APPEND
    X_temporary [z+1][y+1][x]
ELSE IF i = 12 THEN
    APPEND
    X_temporary [z-1][y][x]]
ELSE IF i = 13 THEN
    APPEND
    X_temporary [z+1][y][x]]
ELSE IF i = 14 THEN
    APPEND
    X_temporary [z-1][y-1][x]]
ELSE IF i = 15 THEN
    APPEND
    X_temporary [z][y-1][x]]
ELSE IF i = 16 THEN
    APPEND
    X_temporary [z+1][y-1][x]]
ELSE IF i = 17 THEN
    APPEND
    X_temporary [z-1][y+1][x+1]]
```

ELSE IF i = 18 THEN
APPEND
X_temporary **[**z**][**y+1**][**x+1**]]**
ELSE IF i = 19 THEN
APPEND
X_temporary **[**z+1**][**y+1**][**x+1**]]**
ELSE IF i = 20 THEN
APPEND
X_temporary **[**z-1**][**y**][**x+1**]]**
ELSE IF i = 21 THEN
APPEND
X_temporary **[**z**][**y**][**x+1**]]**
ELSE IF i = 22 THEN
APPEND
X_temporary **[**z+1**][**y**][**x+1**]]**
ELSE IF i = 23 THEN
APPEND
X_temporary **[**z-1**][**y-1**][**x+1**]]**
ELSE IF i = 24 THEN
APPEND
X_temporary **[**z**][**y-1**][**x+1**]]**
ELSE IF i = 25 THEN
APPEND
X_temporary **[**z+1**][**y-1**][**x+1**]]**
END
INCREMENT i
END

split for multi-thread processing; refer to Figure 24 for the LabVIEW dataflow sequence

COMPUTE split index = ARRAY SIZE (***1D for Ti^0 positions around Ti^0 core atom*** **[ ]**)⁄2
SPLIT ***1D for Ti^0 positions around Ti^0 core atom*** **[**split index**]**
OUTPUT 1D top half [ ] AND 1D bottom half [ ]
COMPUTE split index 2 = ARRAY SIZE (1D top half [ ]) ⁄ 2
SPLIT 1D top half [split index 2]

OUTPUT ***1D for multi-thread split 1*** **[ ]** AND ***1D for multi-thread split 2*** **[ ]**

COMPUTE split index 3 = ARRAY SIZE (1D bottom half [ ]) ⁄ 2

SPLIT 1D bottom half [split index 3]

OUTPUT ***1D for multi-thread split 3*** **[ ]** AND ***1D for multi-thread split 4*** **[ ]**

*## Remove **position ID**s already in use, only **1D for multi-thread split 1** [ ] is shown ##*
in Figure 28
Recombine the different threads, like Figure 25
Find a randomised position ID for titanium atoms around the Ti^0 core particle,
illustrated in Figure 29

INCREMENT ***Ti^0 particle ID***

END

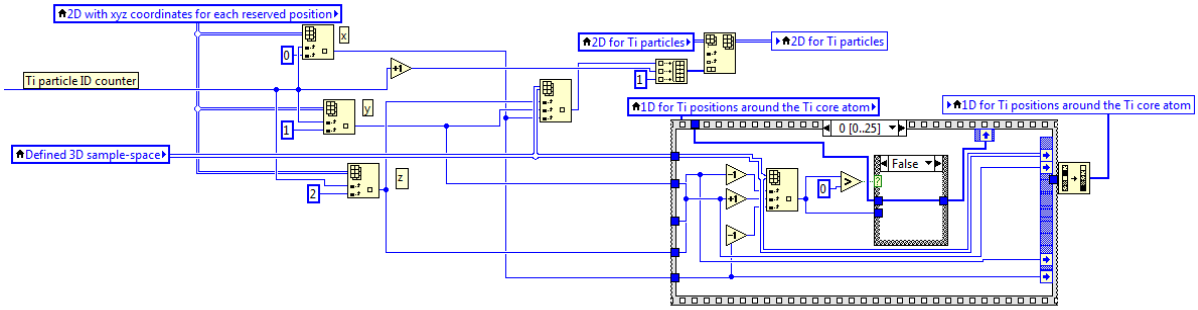

Figure 27: LabVIEW dataflow sequence to extract position IDs for positions available around each Ti^0 core atom

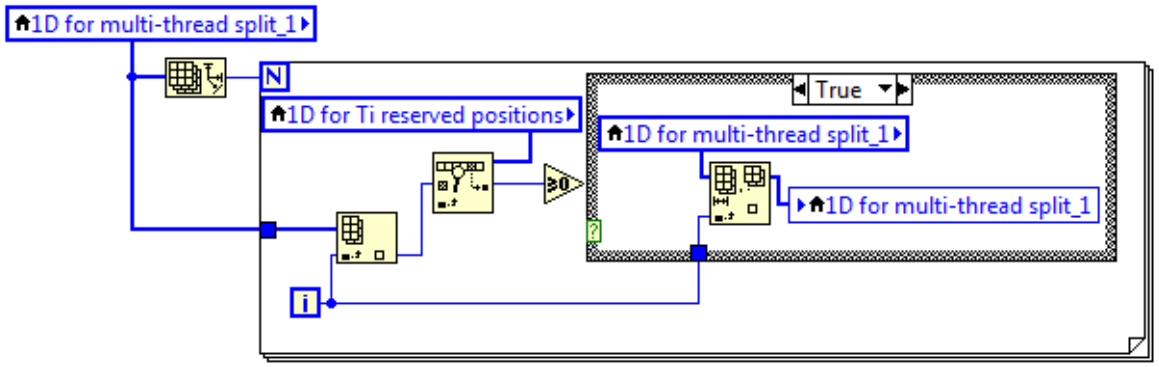

Figure 28: LabVIEW dataflow sequence to remove position IDs already in use from possible positions for randomisation

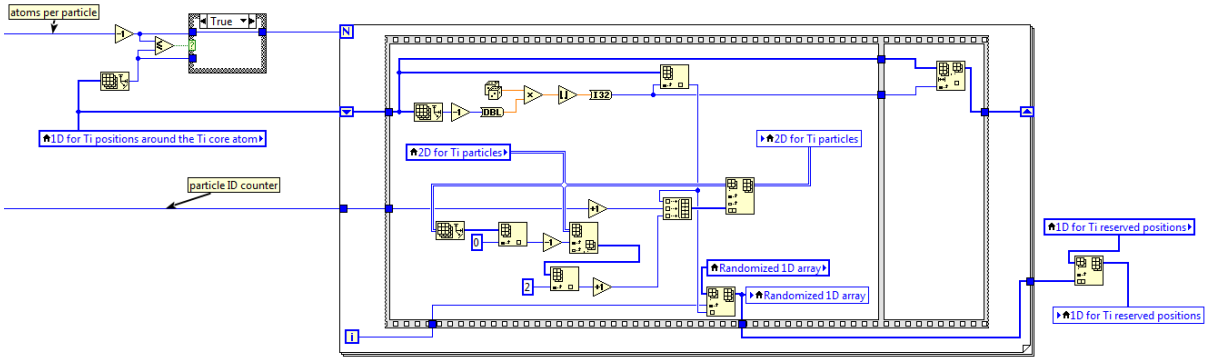

Figure 29: LabVIEW dataflow sequence to randomise Ti^0 atoms around the core atom of a Ti^0 particle

4.3.2.4 – Randomise Ti^{2+} cations in the sample-space

This sequence is similar to that used in Section 4.3.2.2. The pseudo-code for the randomisation is as follows:

ASSIGN size = 0
ASSIGN random-index = 0
  FOR ***Ti^{2+} cation ID*** = 0 to ***Number of Ti^{2+} cations in sample-space***
    COMPUTE size = ARRAY SIZE (***working 1D for unused positions*** **[ ]**) - 1
    COMPUTE random-index = size * random value generator
    COMPUTE random-index = ROUND DOWN (random-index)
    APPEND ***working 1D for unused positions*** **[**random-index**]** TO ***1D for Ti^{2+} reserved positions*** **[ ]**
    DELETE ***working 1D for unused positions*** **[**random-index**]**
    ASSIGN size = 0
    ASSIGN random-index = 0
  INCREMENT ***Ti^{2+} cation ID***
  END

This section's sequence ends by appending ***1D for Ti^{2+} reserved positions*** **[ ]** to another array ***1D for reserved positions*** **[ ]**.

4.3.2.5 – Randomise Na^0 atoms in the sample-space

The sequence applicable to this section is similar to that of Section 4.3.2.5.

4.3.2.6 –Create a text-based three-dimensional array of the resulting sample-space

The text-based three-dimensional sample-space contains the results of sample-space randomisation. This optional sequence is used for validation and debugging.

The LabVIEW dataflow sequence diagram for this section is shown in Figure 30.

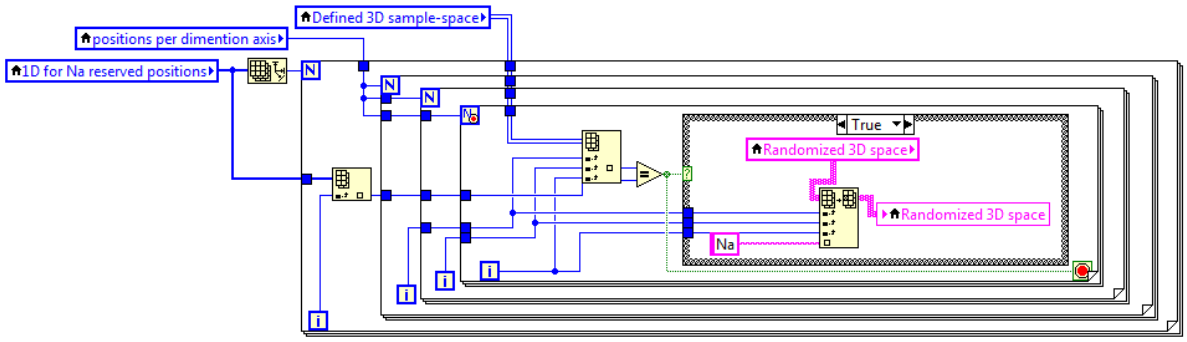

Figure 30: LabVIEW dataflow sequence to create a text output of the randomised sample-space

4.3.3 – Analysis for cluster formation

The cluster formation sequence analyses the three-dimensional sample-space to find (i.e. determine (x,y,z) coordinates) and label (assign a unique identifier) all similar components interacting with each other (i.e. $\lambda = 0$ between them). This sequence is similar to the labelling of atoms in a Ti^0 particle.

This sequence is vital for Ti^{2+} cation and Na^0 atom cluster formation.

4.3.4 – Interaction analysis

This sequence analyses different reagents and reagents-substrate surface interactions in the three-dimensional sample-space. The interactions of interest include:

i. Reagents interactions that meet the required stoichiometry
ii. Reagents-reactor surface interactions
iii. Reagents-suspended Ti^0 particle surface interactions
iv. Component cluster formation, e.g. Ti^{2+} cations that interact.

The three reaction mechanisms considered include LR-EMR, SR-EMR (i.e. precipitation) and postulated autocatalytic electroless deposition on a suspended titanium metal particle.

4.3.4.1 – Ti^{2+} cation cluster ≥ Ti^{0} critical nuclei size

A valid interaction for this scenario is illustrated in Figure 31 when λ 10 is equal to zero for a Ti^{2+} cation cluster equal to the Ti^{0} critical nuclei size.

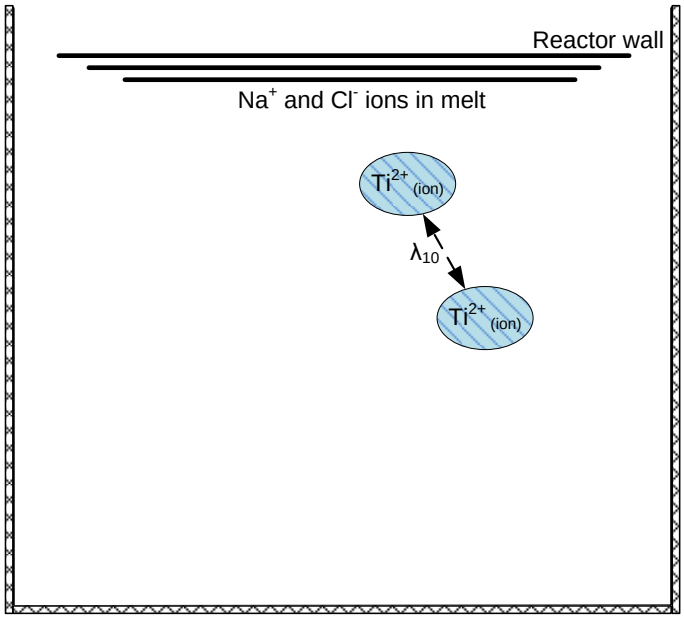

Figure 31: Illustration for a Ti^{2+} cation cluster ≥ Ti^{0} critical nuclei size

Each Ti^{2+} cation cluster labelled in Section 4.3.3 is evaluated to determine whether the Ti^{0} critical nuclei size prerequisite is met.

4.3.4.2 – Ti^{2+} cation cluster ≥ Ti^{0} critical nuclei size AND the number of Na^{0} atoms touching = 2 * Ti^{0} critical nuclei size

This sequence analyses the sample-space surrounding valid Ti^{2+} cation clusters determined in Section 4.3.4.1 to determine whether the stoichiometric requirement for a reaction is met.

This sequence also makes provision for Na^0 atom clusters that interact with Ti^{2+} cation clusters. In other words, only one Na^0 atom in a cluster of Na^0 atoms with the required number of atoms needs to interact with a cluster of Ti^{2+} cations for a reaction to proceed.

A valid interaction for this scenario is illustrated n Figure 32 when four Na^0 atoms "touch" two "connected" Ti^{2+} cations, i.e. in a Ti^{2+} cation cluster. In other words, λ_3, λ_8, λ_{10}, λ_{11}, λ_{12}, λ_{13} and λ_{14} must all be equal to zero for a valid interaction.

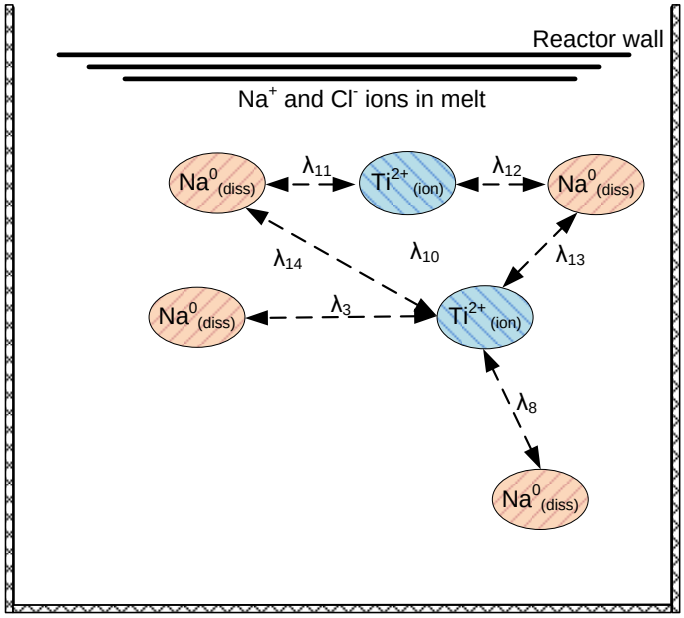

Figure 32: Illustration for SR-EMR prerequisites

4.3.4.3 – Ti^{2+} cation cluster touching Ti^0 AND Ti^0 touching Na^0 AND the number of Na^0 atoms / 2 ≥ 1

This sequence analyses the sample-space surrounding each Ti^0 particle to determine whether the stoichiometric requirement for a reaction is met.

A valid interaction occurs whenever a Ti^{2+} cation interacts with a Ti^0 particle and two Na^0 atoms interact with the Ti^0 particle at the same time.

This scenario's valid interaction is illustrated in Figure 33 when two Na^0 atoms touch different Ti^0 atoms in a Ti^0 particle while a Ti^{2+} cation also touches the Ti^0 particle. In other words, λ_2, λ_5 and λ_6 must all be equal to zero for a valid interaction.

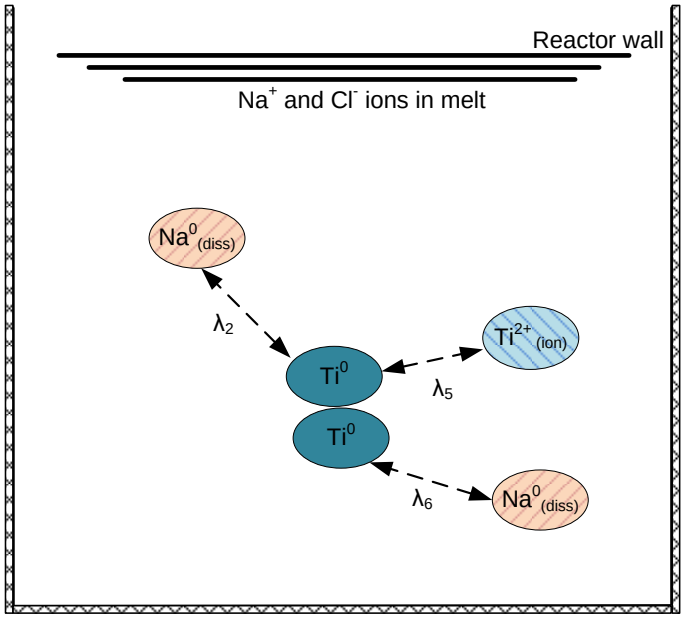

Figure 33: Illustration for autocatalytic electroless deposition prerequisites

4.3.4.4 – Ti^{2+} cation cluster in valid LR-EMR positions AND Na^0 / 2 ≥ 1 in valid LR-EMR positions

This sequence analyses the three LR-EMR cases described in Section 4.3.1.3. A valid LR-EMR interaction can occur when the reagents occupy any of the positions determined in Section 4.3.1.3 and stoichiometry is met.

A valid interaction for this scenario is illustrated in Figure 34 where λ_1, λ_4 and λ_9 are all equal to zero.

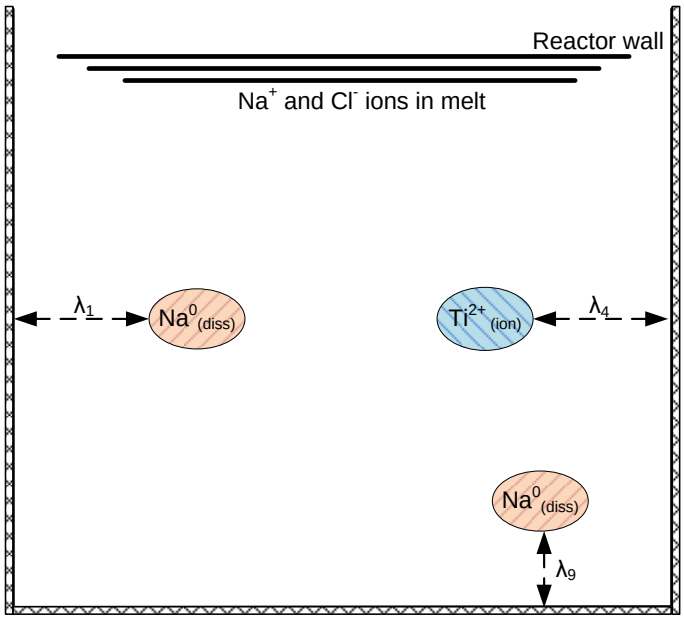

Figure 34: Illustration for LR-EMR prerequisites

4.3.5 – Store results

The number of valid interactions found for each analysis mentioned in Section 4.3.4 is added to a running counter after each iteration. This data is subsequently used in Section 4.3.6 to calculate the output results.

4.3.6 – Repeat for Monte Carlo simulation

The frequency of successful collisions, discussed in Section 3.5, can be used to estimate a reaction mechanism's selectivity by repeatedly randomising the components' positions in a representative three-dimensional sample-space and then determining the number of valid interactions where all prerequisites are met.

This can be achieved by repeating the following steps in the algorithm:

- Section 4.3.2 Sample-space randomisation
- Section 4.3.3 Analysis for cluster formation
- Section 4.3.4 Interaction analysis
- Section 4.3.5 Save results

The number of iterations used determines the confidence with which the results can be presented.

The result of the Monte Carlo simulation is reported using the following statistics:

- The mean of a sample consisting of n numbers is defined by:

$$\bar{x} = \frac{1}{n}\sum_{i=1}^{n} x_i = \frac{1}{n}(x_1 + x_1 + \cdots + x_n) \qquad \text{Equation 12}$$

The mean of a sample effectively describes the frequency of successful collisions.

- The variance is defined by:

$$\sigma^2 = \frac{1}{n-1}\sum_{i=1}^{n}(x_i - \bar{x})^2 = \frac{1}{n-1}[(x_1 - \bar{x})^2 + (x_2 - \bar{x})^2 + \cdots + (x_n - \bar{x})^2] \qquad \text{Equation 13}$$

- The standard deviation (σ) is the square root of variance.
- Confidence error of the mean:

$$E = \frac{100 * z_c * \sigma}{\bar{x}\sqrt{n}} \qquad \text{Equation 14}$$

where z_c is the confidence coefficient and equal to 1.96 for a 95% confidence level.

4.3.7 – Display results

The results produced in Section 4.3.6 are displayed after each iteration. Figure 35 is a screen capture showing the LabVIEW program interface for a completed study.

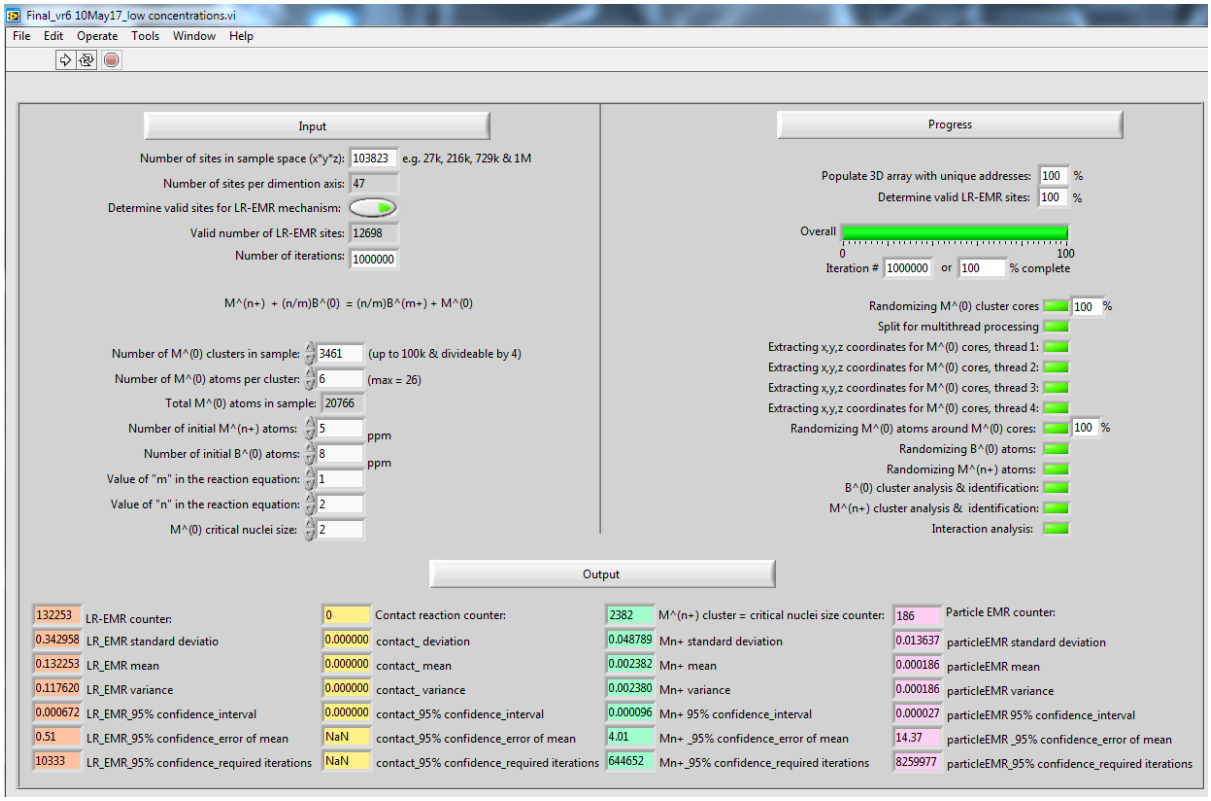

Figure 35: LabVIEW program interface

4.4 – Assumptions and limitations

The following assumptions were made:

- Assume an ideally mixed reaction medium.
- Assume there are no long- or short-range interactions (such as electrostatic or entropic forces) between the reaction medium's different components.
- Assume that all components in the reaction medium are equal in size.
- Assume each component can only be surrounded by 26 other components.
- Assume that the reaction medium consists of only Ti^0, Ti^{2+}, Cl^-, Na^0 and Na^+ (i.e. no contamination).
- Assume negligible activation energy for all reaction mechanisms.
- Assume that all Ti^0 particles contain an equal number of atoms, i.e. there is no Ti^0 particle size distribution.
- Assume that Na^0 can dissolve into molten sodium chloride as single Na^0 atoms.

The following limitations were applicable:

- Each suspended Ti^0 particle can consist of a maximum of 27 Ti^0 atoms.
- The Ti^0 atoms in a Ti^0 particle are randomly distributed during sample-space randomisation. In other words, there is no dominant crystal structure.
- The sample-space evaluated consisted of only 103 823 components (i.e. 47 x 47 x 47 cube) due to limited computational power. A sample-space consisting of 10^6 components (100 x 100 x 100 cube) would have been preferred.

4.5 – Input variable estimation

The reagent concentrations are shown in Figure 13, Section 3.3, would be ideal inputs for the algorithm. However, these concentrations apply to a sample-space consisting of 10^6 components.

The sample-space evaluated in this study is limited to 103 823 components. Therefore, the reagent concentrations illustrated in Figure 13 must be adjusted for a smaller sample-space.

The reaction medium is assumed to be ideally mixed. Assume further that the concentrations of the components scale linearly with sample-space size.

Therefore, the reduced sample-space size's reagent concentrations are approximately 10.38% of the concentrations shown in Figure 13. The results are rounded down to the nearest integer.

Table 10 shows both the original and adjusted values.

Table 10: Ti^{2+} - Na^0 equilibrium concentrations* in ideally mixed molten NaCl at 850 °C

Number of Ti^{2+} cations		Number of Na^0 atoms					
		Ti^0 = 0 mol%		Ti^0 = 10 mol%		Ti^0 = 20 mol%	
Sample-space size = 10^6 positions	Sample-space size = 103 823 positions	Sample-space size = 10^6	Sample - space size = 103 823	Sample - space size = 10^6	Sample-space size = 103 823	Sample-space size = 10^6	Sample - space size = 103 823
500	52	29	3	29	3	19	2
300	31	39	4	39	4	29	3
120	12	58	6	58	6	48	5
80	8	67	7	67	7	58	6
60	6	87	9	77	8	67	7
50	5	96	10	87	9	77	8
30	3	116	12	106	11	96	10
20	2	144	15	125	13	116	12

* $\gamma_{TiCl_2} = 0.04$ & $\gamma_{Na} = 5$

4.6 – Results

4.6.1 – Test for repeatability

Repeatability was evaluated on three different personal computers, and each computer ran three instances of the program. The results obtained after 10^6 iterations are reported in Figure 36 and Table 11.

The mean's average confidence error was approximately 4% for each of the nine repeated simulations.

The results in Table 11 can also be used to calculate the confidence error of the mean between the outputs of the different computers. The mean of nine data sets is 0.002398, with a 1.4% confidence error of the mean.

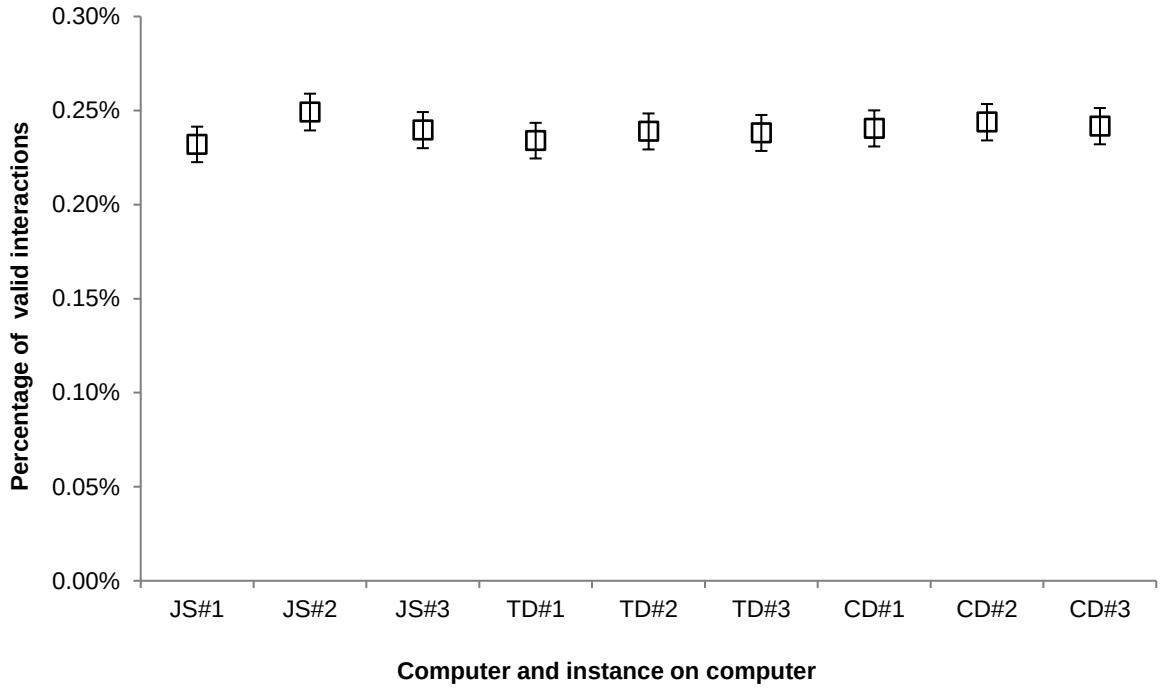

Figure 36: Test for repeatability: formation of Ti^{2+} cation clusters

(Sample-space size = 103 823, 10^6 iterations per study, Ti^0 critical nuclei size = 2, $\gamma_{TiCl_2} = 0.04$ & $\gamma_{Na} = 5$, Ti^{2+} atoms = 5, Na^0 atoms = 8, Ti^0 atoms = 0, 95% confidence level)

Table 11: Test for repeatability*: formation of Ti^{2+} cation clusters

PC	Study mean	Percentage of valid interactions per study	Standard deviation	Confidence error of mean (%)
JS#1	0.002320	0.2320%	0.048131	4.1%
JS#2	0.002492	0.2492%	0.049858	3.9%
JS#3	0.002396	0.2396%	0.048972	4.0%
TD#1	0.002340	0.2340%	0.048317	4.0%
TD#2	0.002389	0.2389%	0.048819	4.0%
TD#3	0.002381	0.2381%	0.048758	4.0%
CD#1	0.002405	0.2405%	0.048982	4.0%
CD#2	0.002438	0.2438%	0.049336	4.0%
CD#3	0.002417	0.2417%	0.049144	4.0%

*Sample-space size = 103 823, 10^6 iterations per study, Ti^0 critical nuclei size = 2, $\gamma_{TiCl_2} = 0.04$ & $\gamma_{Na} = 5$, Ti^{2+} atoms = 5, Na^0 atoms = 8, Ti^0 atoms = 0, 95% confidence level

4.6.2 – Autocatalytic electroless deposition on suspended titanium metal particles

Refer to Figure 33 in Section 4.3.4.3 for the background to the prerequisites needed for a valid interaction in Section 4.6.2.

4.6.2.1 – Function of reagent concentrations

The effect of reagent concentration on the postulated growth mechanism was evaluated at a constant 20 mol % Ti^0 particle concentration.

The results are reported in Figure 37 and Table 12.

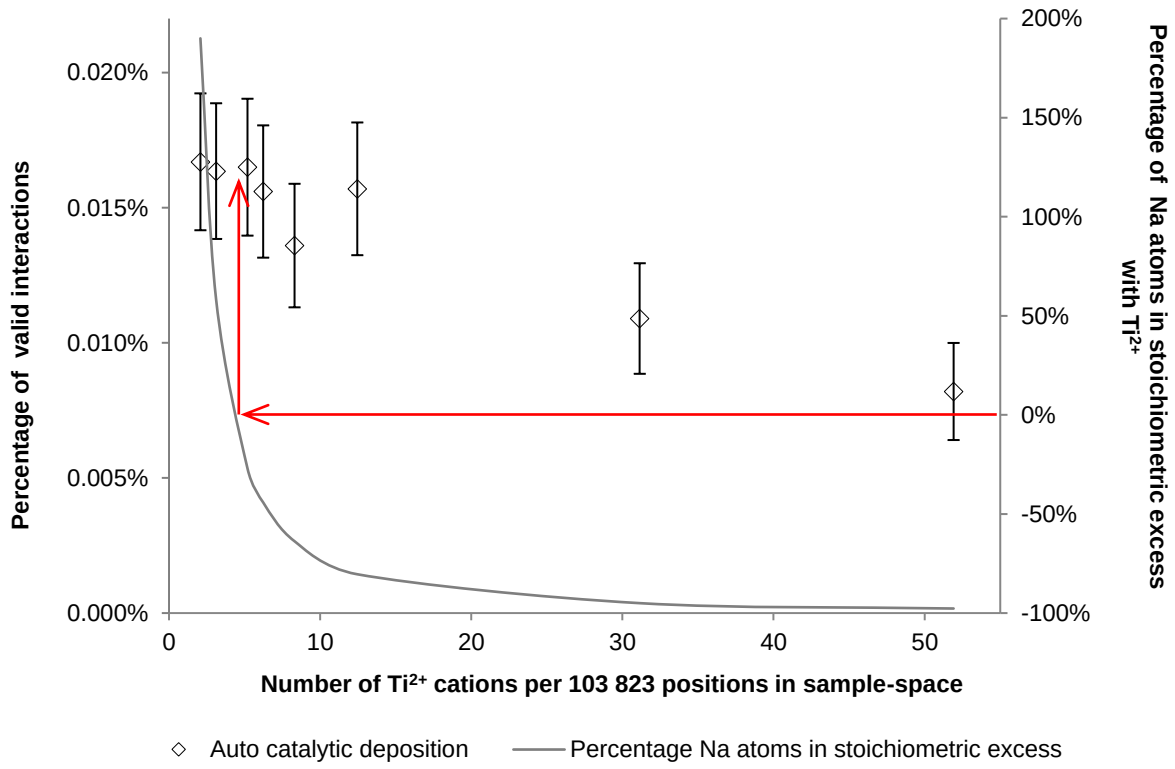

Figure 37: Autocatalytic electroless deposition as a function of reagent concentrations

(Ti^0 mol fraction = 0.2, Ti^0 atoms per Ti^0 particle =14, 10^6 iterations per study, $\gamma_{TiCl_2} = 0.04$ & $\gamma_{Na} = 5$, 95% confidence level)

The postulated growth mechanism was observed for all concentrations where Na^0 and Ti^{2+} cations co-exist. The percentage of valid interactions reduced sharply with an increase in Ti^{2+} cation concentration. The percentage of valid interactions seem to reach a maximum when the reagent concentrations are close to the stoichiometric equilibrium.

Table 12: Autocatalytic electroless deposition as a function of reagent concentration

Number of Ti^{2+} cations per 103 823 positions	Number of Na^0 atoms per 103 823 positions	Study mean	Percentage of valid interactions per study	Standard deviation	Confidence error of mean (%)
52	2	0.000082	0.0082%	0.009165	21.9%
31	3	0.000109	0.0109%	0.010440	18.8%
12	5	0.000157	0.0157%	0.012529	15.6%
8	6	0.000136	0.0136%	0.011662	16.8%
6	7	0.000156	0.0156%	0.012490	15.7%
5	8	0.000165	0.0165%	0.012923	15.4%
3	10	0.000164	0.0164%	0.012788	15.4%
2	12	0.000167	0.0167%	0.012922	15.2%

(Ti^0 mol fraction = 0.2, Ti^0 atoms per Ti^0 particle =14, 10^6 iterations per study, $\gamma_{TiCl_2} = 0.04$ & $\gamma_{Na} = 5$, 95% confidence level)

Table 12 shows a very high error of mean for a 95% confidence level. The number of iterations required per study needs to increase significantly to reduce this error.

The number of iterations required can be estimated using (Driels & Shin, 2004: 10):

$$\mathrm{n} = \left[\frac{100 * \mathrm{z_c} * \sigma}{E * \bar{\mathrm{x}}}\right]^2 \qquad \text{Equation 15}$$

Applying Equation 15 to the first row of data in Table 12 indicates that approximately 18 000 000 more iterations would be needed to report an answer with a 5% error of the mean at a 95% confidence level. This would take an exceptionally long time to complete with computational power available.

A trade-off between accuracy and time is, therefore needed. The number of iterations per study is fixed at 10^6 for all scenarios evaluated.

4.6.2.2 – Function of Ti^0 particle concentration

A suspended Ti^0 particle is a prerequisite for the postulated growth mechanism. As expected, the results illustrated in Figure 38 indicate that an increase in the available surface area also increases the percentage of valid interactions observed.

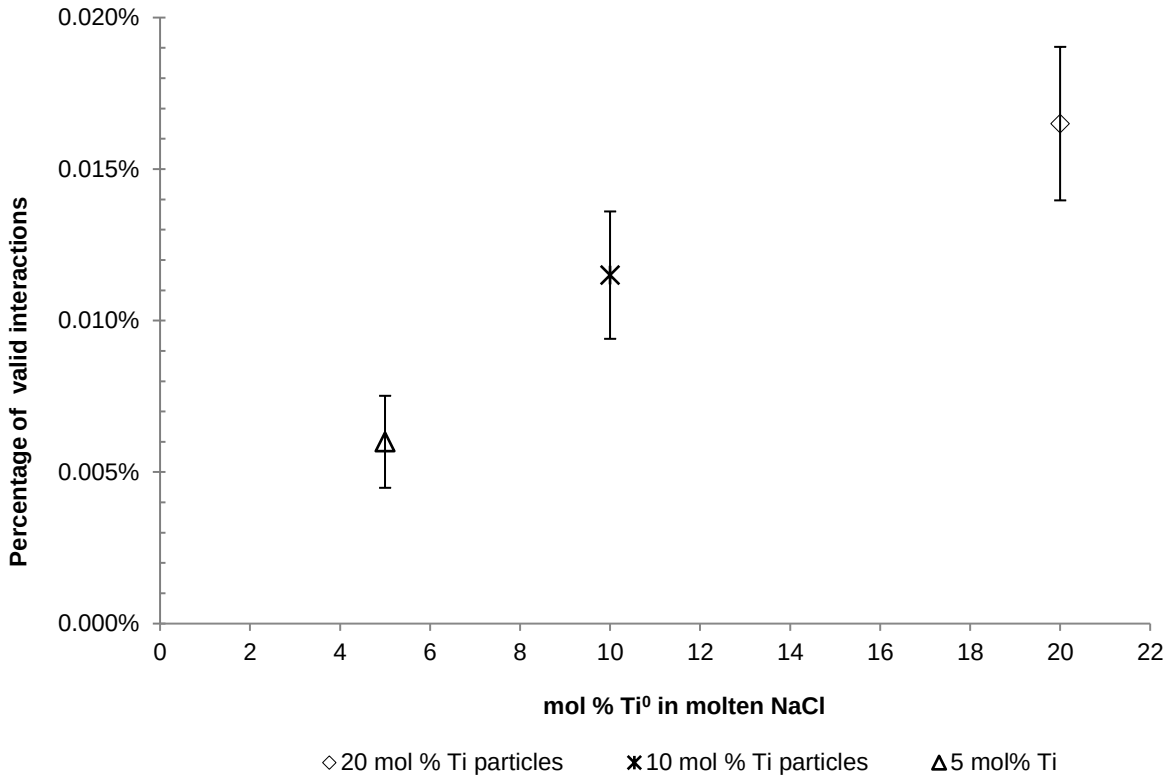

Figure 38: Autocatalytic electroless deposition as a function of Ti^0 particle concentration

(Sample-space size = 103 823, Ti^0 atoms per Ti^0 particle = 14, 10^6 iterations per study, $\gamma_{TiCl_2} = 0.04$ & $\gamma_{Na} = 5$, Ti^{2+} atoms = 5, Na^0 atoms = Refer Table 10, 95% confidence level)

Table 13: Autocatalytic electroless deposition as a function of Ti^0 particle concentration

Ti^0 mol %	Study mean	Percentage of valid interactions per study	Standard deviation	Confidence error of mean (%)
5	0.000060	0.0060%	0.007746	25.3%
10	0.000115	0.0115%	0.010723	18.3%
20	0.000165	0.0165%	0.012923	15.4%

(Sample-space size = 103 823, Ti^0 atoms per Ti^0 particle = 14, 10^6 iterations per study, $\gamma_{TiCl_2} = 0.04$ & $\gamma_{Na} = 5$, Ti^{2+} atoms = 5, Na^0 atoms = Refer Table 10, 95% confidence level)

4.6.2.3 – Function of suspended Ti^0 particle size

The postulated growth mechanism was evaluated as a function of the number of Ti^0 atoms in a Ti^0 particle. The results illustrated in Figure 39 indicate that the percentage of valid interactions reduces with an increase in Ti^0 particle size.

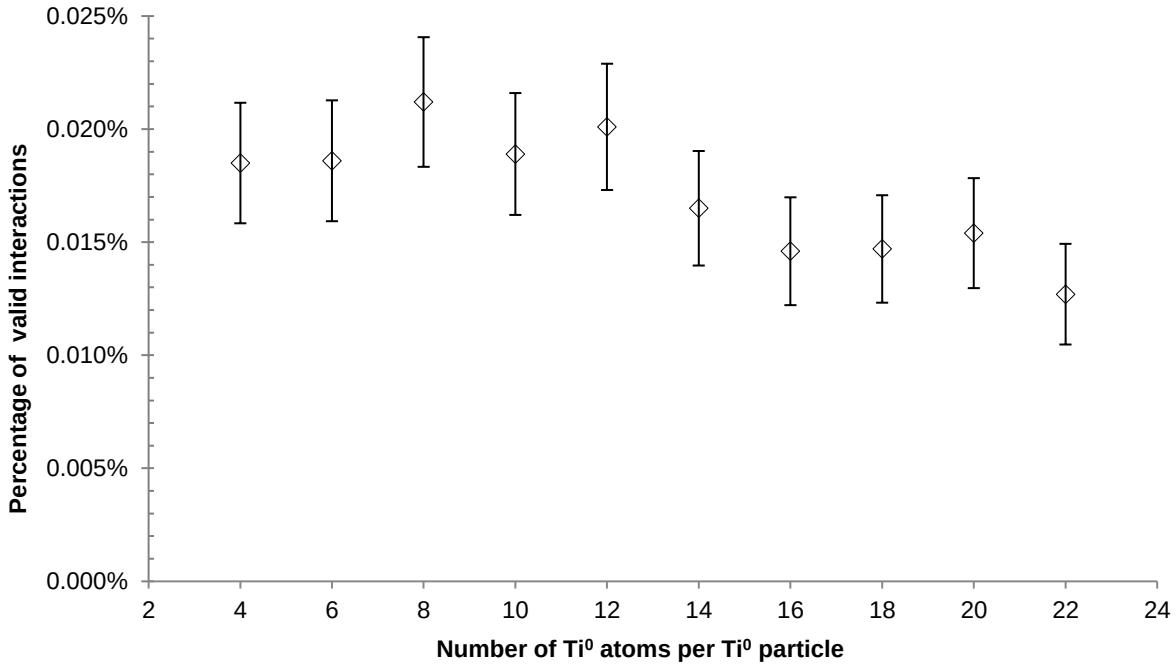

Figure 39: Autocatalytic electroless deposition as a function of suspended Ti^0 particle size

(Sample-space size = 103 823, Ti^0 mol % = 20, 10^6 iterations per study, $\gamma_{TiCl_2} = 0.04$ & $\gamma_{Na} = 5$, Ti^{2+} atoms = 5, Na^0 atoms = 8, 95% confidence level)

This correlation can be explained by how the Ti^0 surface area ratio relative to volume reduces as the Ti^0 particle size increases.

The results illustrated in Figure 39 suggest that smaller Ti^0 particles are more likely to grow than larger Ti^0 particles when both are present.

Table 14: Autocatalytic electroless deposition as a function of suspended Ti^0 particle size

Number of Ti^0 atoms per Ti^0 particle	Study mean	Percentage of valid interactions per study	Standard deviation	Confidence error of mean (%)
4	0.000185	0.0185%	0.013600	14.4%
6	0.000186	0.0186%	0.013637	14.4%
8	0.000212	0.0212%	0.014627	13.5%
10	0.000189	0.0189%	0.013746	14.3%
12	0.000201	0.0201%	0.014246	13.9%
14	0.000165	0.0165%	0.012922	15.3%
16	0.000146	0.0146%	0.012165	16.3%
18	0.000147	0.0147%	0.012123	16.2%
20	0.000154	0.0154%	0.012409	15.8%
22	0.000127	0.0127%	0.011357	17.5%

(Sample-space size = 103 823, Ti^0 mol % = 20, 10^6 iterations per study, $\gamma_{TiCl_2} = 0.04$ & $\gamma_{Na} = 5$, Ti^{2+} atoms = 5, Na^0 atoms = 8, 95% confidence level)

4.6.3 – The LR-EMR mechanism

Refer to Figure 34 in Section 4.3.4.4 for a background to the prerequisites needed for a valid interaction in Section 4.6.3.

4.6.3.1 – Function of reagent concentrations

The LR-EMR mechanism is similar to the postulated growth mechanism in that both allow a reaction to proceed through a substrate surface. However, the surface area available for electron transfer is significantly larger in the LR-EMR mechanism. To illustrate, the sample-space simulated by this algorithm has 2 209 available positions (47 x 47 for one plane) in which the stoichiometric requirements can be met for a valid LR-EMR interaction.

Therefore, the results presented in this section should correlate with those in Section 4.6.2. This expected correlation is confirmed by the results illustrated in Figure 40. Figure 40 also shows that the maximum percentage of valid interactions is observed at stoichiometric equilibrium.

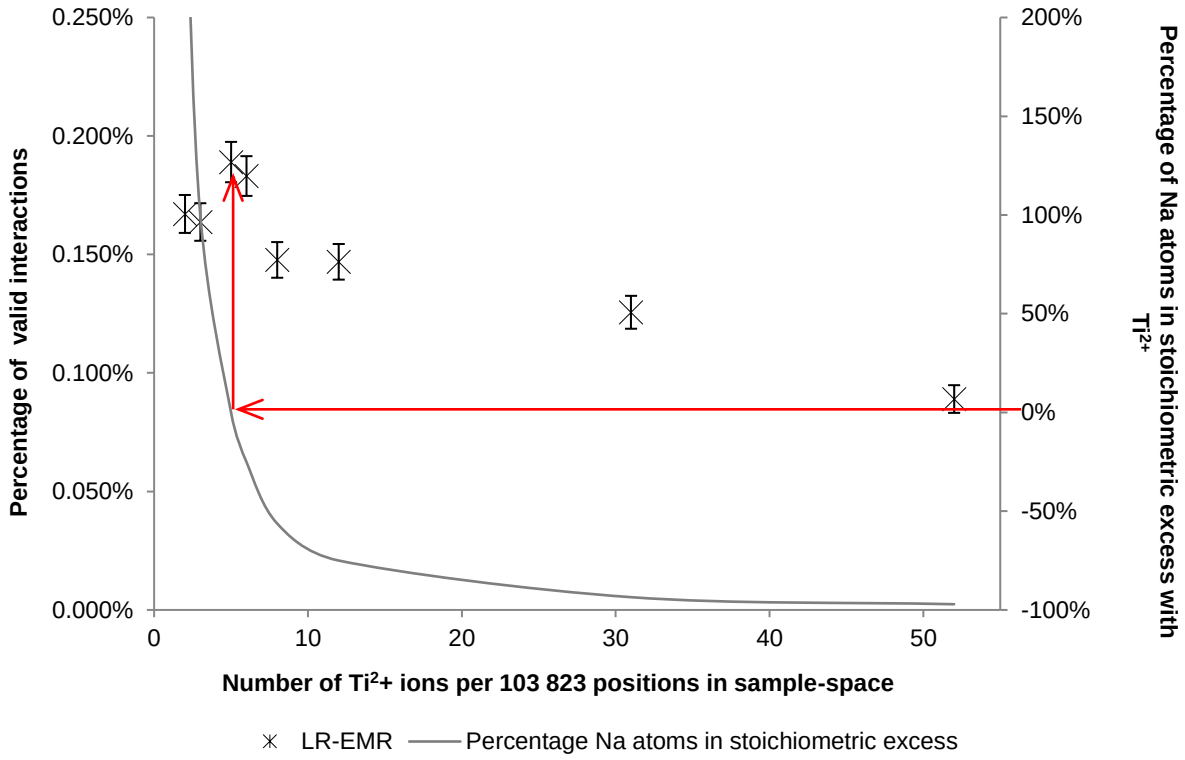

Figure 40: LR-EMR as a function of reagent concentrations

(Ti^0 mol % = 0, 10^6 iterations per study, $\gamma_{TiCl_2} = 0.04$ & $\gamma_{Na} = 5$, 1 side LR-EMR, 95% confidence level)

Table 15: LR-EMR as a function of reagent concentration

Number of Ti^{2+} cations per 103 823 positions	Number of Na^0 atoms per 103 823 positions	Study mean	Percentage of valid interactions per study	Standard deviation	Confidence error of mean (%)
52	3	0.000890	0.089%	0.02982	6.6%
31	4	0.001256	0.126%	0.035418	5.5%
12	6	0.001469	0.147%	0.038325	5.1%
8	7	0.001477	0.148%	0.038403	5.1%
6	9	0.001831	0.183%	0.042770	4.6%
5	10	0.001890	0.189%	0.043433	4.5%
3	12	0.001637	0.164%	0.040427	4.8%
2	15	0.001671	0.167%	0.040844	4.8%

(Ti mol % = 0, 10^6 iterations per study,
$\gamma_{TiCl_2} = 0.04$ & $\gamma_{Na} = 5$, 1 side LR-EMR, 95% confidence level)

4.6.3.2 – LR-EMR as a function of exposed surface area and sample-space size

The LR-EMR mechanism is a function of exposed surface area (i.e. viable LR-EMR positions) and sample-space volume.

Figure 41 illustrates the effect when the sample-space size is kept constant while increasing the number of sides (flat planes) in the cube exposed to the sample-space (refer to Section 4.3.1.3).

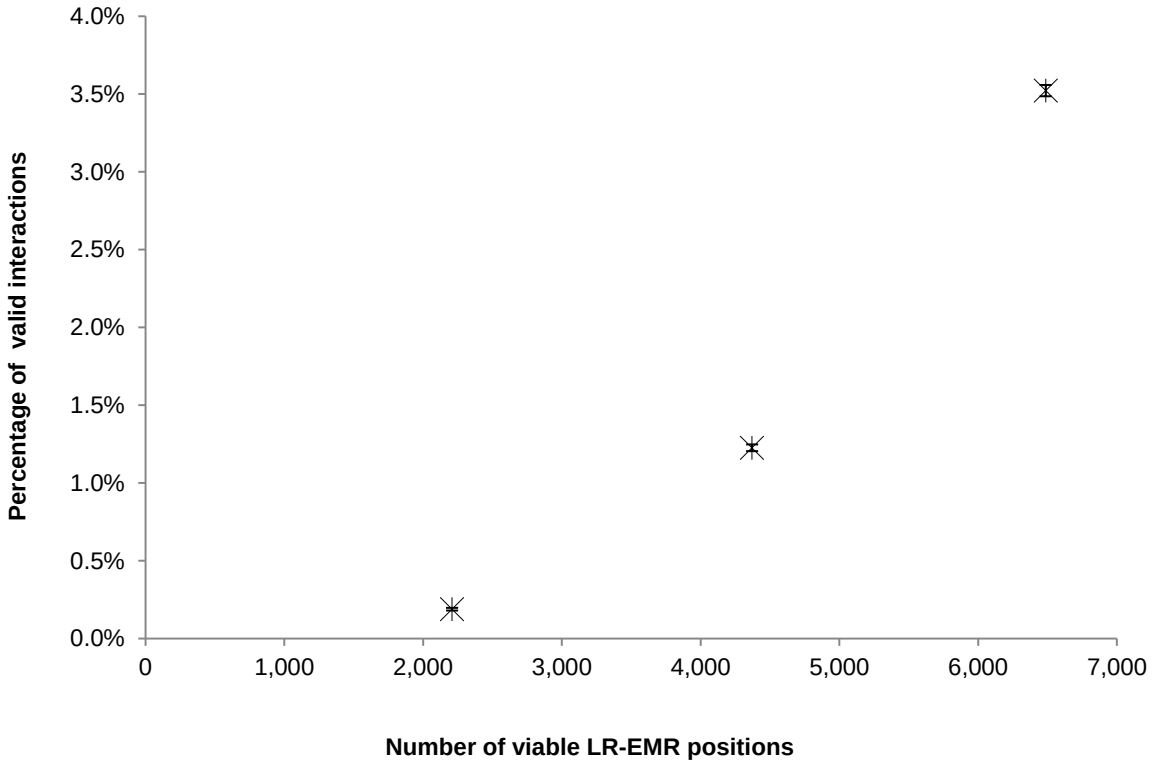

Figure 41: LR-EMR as a function of the number of positions available for the LR-EMR mechanism

(Sample-space size = 103 823, Ti^0 mol % = 0, 10^6 iterations per study, $\gamma_{TiCl_2} = 0.04$ & $\gamma_{Na} = 5$, Ti^{2+} atoms = 5, Na^0 atoms = 10, 95% confidence level)

In turn, Figure 42 shows that the number of available LR-EMR positions reduces when the cubic sample-space size increases.

Therefore, the sample-space size (or volume) exposed to the reactor surface is an important consideration for the LR-EMR mechanism. Increasing the sample-space size while reducing the exposed surface area will reduce the likelihood of observing the LR-EMR mechanism.

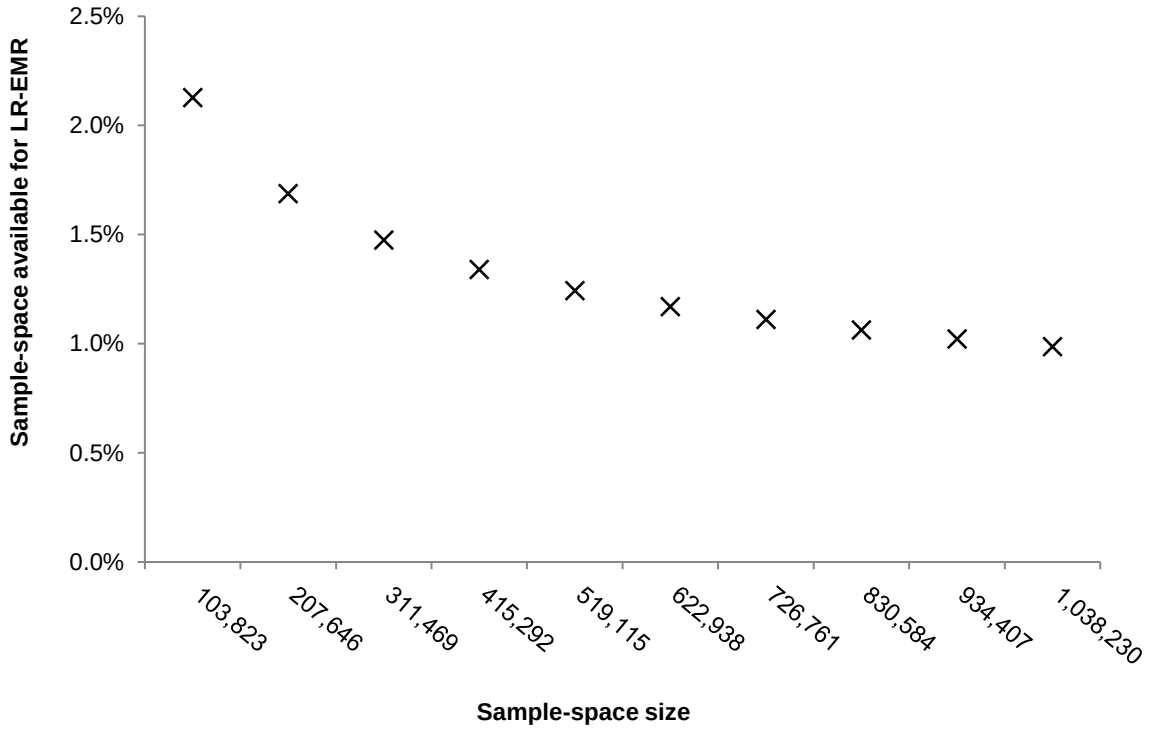

Figure 42: Percentage sample-space available for the LR-EMR mechanism as a function of the cubic sample-space size

4.6.4 – The SR-EMR mechanism

Not a single valid SR-EMR interaction was observed in all the scenarios evaluated. The prerequisites needed for this interaction seem to be exceedingly difficult to meet. Section 4.3.4.2 described these prerequisites in more detail.

The formation of a cluster of Ti^{2+} cations equal to the Ti^{0} critical nuclei size is the first prerequisite needed for this mechanism. Section 4.3.4.1 discusses a Ti^{0} critical nuclei size cluster formation in more detail.

The results obtained for forming a cluster of Ti^{2+} cations equal to the Ti^{0} critical nuclei size are illustrated in Figure 43 as a function of reagent concentrations.

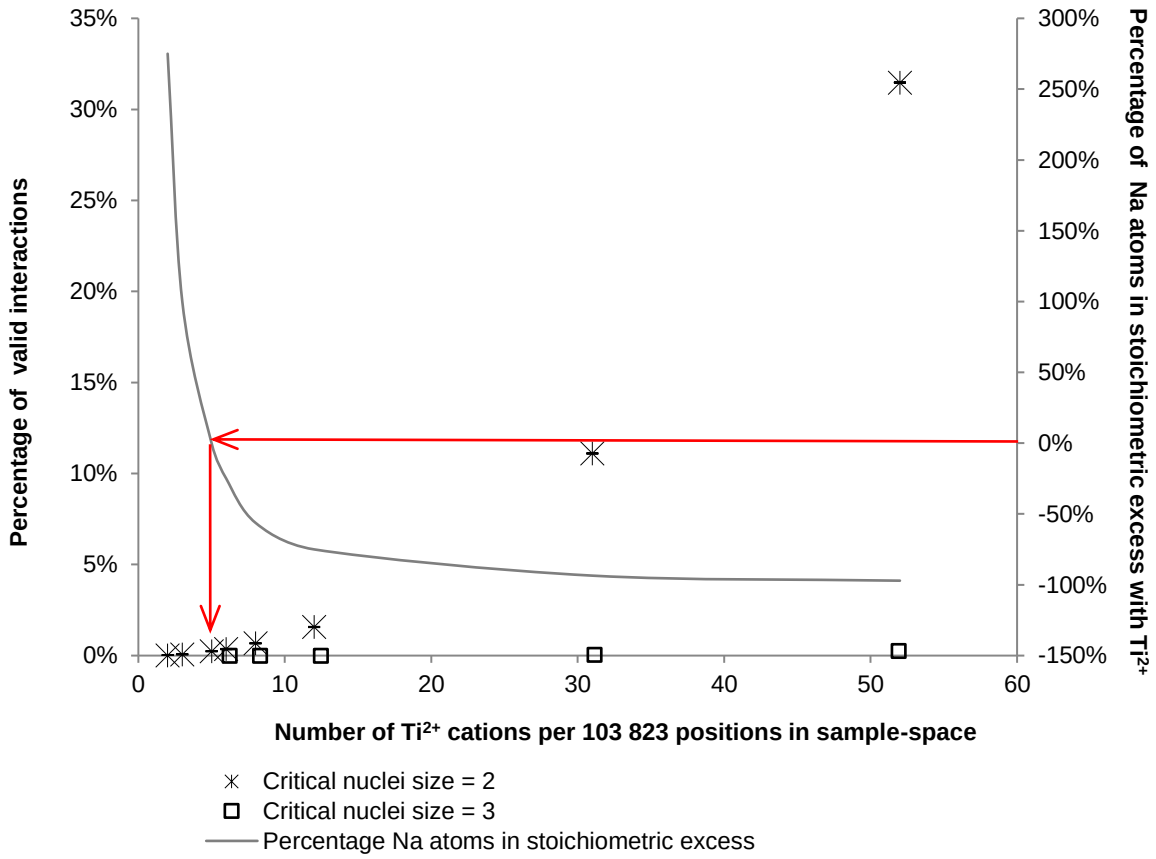

Figure 43: Ti^{2+} cluster formation as a function of Ti^{2+} cation concentration

The cluster formation of two Ti^{2+} cations increases significantly as the Ti^{2+} concentration increases. Figure 43, however, also shows that Na^0 concentration reduces significantly as the Ti^{2+} cation concentration increases. The formation of three Ti^{2+} cations in a cluster has a significantly reduced likelihood.

Table 16 summarises the results illustrated in Figure 43.

Ti^{2+} cations likely exist as clusters rather than individual ions. This requirement was not included in the algorithm design.

Therefore, the algorithm should make provision for randomising variable clusters of both sodium and Ti^{2+} cations into the sample-space. The sequences described in Sections 4.3.2.2 and 4.3.2.3 can be used as references.

Table 16: Ti^{2+} cluster formation as a function of Ti^{2+} cation concentration

Number of Ti^{2+} cations per 103 823 positions	Number of Na^0 atoms per 103 823 positions	Percentage of valid interactions Crit. nucl. = 2	Percentage of valid interactions Crit. nucl. = 3
52	3	31.476%	0.264%
31	4	11.103%	0.052%
12	6	1.570%	0.003%
8	7	0.675%	0.001%
6	9	0.357%	0.000%
5	10	0.239%	0.000%
3	12	0.071%	0.000%
2	15	0.021%	0.000%

A linear relationship is illustrated in Figure 44 when plotting the percentage of valid interactions for Ti^0 critical nuclei cluster formation as a function of sample-space size.

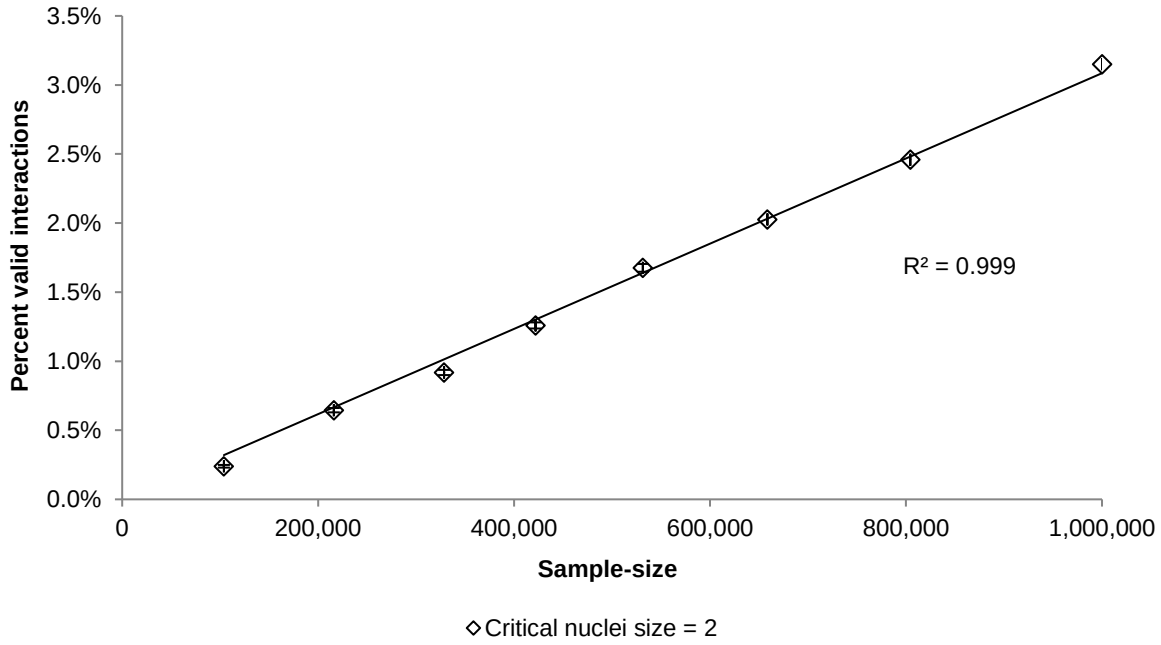

Figure 44: Ti^{2+} cation cluster formation as a function of sample-space size

4.7 – Concluding remarks

The results provided in Chapter 4 indicate that the postulated Ti^0 particle growth mechanism is possible, but only under very specific and low reagent concentrations.

The postulated growth mechanism and the LR-EMR mechanism both allow the reaction to proceed through a substrate surface. However, the nature of the substrate surface differs for each in size, position, and contact with the reaction medium.

In other words,

- The substrate surface available for the LR-EMR mechanism is dependent on the reactor geometry and is stationary relative to the reaction medium.
- The substrate surface available for the postulated growth mechanism is small and moves around actively within the reaction medium.

Correlation of results is therefore expected. This correlation was confirmed in Sections 4.6.2 and 4.6.3.

Other observations include:

- Both LR-EMR and the postulated growth mechanism reported a maximum percentage of valid interactions at the stoichiometric equilibrium concentration.
- Both LR-EMR and the postulated growth mechanism showed an increase in the available surface area directly increases the percentage of valid interactions observed.
- The results in Section 4.6.2.3 suggested that smaller Ti^0 particles are more likely to grow than larger Ti^0 particles when both are present in the reaction medium.
- Section 4.6.3.2 indicated that the number of available LR-EMR positions reduces as sample-space size increases.
- Not a single valid SR-EMR interaction was observed in all the scenarios evaluated.

The following inference can be made from the observations above:

- It is unlikely that the postulated growth mechanism will be observed without the LR-EMR mechanism whilst a metallic reactor in contact with the reaction medium is being used.
- The LR-EMR mechanism's selectivity can be reduced by maximising the ratio between reaction volume and exposed surface area.
- The reaction medium must be maintained at this narrow stoichiometric equilibrium concentration; any deviation from it will be detrimental to controlled particle growth.
- The likelihood of observing the postulated growth mechanism is directly proportional to the concentration of suspended Ti^0 particles. Therefore, either the reactor should be seeded with Ti^0 particles, or the product obtained from precipitation should be allowed to accumulate.

CHAPTER 5 – EXPERIMENTAL

5.1 – Chapter overview

The modelling and simulation results presented in Chapter 4 indicate that titanium metal particle growth is possible through an electrochemical autocatalytic electroless deposition mechanism, but only in a very specific and narrow range of reagent concentration. To establish and maintain the reaction medium practically at these conditions is technically complex.

Confidentiality restrictions limit the disclosure of experimental effort to information already available in the public domain, i.e. patents, journal articles, conference presentations and book chapters.

This chapter intends to demonstrate that titanium metal particle growth is possible through controlled metallothermic reduction on particles suspended in a molten chloride salt without disclosing commercially sensitive information.

Chapter 5 contains the following sections:

1. Section 5.2 provides a brief overview of the reaction system requirements.
2. A hypothesis test is discussed in Section 5.3 to demonstrate the postulated growth mechanism.
3. Various experimental considerations are briefly discussed in Section 5.4.
4. Limitations applicable to the experimental investigation are listed in Section 5.5.
5. Section 5.6 presents the results obtained from the experimental investigation.

5.2 – Three independent electrochemical zones

The Department Science and Technology (DST) contracted the Council for Scientific and Industrial Research (CSIR) in South Africa to develop a process that can produce a primary titanium metal powder product (CSIR, 2018).

The CSIR's research and development efforts resulted in the CSIR-Ti process. A simplified block flow diagram of the CSIR-Ti process's reduction section is illustrated in Figure 45.

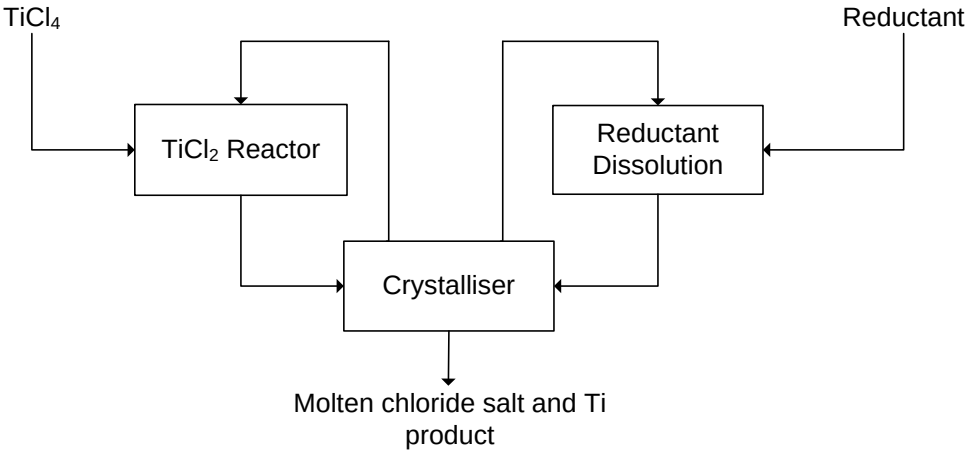

Figure 45: Simplified block flow diagram of the CSIR-Ti process's reduction section

In Figure 45, each reagent is fed to a dedicated system where it is prepared for addition into the Crystalliser. In the Crystalliser, the diluted reagents react with each other in a controlled manner to produce titanium powder dispersed in molten chloride salt.

The molten salt slurry is then recycled back to the $TiCl_2$ Reactor and Reductant Dissolution systems respectively for reagent re-loading. The final product stream can be obtained via pump discharge or overflow from the Crystalliser.

The metallothermic reduction reaction is exothermic and kinetically fast. The CSIR-Ti process's reduction section is designed to enforce control over this reaction by slowing it down as much as possible.

The block flow diagram illustrated in Figure 45 shows two methods used in the CSIR-Ti process to slow down the reaction rate. These are:

- Reduce the concentration of reagents through dilution before they interact with each other.

- Reduce the reagents' electrochemical potential by using dissolved $TiCl_2$ and reductant for controlled Ti^0 deposition.

Therefore, the CSIR-Ti process essentially divides the metallothermic reduction reaction into three independent electrochemical zones.

5.3 – Hypothesis test description

The postulated Ti^0 particle growth mechanism was observed when spherical titanium metal particles were used as seed material in a reactor prototype.

Figure 46 is a scanning electron micrograph (SEM) image of spherical titanium particles without deposition, and Figure 47 is an SEM image of spherical titanium particles with titanium metal deposited on the surface.

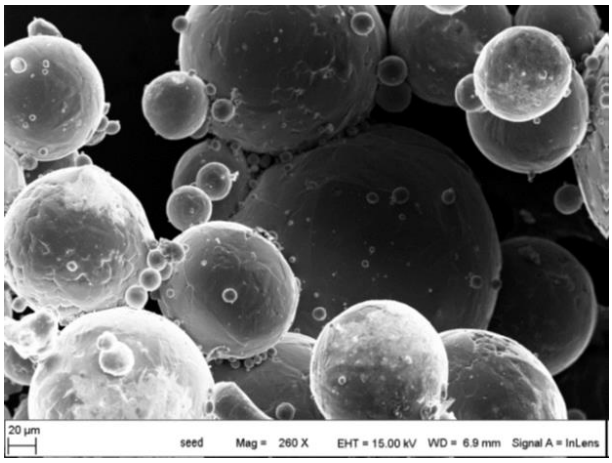

Figure 46: SEM image of spherical titanium particles

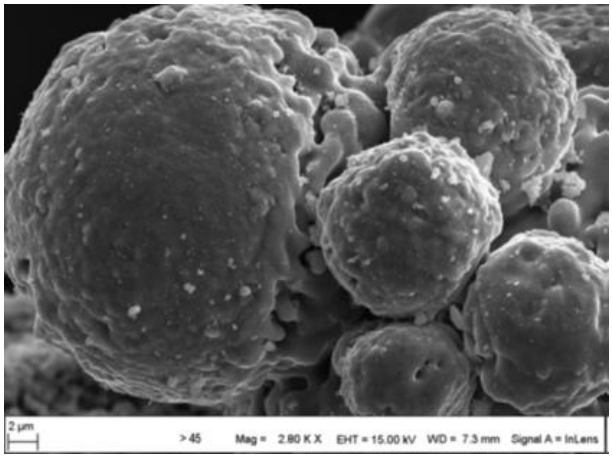

Figure 47: Spherical particles with titanium metal deposit

An integrated reaction system similar to that illustrated in Figure 45 is the preferred method to demonstrate the postulated titanium metal particle growth mechanism.

However, an integrated reaction system is not possible with the available resources. The existence of the postulated titanium metal particle growth mechanism was evaluated through a hypothesis test.

The hypothesis is as follows:

> *Titanium metal particle growth is possible through a mechanism known as autocatalytic electroless deposition.*

The hypothesis test aims to demonstrate autocatalytic electroless deposition on suspended metal particles.

Therefore, if the hypothesis test validates the postulated growth mechanism, then titanium metal particle growth should be possible through the same mechanism.

The nature of the autocatalytic electroless deposition mechanism should allow deposition of titanium metal on the surface of another metal particle.

Another characteristic of autocatalytic electroless deposition is that a non-metallic substrate surface can be metallised before metal deposition (Section 2.4.1).

Figure 48 is a schematic illustration showing how autocatalytic electroless titanium metal deposition can occur on the surface of ilmenite ($FeO.TiO_2$) particles.

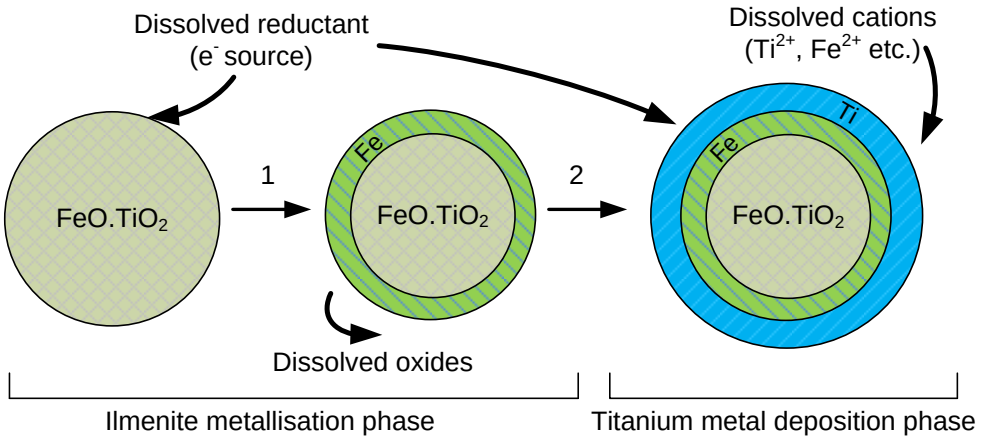

Figure 48: Schematic illustration showing how autocatalytic electroless titanium metal deposition can occur on ilmenite

Figure 48 illustrates the two phases needed to promote titanium metal deposition on ilmenite particles' surface.

In the first phase, i.e. metallisation, the reductant is added to the reactor to reduce the metal oxide surface of ilmenite particles, to result in a metal layer and soluble metal oxide product of the reductant. Most molten chloride salts dissolve metal oxides to varying extents. After metallisation, the surface layer meets the prerequisites needed to become a mixed electrode (Section 2.4.3) for autocatalytic electroless deposition, i.e. electron and ion transfer.

In the second phase, metal cations (Ti^{4+}, Ti^{2+}) are fed into the growth zone at a rate that does not exceed the allowable concentration range (parts per million) prescribed for meta-stable equilibrium (Section 3.3). These metal cations deposit onto the surface of suspended metal particles in contact with a dissolved reductant.

The chemical composition for unroasted Hillendale ilmenite is provided in Table 17.

Table 17: Chemical composition of unroasted Hillendale ilmenite

Constituent	Mass %
Fe_2O_3	12.29
FeO	36.15
TiO_2	48.40
MnO	1.06
SiO_2	0.44
Al_2O_3	0.27
P_2O_5	0.01
V_2O_5	0.25
ZrO_2	0.08
Cr_2O_3	0.09
MgO	0.50
CaO	0.02
Other	0.44

The typical particle size distribution of unroasted Hillendale ilmenite is illustrated in Figure 49.

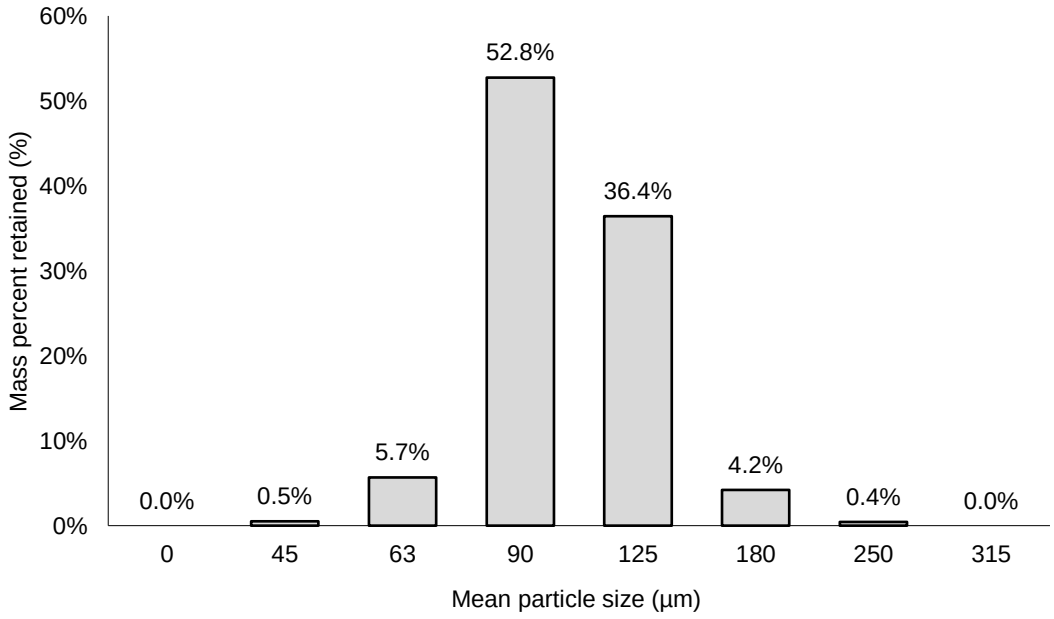

Figure 49: Particle size distribution of ilmenite used

Figure 50 is a stereo-micrograph showing the surface of unroasted Hillendale ilmenite.

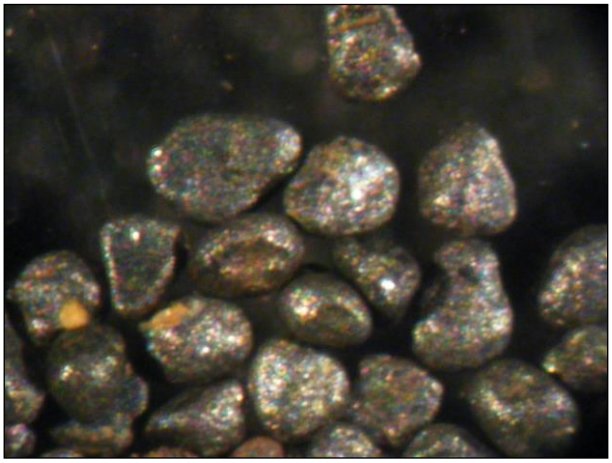

Figure 50: Photograph showing the surface of unroasted Hillendale ilmenite particles (200–350 µm)

5.4 – Experimental

5.4.1 – Standalone operation of the experimental reactor

Crystallisation theory is relatively complicated in that it requires an understanding of various topics Demopoulos (2009: 200).

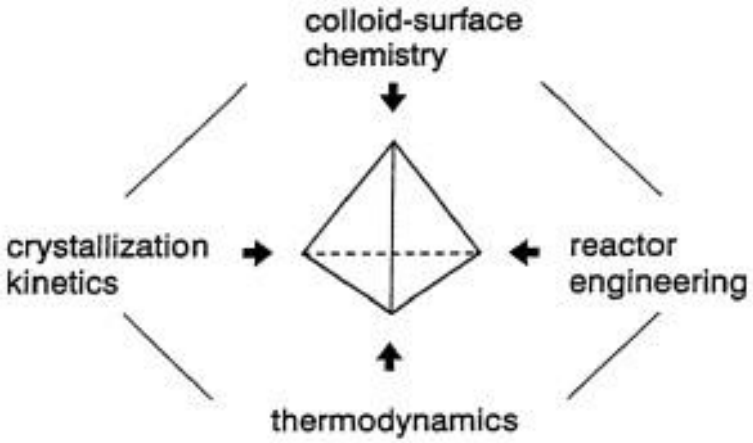

Figure 51: Demopoulos's proposed approach to reactive crystallisation studies
(Source: Demopoulos, 2009: 200)

The paradigm proposed in Figure 51 is also applicable to metal powder production through the controlled metallothermic reduction in a molten chloride salt.

Reactor engineering is especially essential to this research considering the various difficulties inherent to the metallothermic reduction system and required operating conditions.

Consequently, a novel reactor design was developed in this study based on principles presented in the Segregated Feed Model (SFM). The SFM, illustrated in Figure 52, is a compartmental mixing model used in aqueous precipitation processes (Zauner & Jones, 2002: 823).

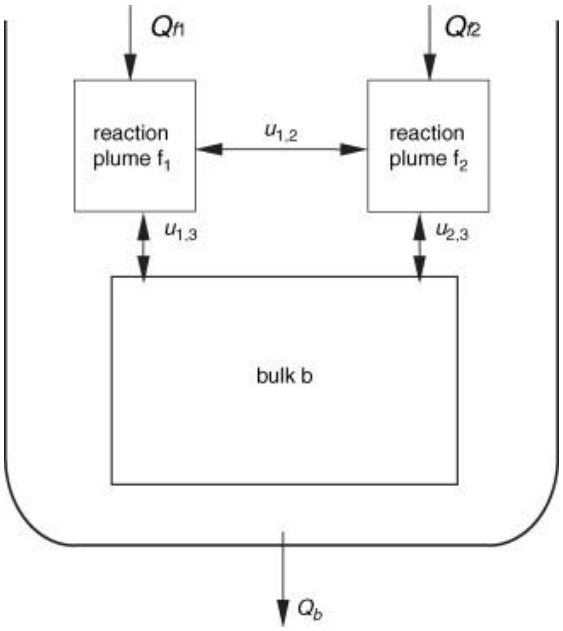

Figure 52: The Segregated feed model
(Source: Zauner & Jones, 2002: 823)

The SFM divides the reactor into three well-mixed zones: two feed zones "f_1" and "f_2" and the reaction bulk, "bulk b". The feed zones exchange mass with each other (flow rates $u_{1,2}$, $u_{1,3}$ and $u_{2,3}$) and with the bulk as depicted in Figure 52 (Zauner & Jones, 2000a: 2393, Zauner & Jones, 2000b: 895, Zauner & Jones, 2002: 823).

Figure 53 is an illustration showing the mixing profile inside the experimental reactor.

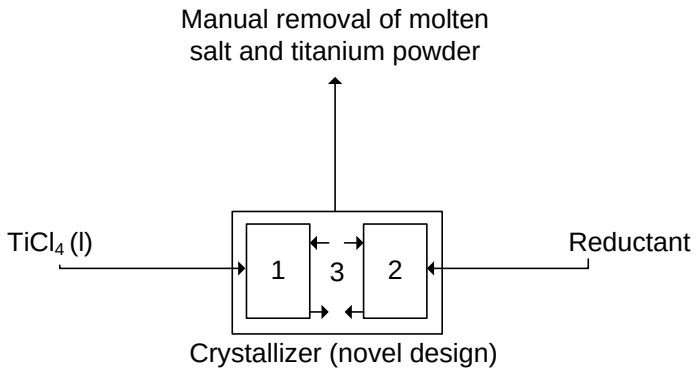

Figure 53: Illustration showing the mixing profile within the experimental reactor

Consideration was also given in the experimental reactor to reduce or eliminate the $u_{1,2}$ interaction while maximising the $u_{1,3}$ and $u_{2,3}$ flow streams in Figure 52.

Zone 1 indicated in Figure 53 represents the β-phase in Figure 9, while zone 2 represents the α-phase. Zone 3 in Figure 53 is the titanium metal growth zone, i.e. the σ-interfacial region in Figure 9.

Figure 54 is a photograph showing molten salt circulating inside an operational reactor.

Figure 54: Photograph showing molten salt flow inside an operational reactor

The experimental reactor (illustrated in Figure 53) can be regarded as the worst-case scenario as a level of control is lost by not having dedicated zones for titanium dichloride production and reductant dissolution.

Figures 55 and 56 are photographs showing the experimental reactor in operation.

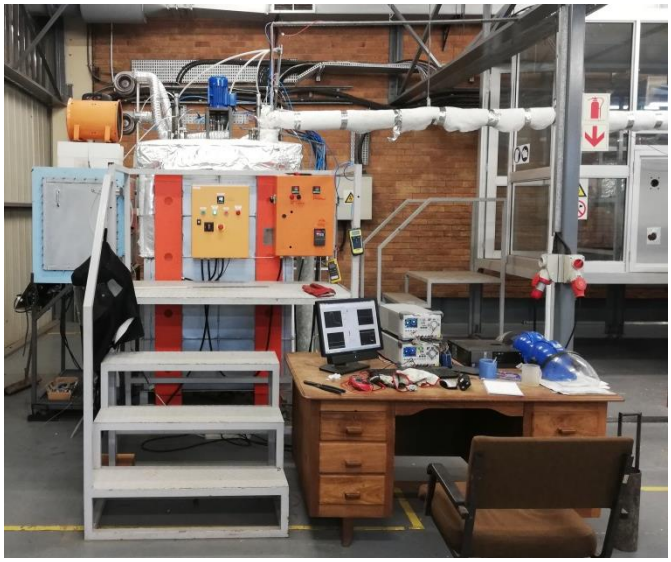

Figure 55: Photograph showing an overview of the experimental setup in operation

Figure 56: Photograph showing an overview of the reactor's lid

5.4.2 – Reaction control at meta-stable equilibrium

Reaction control at meta-stable equilibrium is a critical prerequisite needed to demonstrate the postulated growth mechanism. Reaction control is achieved by varying the molten reductant and liquid titanium tetrachloride feed rates. Each reagent, in turn, requires various handling and safety considerations.

The dissolved reductant concentration in the growth zone is the response variable used for control.

The dissolved reductant concentration is measured using controlled potential coulometry in a three-electrode configuration with a pseudo-reference electrode. The difference between a true reference electrode and a pseudo-reference electrode is the latter's lack of thermodynamic equilibrium (Inzelt, Lewenstam & Scholz, 2013: 331).

A screen capture of the reaction monitoring system is shown in Figure 57.

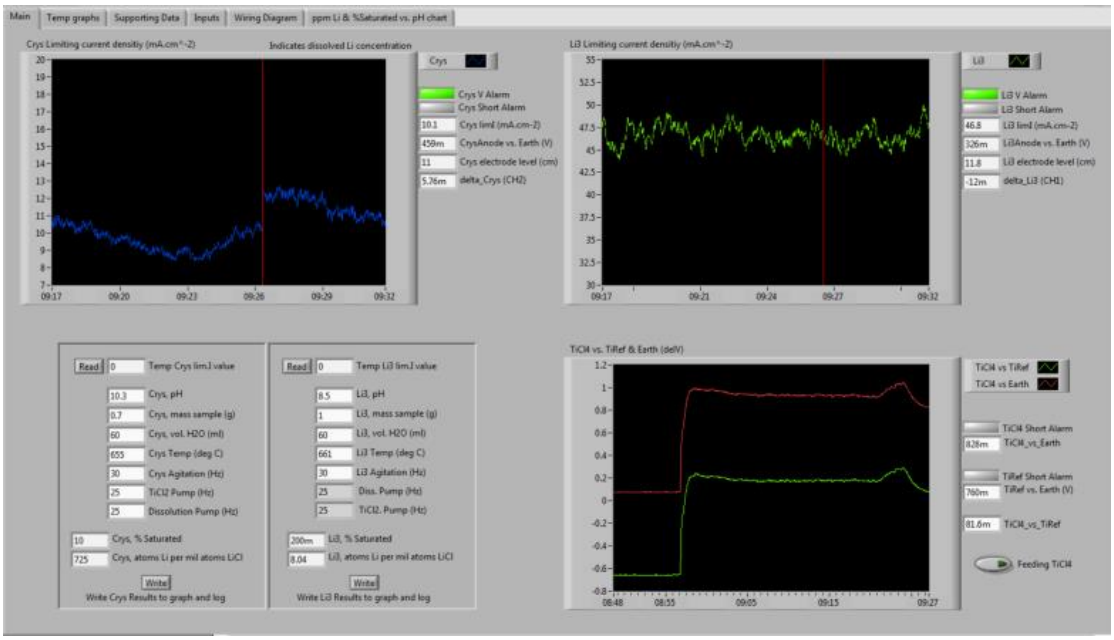

Figure 57: Output for reaction monitoring in LabVIEW

5.4.3 – Operational, health and safety considerations

Working at high temperature with hazardous chemicals is dangerous and technically challenging.

Molten chloride salts are highly corrosive when exposed to the normal atmosphere. Figure 58 is a photograph of a reactor prototype which suffered excessive molten salt corrosion damage.

Figure 58: Photograph of a reactor prototype with excessive corrosion damage

Titanium tetrachloride is a highly corrosive substance that forms hydrochloric acid and titanium oxychlorides on exposure to the atmosphere.

Molten alkali and alkali earth metals are highly reactive substances requiring specialised equipment and procedures to ensure safe handling and transport.

Significant engineering due diligence is required.

5.5 – Limitations

- The experimental reactor is operated in a standalone configuration.
- The use of ilmenite as seed material introduces dissolved oxides into the molten salt. Contamination from oxygen and corrosion products are therefore expected.
- No $TiCl_4$(l) pre-evaporation or purification is applied.
- The $TiCl_4$ feed nozzle is submerged in the circulating molten salt stream.
- The submerged $TiCl_4$ feed nozzle is made from 316 stainless steel.

5.6 – Results

The powder product removed from the reactor was prepared for analysis using the following steps:

1. Dissolve solid salt with a pH 1.5 hydrochloric acid solution.
2. Wet screen with 90 µm and 40 µm sieves to remove metal powder product.
3. Wash the metal powder product with hot water.
4. Vacuum dry the metal powder product at 60 °C and 10 mbar gauge.
5. Separate magnetic particles manually with a permanent handheld magnet. Only the magnetic particles are needed for evaluation since these would correspond with the ilmenite particles fed into the reactor.

The following evaluation steps were followed:

1. Visual inspection for ilmenite surface metallisation
2. An internal SEM-EDS elemental map investigation
3. An external SEM-EDS elemental map investigation
4. An EBSD study of samples to confirm findings

The results of each investigation are reported in the sections below.

5.6.1 – Surface layer metallisation of ilmenite particles

Surface layer metallisation of ilmenite particles was the first phase objective, shown in Figure 48.

Figure 59 is a photograph of particles removed from the reactor revealing a change in surface appearance due to metallisation.

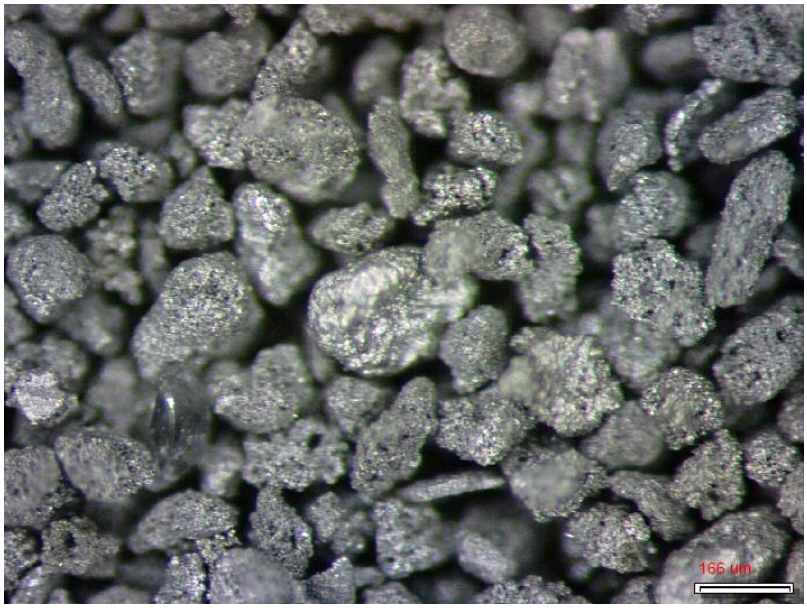

Figure 59: Metallised particles removed from the reactor

The metallic lustre visible on the particles shown in Figure 59 indicates that metallisation was successful.

5.6.2 – Internal SEM/EDS investigation

Figure 60 is an SEM-BEC image of a -40 µm magnetic particle removed from the experimental reactor. Table 18 reports the results obtained from different spot analyses on this particle.

Figure 61 is an iron and titanium elemental map of the particle shown in Figure 60.

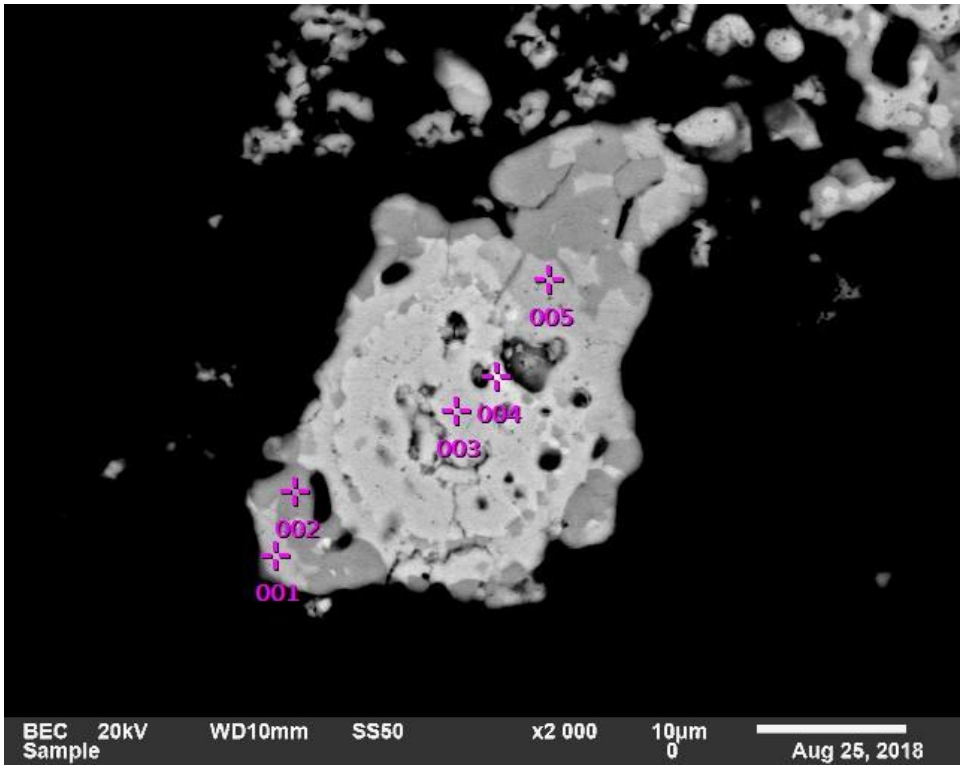

Figure 60: SEM-BEC image of a -40 µm magnetic particle with spot analysis indicated

Table 18: Spot analysis estimation for mass % composition of Figure 60

	Ti	Fe
Spot 1	82.63	16.23
Spot 2	100.00	
Spot 3	49.23	50.10
Spot 4	60.30	38.94
Spot 5	84.30	14.65

The results shown in Figures 60 and 61 combined with the data reported in Table 18 indicate a particle consisting of an iron/titanium core and a titanium shell, as expected, and illustrated in Figure 48. The iron:titanium ratio for spots 3 and 4 in Table 18 is also similar to that of the iron:titanium ratio of ilmenite reported in Table 17.

Figure 61 also shows an area, indicated with a red circle, where titanium deposition was preferential.

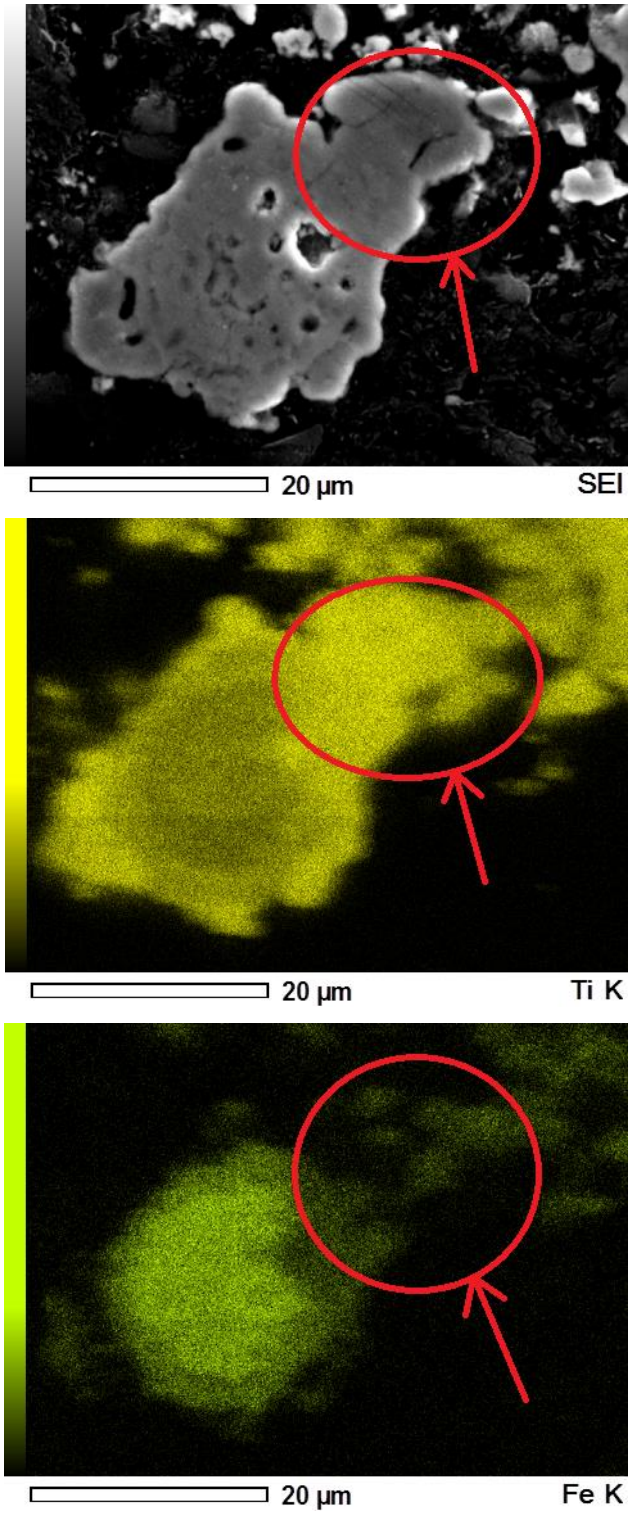

Figure 61: Iron and titanium elemental maps of Figure 60

5.6.3 – External SEM/EDS investigation

The National Metrology Institute of South Africa (NMISA) was contracted to generate SEM-EDS elemental maps of the particles.

The results obtained are illustrated in this section. A theme common to all the results is that a layer of deposited material is visible on the surface of these magnetic particles.

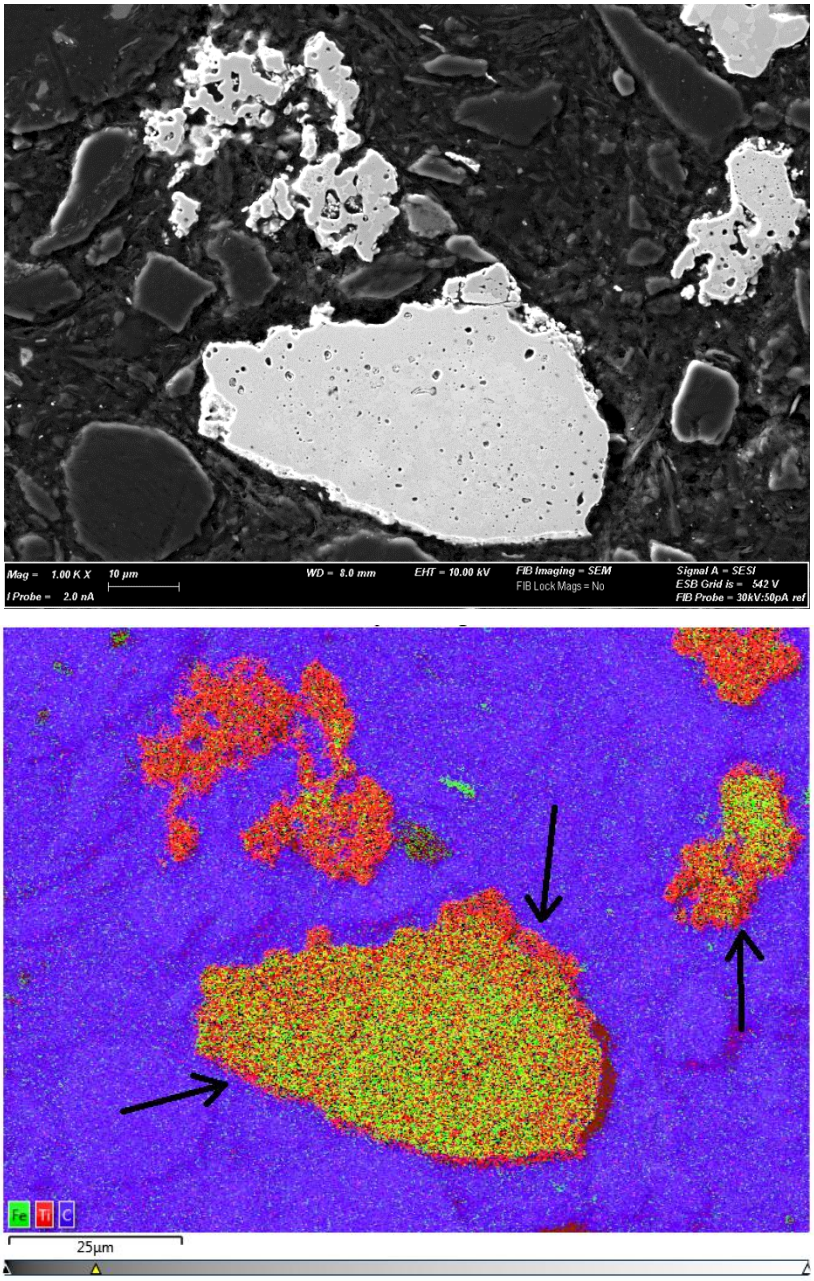

Figure 62: SEM-BEC image and a stacked iron/titanium EDS elemental map: -40 µm, x1 000 magnification

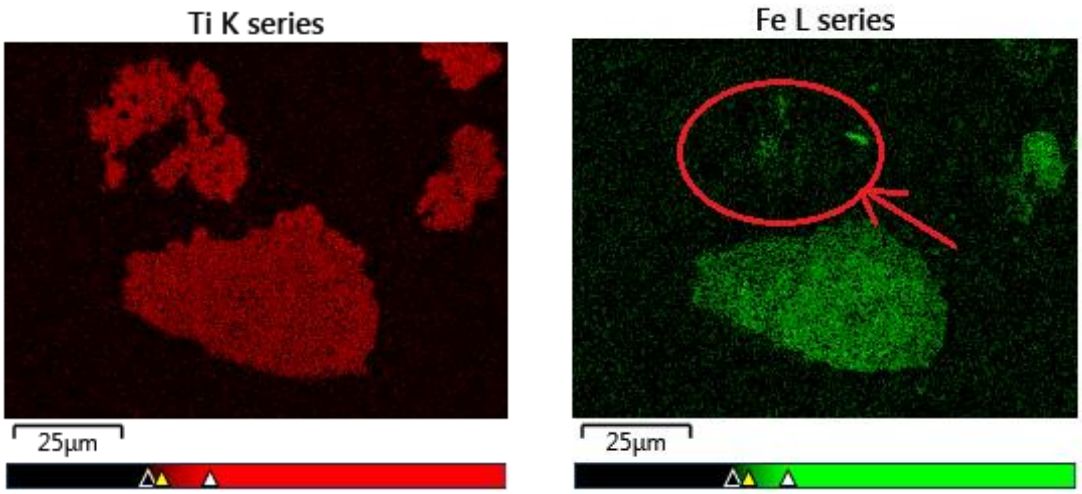

Figure 63: Iron and titanium elemental maps of Figure 62

Table 19: Spectrum analysis estimation for mass % composition of Figure 62

	Ti	Fe	Ni
Centre Edge	45.32 100.00	34.48	20.20

Figure 63 also shows an area similar to that in Figure 61, where titanium deposition was preferential.

The difference between the substrate and the deposited layer is evident in Figure 64. The deposition of nickel in this layer can be clearly seen in Figure 65.

The presence of iron and nickel cations is attributed to titanium tetrachloride corroding the submerged $TiCl_4$ (g) feed nozzle constructed from 316 stainless steel.

Co-deposition of different metal cations on a metallic substrate surface is a positive indicator supporting the role of an electrochemical autocatalytic electroless deposition mechanism.

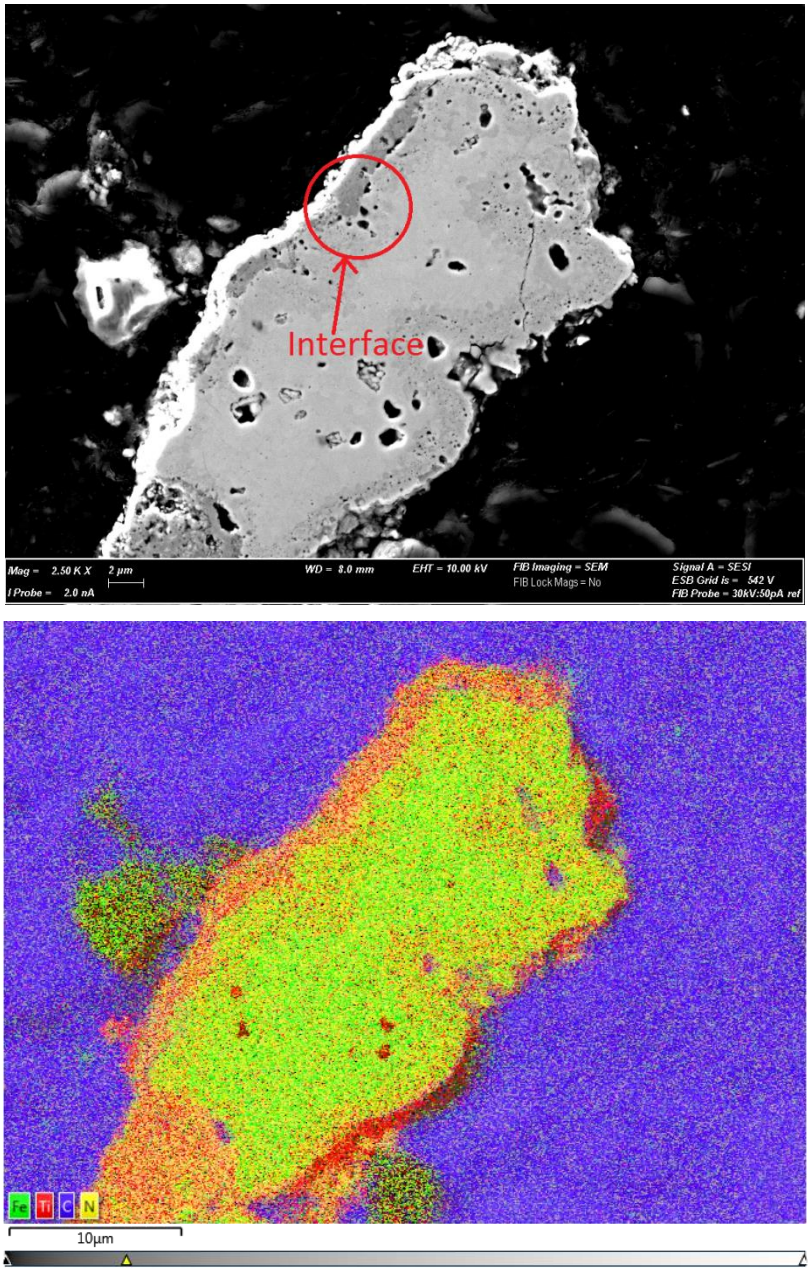

Figure 64: SEM-BEC image and a stacked iron/titanium EDS elemental map: -40 µm, x2 500 magnification

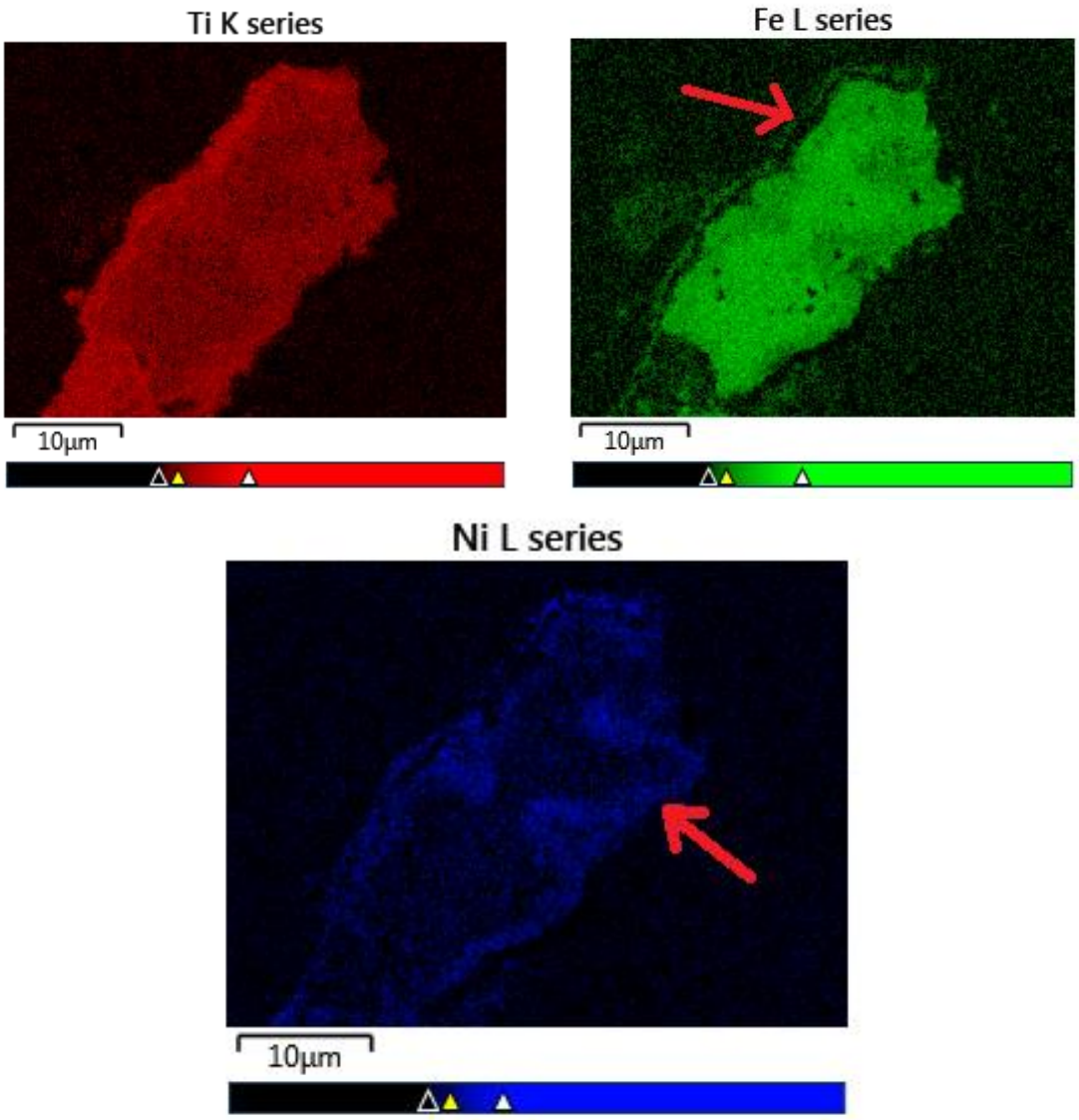

Figure 65: Iron, titanium, and nickel elemental maps of Figure 64

Table 20: Spectrum analysis estimation for mass % composition of Figure 64

	Cl	Si	Ti	Fe	Ni
Centre (a)		0.41	30.68	63.77	5.13
Centre (b)			29.25	64.83	2.98
Edge (b)	0.47	0.54	71.24	20.90	6.85

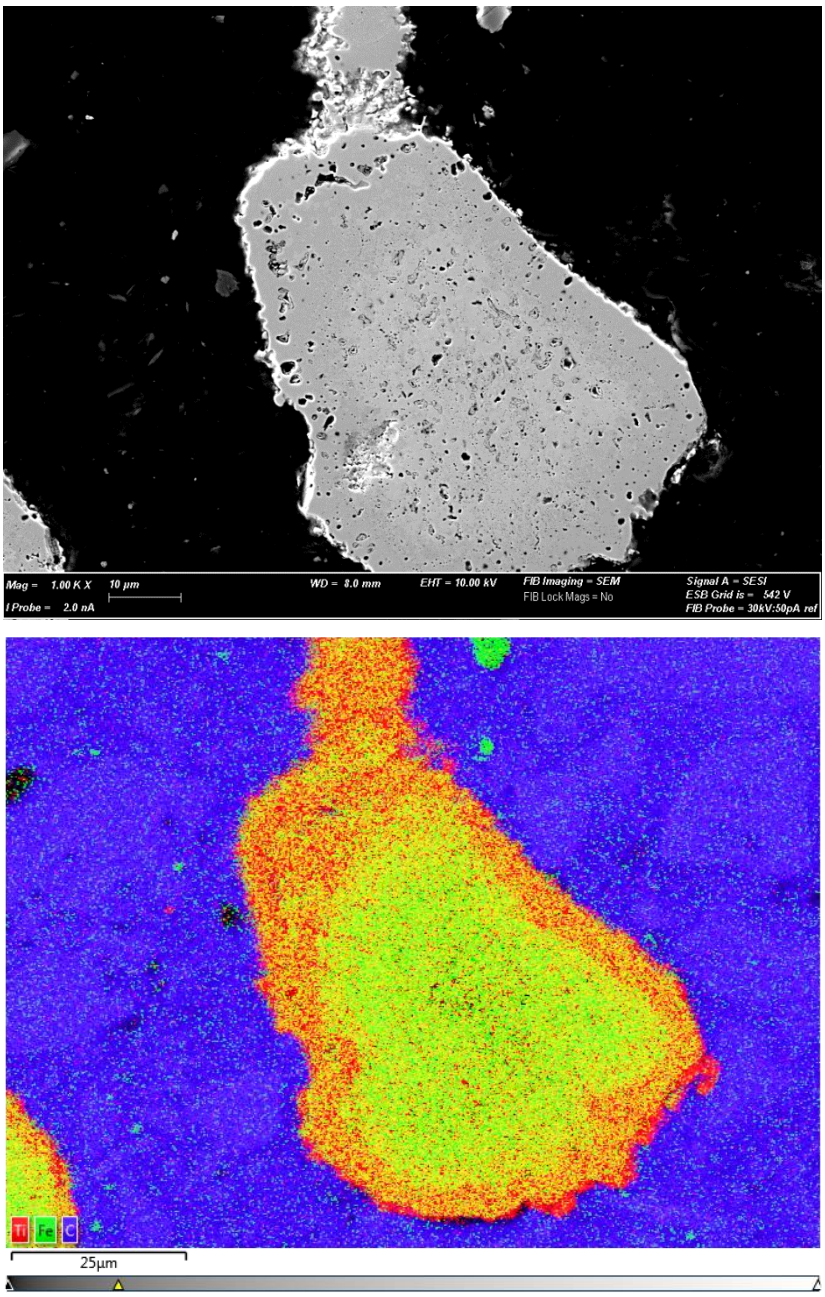

Figure 66: SEM-BEC image and a stacked iron/titanium EDS elemental map: +90 µm, x1 000 magnification

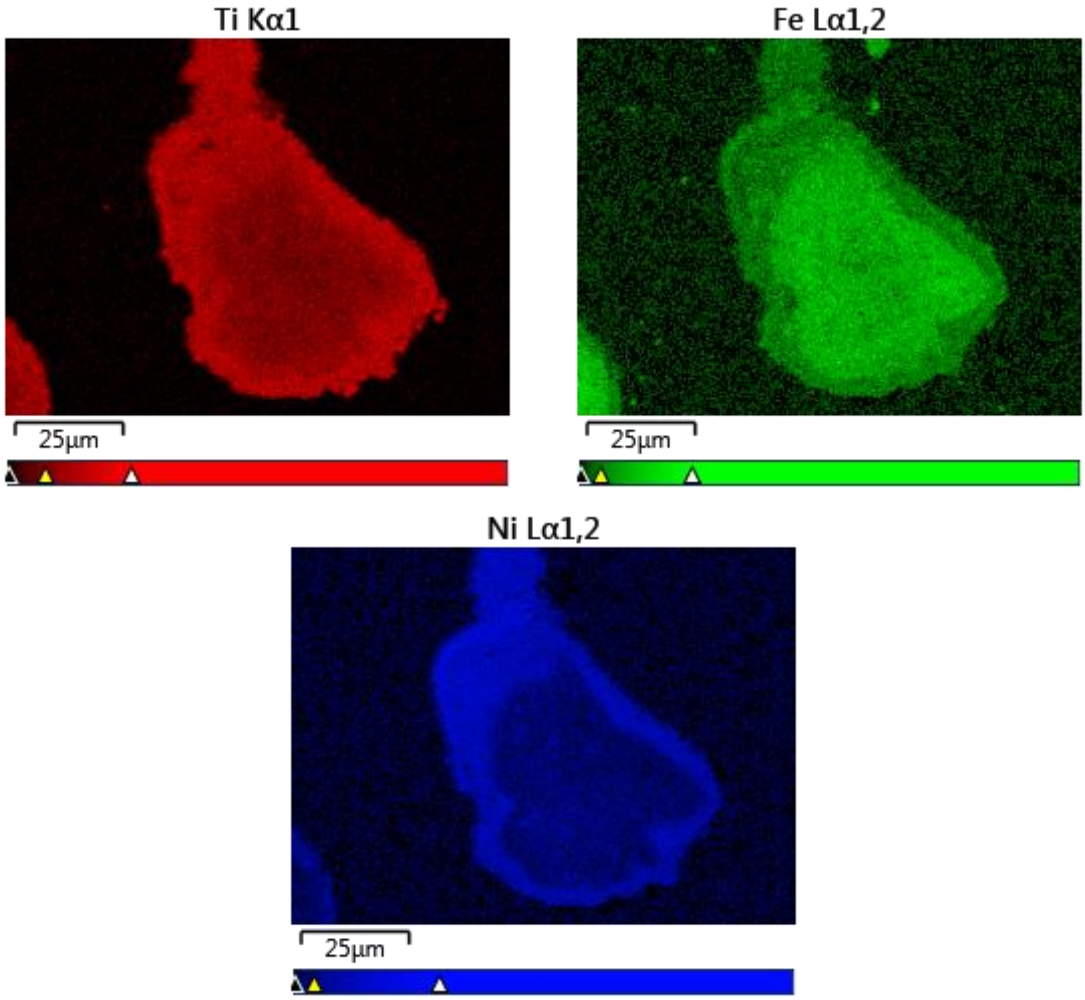

Figure 67: Iron, titanium and nickel elemental maps of Figure 66

5.6.4 – External EBSD investigation

Electron backscatter diffraction (EBSD) analysis was then conducted on particles from the -40 µm magnetic fraction. The EBSD technique is able to provide an elemental map (with phase identification) at a higher resolution than that of standard SEM-EDS elemental mapping. The goal was to identify a phase transition between the substrate particle and the deposited layer.

NMISA also performed the EBSD analysis. The results obtained are shown in Figures 68 and 69.

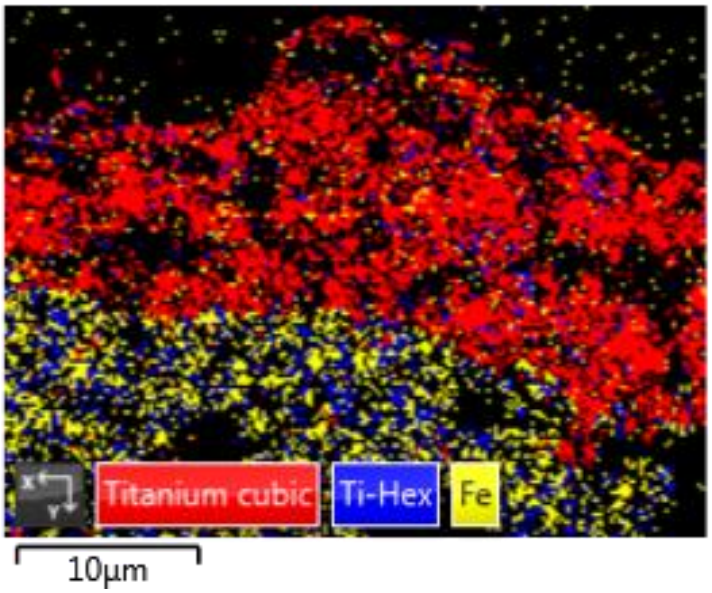

Figure 68: EBSD image showing the transition between two distinct titanium phases

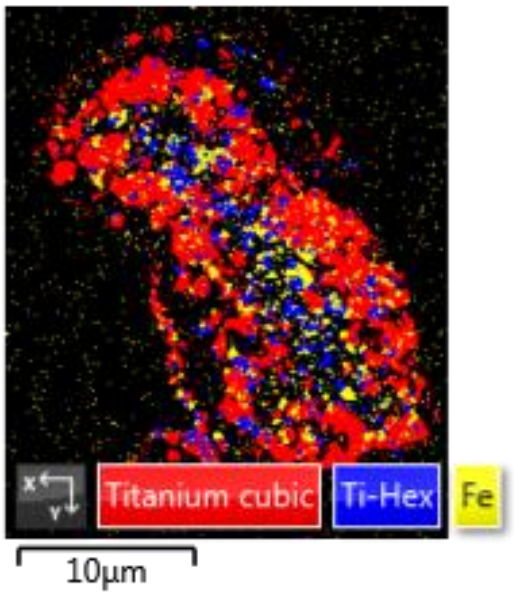

Figure 69: EBSD image indicating the presence of two distinct titanium phases

The result shown in Figures 68 and 69 indicates the presence of two distinct titanium phases separated by an interface. Ilmenite is part of the hexagonal crystal family (hcp crystal structure, i.e. α-titanium), whereas β-titanium has a cubic crystal structure. Deposition of β-titanium appears to have occurred due to the significant co-deposition of iron and nickel on the ilmenite surface. Both elements are beta-phase stabilisers for titanium.

CHAPTER 6 –CONCLUSIONS

6.1 – Titanium metal particle growth

This thesis's main objective was to demonstrate that titanium metal particle growth is possible through controlled metallothermic reduction on metal particles suspended in a molten chloride salt.

A literature review and theory building resulted in a postulated growth mechanism termed “autocatalytic electroless deposition”.

Modelling and simulation efforts indicated that the postulated growth mechanism is possible, but only in a very specific and low reagent concentration range.

Subsequently, a hypothesis test was conducted experimentally.

The hypothesis is as follows:

> *Titanium metal particle growth is possible through a mechanism known as autocatalytic electroless deposition*.

The hypothesis test's purpose was to demonstrate autocatalytic electroless deposition on suspended metal particles. Therefore, if the hypothesis test validates the postulated growth mechanism's existence, then titanium metal particle growth on titanium metal particles suspended in the same molten salt should also be possible through the same mechanism.

The results presented in Section 5.6 demonstrated successful autocatalytic electroless deposition of titanium, iron, and nickel on the surface of metallised ilmenite particles, thereby confirming the hypothesis of metal particle growth via autocatalytic electroless deposition.

6.2 – Producing high-quality primary titanium metal powder product

Figure 70 shows some of the titanium powder produced during this experimental investigation.

Figure 70: Titanium metal powder produced during the experiment

Not all metal powder products are equal. Powder product quality is too general a term to use in that it can mean various things to whoever uses it (Section 2.2.1).

The three most important properties that determine powder product quality are (Neikov, 2009: 3):

- Chemical composition
- Particle morphology
- Particle size distribution

Producing high-quality primary titanium metal powder products requires control over all three properties. Each property can be related to process performance as follows:

- Chemical composition relates to the production technique, i.e. preventing contaminated reagents from being fed to the system, preventing oxygen ingress into the reactor atmosphere, using appropriate construction materials, etc.
- Morphology and particle size distribution are determined by how well the

metallothermic reduction reaction is controlled at the conditions needed for the postulated autocatalytic electroless deposition of titanium on suspended titanium particles.

The patented CSIR-Ti process's reduction section (illustrated in Figure 45) is designed to enable control over particle morphology and size distribution (Section 5.2).

Some interesting product morphologies obtained throughout the experimental efforts are shown in Figures 71 to 76.

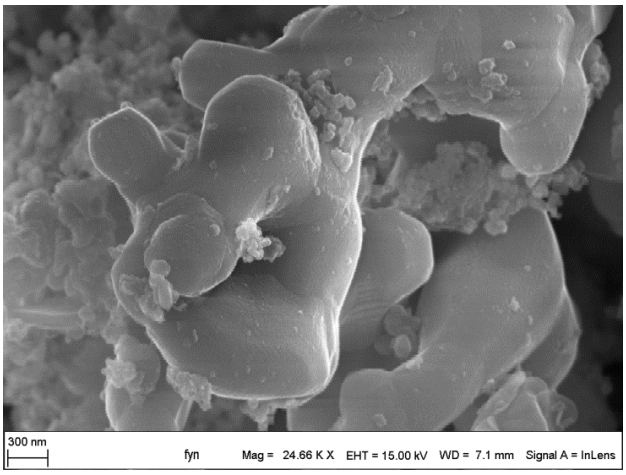

Figure 71: Close-up magnification of coral-like morphology

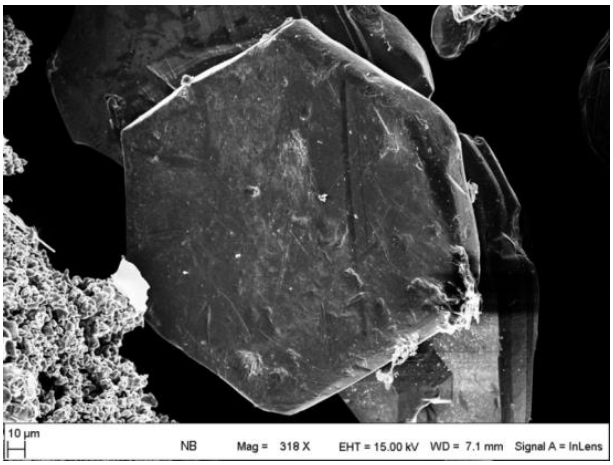

Figure 72: Hexagonal titanium crystal

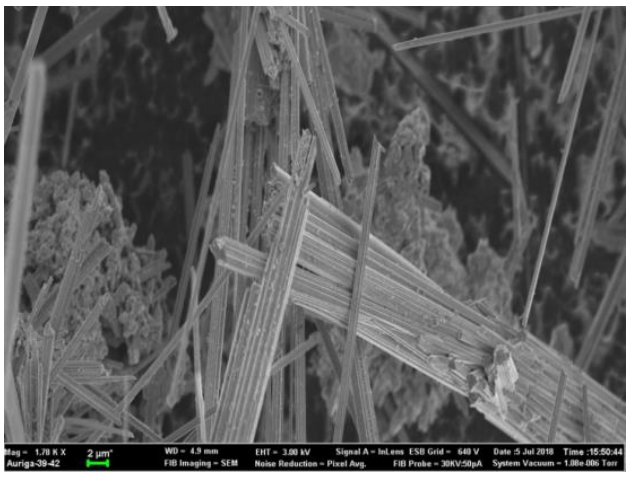

Figure 73: Crystalline titanium fibres

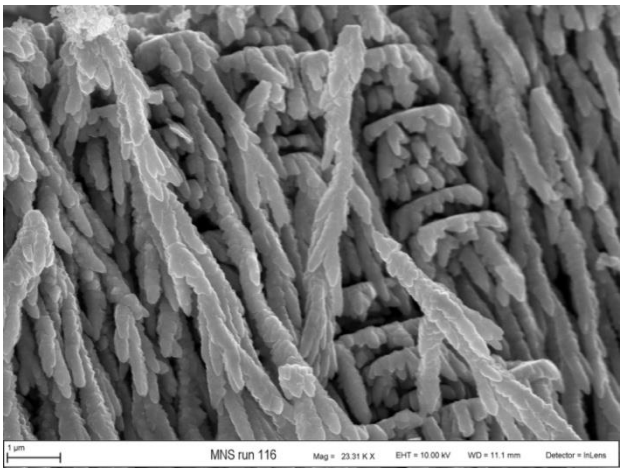

Figure 74: Dendrite-like growth but without crystal edges

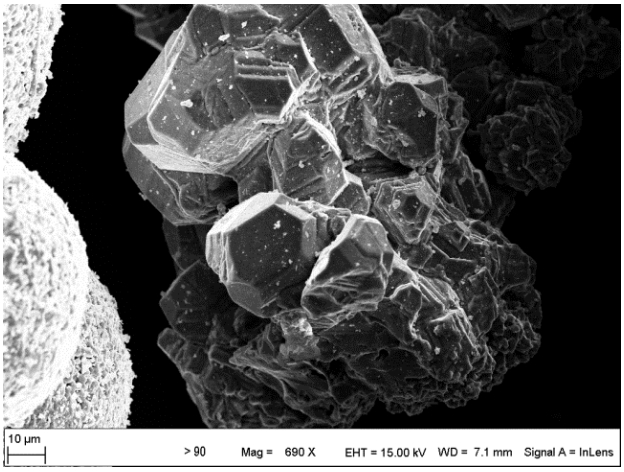

Figure 75: Agglomerate of crystals

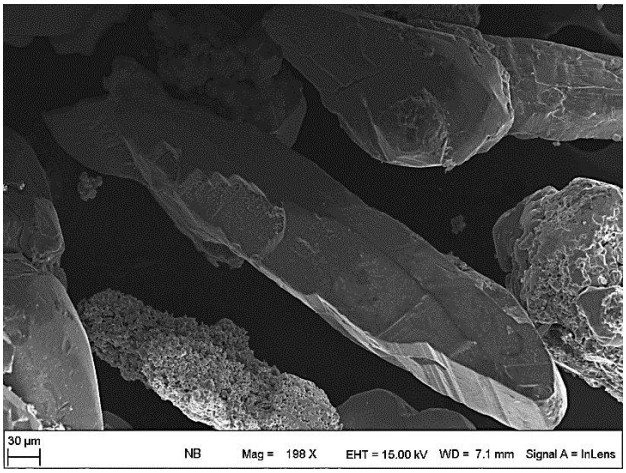

Figure 76: Elongated crystals

6.3 – Technical complexity

Working with hazardous chemical substances in molten chloride salts is technically very challenging. Other considerations adding to the complexity include:

- High circulating molten salt slurry streams with suspended metal particles
- The mechanical integrity of materials at elevated temperatures
- Design for reactor maintainability. Section 4.7 showed that LR-EMR and autocatalytic electroless deposition would always occur at the required conditions. Provision should therefore be made to accommodate this
- Removing the heat of reaction
- Corrosion damage (and product contamination) due to the presence of titanium tetrachloride in contact with molten salt and the reactor materials of construction

Therefore, the work presented in this thesis is intricate, requiring specialist expertise from various other disciplines.

CHAPTER 7 – RECOMMENDED FUTURE WORK

The work presented in this thesis can be used as a starting point to further improve understanding of reactive metal powder production through controlled metallothermic reduction. There are numerous research and developmental questions still unanswered.

An ideal project based on the current understanding would be to integrate the experimental reactor developed in this research into the CSIR-Ti process's reduction section. This concept is illustrated in Figure 77.

This integration should provide the ideal conditions to demonstrate whether or not a primary titanium metal powder product is possible (Section 2.2.1) and allow improved control over the reaction to study the influence of various process parameters on product morphology.

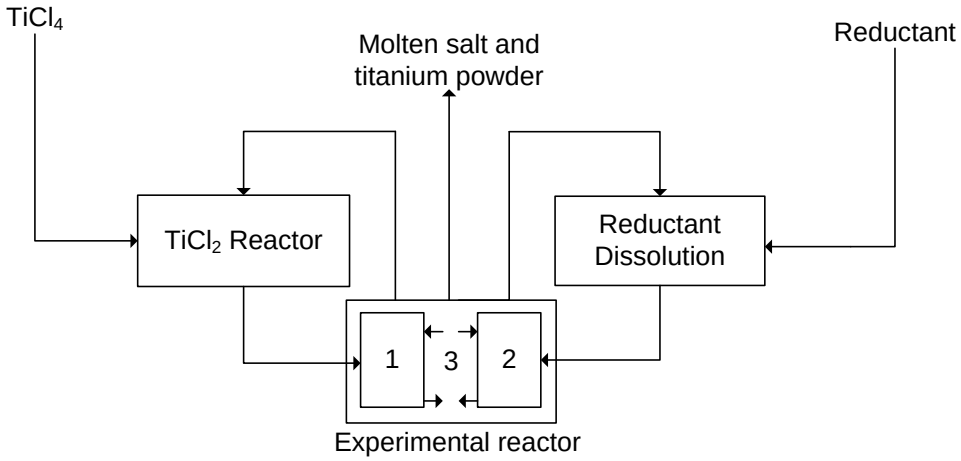

Figure 77: Experimental reactor integrated with the CSIR-Ti process's reduction section

CHAPTER 8 – CONTRIBUTIONS TO THE FIELD

Journal articles/conference papers that are relevant/used in the thesis include:

1. Van VUUREN, D.S., OOSTHUIZEN, S.J. & SWANEPOEL, J.J., 2013, Development of a continuous process to produce Ti via metallothermic reduction of $TiCl_4$ in molten salt. *Key Engineering Materials*, 551, 16-24.
2. Van VUUREN, D.S., OOSTHUIZEN, S.J. & SWANEPOEL, J.J., 2014, Challenges experienced in scaling-up the CSIR-Ti process. *Advanced Materials Research*, 1019, 187-194.
3. OOSTHUIZEN, S.J. & SWANEPOEL, J.J., 2018, Development status of the CSIR-Ti process. *IOP Conference Series: Materials Science and Engineering*, 430, 012008.

The CSIR-Ti process, entitled “Process for the production of crystalline titanium powder” is patented in various territories. The author is one of the three inventors of this technology. The patent has been granted in the following territories:

- United States: US 9,567,690 B2 (Granted: 14 February 2017)
- Australia: AU 2013 270 660 B2 (Granted 21 September 2017)
- China: CN 104736273 B (Granted: 1 May 2018)
- Japan: JP 6216372 B2 (Granted: 18 October 2017)
- Russia: RU 2 635 587 C2 (Granted: 14 November 2017)
- European Patent Office: EP 2844411 B1 (Granted: 27 September 2017)

Research relating to the experimental reactor used in this thesis led to a new patent application. This patent application is entitled “Electroless titanium process”. The UK patent application was recently published as GB 2567007 A (3 March 2019).

REFERENCES

ALCOCK, C.B., 2001, *Thermochemical Processes – Principles and Models*. Oxford: Butterworth-Heinemann.

ATKINS, P., & de PAULA, J., 2002, *Atkins' Physical Chemistry*, 7th ed. Oxford: Oxford University Press.

BOOZENNY, A., 1962, Na-$TiCl_2$-$TiCl_3$ equilibrium in NaCl melts. *Transactions of the Metallurgical Society of the AIME*, 224, 950-956.

CARDARELLI, F., 2008, *Materials Handbook: A Concise Desktop Reference,* 2nd ed. New York: Springer Science & Business Media.

CSIR, 2018, *Titanium pilot plant*. Online: https://www.csir.co.za/titanium-pilot-plant

DEMOPOULOS, G.P., 2009, Aqueous precipitation and crystallization for the production of particulate solids with desired properties. *Hydrometallurgy*, 96, 199-214.

DJOKIĆ, S.S., 2002, Electroless deposition of metals and alloys. In Conway, B.E., & White, R.E. (Eds), *Modern Aspects of Electrochemistry*, Vol. 35. New York: Springer, pp. 51-133.

DJOKIĆ, S.S., & CAVALLOTTI, P.L., 2010, Electroless deposition: theory and practice. In Djokić, S.S. (Ed.), *Modern Aspects of Electrochemistry. Electrodeposition: Theory and Practice*, Vol. 48. New York: Springer, pp. 251-289

DRIELS, M.R. & SHIN, Y.S., 2004, *Determining the number of iterations for Monte Carlo simulations of weapons effectiveness,* Report No. NPS-MAE-04-005. Monterey, CA: Naval Postgraduate School, Department of Mechanical & Astronautical Engineering.

DRYFE, R.A.W., 2007, Liquid junction potential. In ZoskiI, C.G. (Ed.), *Handbook of Electrochemistry*, 1st ed. Amsterdam, Boston, MA: Elsevier, pp. 849–877.

EHK TECHNOLOGIES, 2004, *Summary of emerging titanium cost reduction technologies*. Study performed for the US Department of Energy and Oak Ridge National Laboratory, Subcontract 4000023694. Vancouver, WA: EHK Technologies.

FANG, Z.F., PARAMORE, J.D., SUN, P., CHANDRAN, K.S.R., ZHANG, Y., XIA, Y., *et al.*, 2017, Powder metallurgy of titanium – Past, present, and future. *International Materials Reviews*, 63(7), 407-459. DOI: 10.1080/09506608.2017.1366003

FOGLER, H.S., 2006, *Elements of Chemical Reaction Engineering*, 4th ed. London: Pearson International.

FROES, F.H., 2012, Titanium Powder Metallurgy: A Review – Part 1. *Advanced Materials & Processes,* 170(10), 26-29.

FROES, F.H., 2015, A historical perspective of titanium powder metallurgy. In Froes, F.H. & Qian, M, (Eds), *Titanium Powder Metallurgy – Science, Technology and Applications*. Amsterdam, Boston: Elsevier.

FROES, F.H., EYLON, D., & BOMBERGER, H.B., 2015, Melting, Casting, and Powder Metallurgy. In *Titanium – Physical Metallurgy, Processing, and Applications*. Materials Park, OH: ASM International.

HANSEN, D.A., & GERDEMANN, S.J., 1998, Producing titanium powder by continuous vapour-phase reduction. *JOM*, 50(11), 56-58.

HENRIE, T.A., & BAKER, D.H. 1960, *Mechanism of sodium reduction of titanium chlorides in fused salts*. Washington, DC: U.S. Dept. of the Interior, Bureau of Mines.

HENRIE, T.A., 1965. Extractive metallurgy of titanium, high temperature refractory materials. *Meteorological Society Conference*, 34(1), 139-154.

HOUSLEY, K.L., 2007, *Black Sand the History of Titanium*, 1st ed. Hartford, CA: Metal Management Aerospace, Inc.

INZELT, G., LEWENSTAM, A., & SCHOLZ, F., 2013, *Handbook of Reference Electrodes*. Berlin, Heidelberg: Springer, p. 351.

KAYE, B.H., 1998, Particle shape characterization. In Lee, P.W. (Ed.), *Powder Metal Technologies and Applications*, ASM Handbook, Vol. 7. Materials Park, OH: ASM International.

KOTZ, J.C., & TREICHEL, P.M., 2003, *Chemistry and Chemical Reactivity*, 5th ed. Stamford, CT: Brooks/Cole.

MALLORY, G.O., & HAJDU, J.B., 1990, *Electroless Plating: Fundamentals and applications*. Park Ridge, NJ: Noyes Publications.

NEIKOV, D.O., 2009, Introduction. In Neikov, O.D., Naboychenko, S.S., & Dowson, G. (Eds), *Handbook of Non-Ferrous Metal Powders*. Amsterdam: Elsevier, pp. 1-5.

OKABE, T.H. & WASEDA, Y., 1997, Producing titanium through an electronically mediated reaction. *JOM,* 49(6), 28-32.

OKABE, T.H. & SADOWAY, D.R., 1998. Metallothermic reduction as an Electronically Mediated Reaction (EMR). *Journal of Materials Research*, 13(12), 3372-3377.

OOSTHUIZEN, S.J., & Van VUUREN, D.S., 2011. *Titanium powder production process*. US Patent 8,790,441.

OOSTHUIZEN, S.J., Van VUUREN, D.S., & HEYDENRYCH, M.D., 2011, Titanium production via metallothermic reduction of $TiCl_4$ in molten salt: problems and products. *Journal of the Southern African Institute of Mining and Metallurgy*, 111(3), 141–148.

OOSTHUIZEN, S.J., Van VUUREN, D.S., & SWANEPOEL, J.J., 2015. *Process for the production of crystalline titanium powder.* US Patent 20150144055 A1.

OOSTHUIZEN, S.J., 2016, Development of a novel cost-effective metallic titanium production process. PhD Thesis, North-West University, South Africa.

POPOV, K.I., DJOKIĆ, S.S., NIKOLIĆ, N.D., & JOVIĆ, V.D., 2016, *Morphology of electrochemically and chemically deposited metals*. Cham, Switzerland: Springer.

PAUNOVIC, M., & SCHLESINGER, M., 2006, *Fundamentals of Electrochemical Deposition*. 2nd ed. New York: Wiley.

QIAN, M., & FROES, F.H., 2015, *Titanium Powder Metallurgy: Science, Technology and Applications.* Oxford: Butterworth-Heinemann.

ROSKILL INFORMATION SERVICES, 2013, *Titanium Metal: Market Outlook to 2018*, 6th ed. London.

SANDEROW, H.I., 1998, Powder metallurgy methods and design. In Lee, P.W. (Ed.), *Powder Metal Technologies and Applications*, ASM Handbook, Vol. 7. Materials Park, OH: ASM International.

SUBRAMANYAM, R.B., 1993, Some recent innovations in the Kroll process of titanium sponge production. *Bulletin of Materials Science*, 16(6), 433-451.

SWANEPOEL, J.J., OOSTHUIZEN, S.J., & SWANEPOEL, E., 2017. *Electroless titanium process*. UK Patent Office 1716024.3 (application submitted 2017).

TRUDEL, Y., 1998, Introduction to metal powder production and characterization. In Lee, P.W. (Ed.), *Powder Metal Technologies and Applications*, ASM Handbook, Vol. 7. Materials Park, OH: ASM International.

TURNER, P.C., HARTMAN, A.D., HANSEN, J.S., & GERDEMANN, S.J., 2001, *Low cost titanium – Myth or reality.* Paper presented the EPD Congress 2001, held at the 2001 TMS Annual Meeting, New Orleans, LA, 11–15 February.. DOI: https://www.osti.gov/servlets/purl/899609

Van VUUREN, D.S., 2009a, *Titanium – An opportunity and challenge for South Africa*. Keynote address presented at the 7th International Heavy Minerals Conference, Champagne Sports Resort, Drakensberg, 20–23 September.

Van VUUREN, D.S., 2009b, A critical evaluation of processes to produce primary titanium. *Journal of the Southern African Institute of Mining and Metallurgy*, 109(8), 455-461.

Van VUUREN, D.S., 2010, *In search of low-cost titanium*. PhD Thesis, University of Pretoria, South Africa.

Van VUUREN, D.S., 2015, Direct titanium powder production by metallothermic processes. In Qian, M., & Froes, F.H. (Eds), *Titanium Powder Metallurgy: Science, Technology and Applications*, Oxford: Butterworth-Heinemann, pp. 69-93.

VILLERMAUX, J., 1989. *A simple model for partial segregation in a semi batch reactor*. Paper presented at the American Institute of Chemical Engineers Annual Meeting, San Francisco, CA, Paper 114a.

WITHERS, J.C., 2015, Production of titanium powder by an electrolytic method and compaction of the powder. In Qian, M., & Froes, F.H. (Eds), *Titanium Powder Metallurgy: Science, Technology and Applications*. Oxford: Butterworth-Heinemann, pp. 33–50.

YOLTON, C.F. & FROES, F.H., 2015, Conventional titanium powder production. In Qian, M., & Froes, F.H. (Eds), *Titanium Powder Metallurgy: Science, Technology and Applications*. Oxford: Butterworth-Heinemann, pp. 21-32.

ZAUNER, R. & JONES, A.G., 2000a. Scale-up of continuous and semi batch precipitation processes. *Industrial and Engineering Chemistry Research*, 39(7), 2392-2403.

ZAUNER, R. & JONES, A.G., 2000b. Mixing effects on product characteristics from semi-batch precipitation. *Transactions of the Institution of Chemical Engineers*, 78(A), 894-901.

ZAUNER, R. & JONES, A.G., 2002, On the influence of mixing on crystal precipitation processes – Application of the segregated feed model. *Chemical Engineering Science*, 57(5), 821-831.

APPENDICES

Appendix 1 – Modelling and simulation data

A.1 – Repeatability test

Table 21: Output data for repeatability test

Number of iterations	Ti^{2+} cluster = Ti^{0} critical nuclei size (hits)	Standard deviation
1 000 000	2 320	0.048131
1 000 000	2 492	0.049858
1 000 000	2 396	0.048972
1 000 000	2 340	0.048317
1 000 000	2 389	0.048819
1 000 000	2 381	0.048758
1 000 000	2 405	0.048982
1 000 000	2 438	0.049336
1 000 000	2 417	0.049144

A.2 – Autocatalytic electroless deposition

Table 22: Output data for autocatalytic electroless deposition as function of reagent concentrations

Ti^{2+} (ppm)	Na^0 (ppm)	Number of iterations	Auto. catalytic deposition (hits)	Standard deviation
52	2	1 000 000	82	0.009165
31	3	1 000 000	109	0.010440
12	5	1 000 000	157	0.012529
8	6	1 000 000	136	0.011662
6	7	1 000 000	156	0.012490
5	8	1 000 000	165	0.012923
3	10	996 628	163	0.012788
2	12	1 000 000	167	0.012922

Table 23: Output data for autocatalytic electroless deposition as a function of Ti^0 particle concentration

Ti^{2+} (ppm)	Na^0 (ppm)	Mol % Ti^0 in melt	Number of iterations	Auto. catalytic deposition (hits)	Standard deviation
5	9	5	1 000 000	60	0.007746
5	9	10	1 000 000	115	0.010723
5	8	20	1 000 000	165	0.012923

Table 24: Output data for autocatalytic electroless deposition as a function of suspended Ti^0 particle size

Ti^0 atoms per Ti^0 particle	Number of Ti^0 particles	Number of iterations	Auto. catalytic deposition (hits)	Standard deviation
4	5 191	1 000 000	185	0.0136
6	3 461	1 000 000	186	0.013637
8	2 596	1 000 000	212	0.014627
10	2 076	1 000 000	189	0.013746
12	1 730	1 000 000	201	0.014246
14	1 483	1 000 000	165	0.012922
16	1 298	1 000 000	146	0.012165
18	1 154	1 000 000	147	0.012123
20	1 038	1 000 000	154	0.012409
22	944	1 000 000	127	0.011357

A.3 – LR-EMR

Table 25: Output data for the LR-EMR mechanism as a function of reagent concentration

Ti^{2+} (ppm)	Na^0 (ppm)	Number of iterations	LR-EMR (hits)	Standard deviation
52	3	1 000 000	890	0.02982
31	4	1 000 000	1256	0.035418
12	6	1 000 000	1469	0.038325
8	7	1 000 000	1477	0.03840
6	9	1 000 000	1831	0.04277
5	10	1 000 000	1890	0.043433
3	12	1 000 000	1637	0.040427
2	15	1 000 000	1671	0.040844

Table 26: Output data for the LR-EMR mechanism as a function of positions available for LR-EMR

Number of positions available for LR-EMR	Number of iterations	LR-EMR (hits)	Standard deviation
2 209	1 000 000	1 890	0.043433
4 371	1 000 000	12 264	0.110116
6 487	1 000 000	35 222	0.184763

Table 27: Output data for the LR-EMR mechanism as a function of the sample-space size

Ti^{2+} (ppm)	Na^{0} (ppm)	Sample-space size	Number of iterations	LR-EMR (hits)	Standard deviation
5	10	103 823	1 000 000	1 890	0.043433
11	21	216 000	1 000 000	8004	0.089241
16	32	328 509	1 000 000	16 481	0.12745
21	41	421 875	1 000 000	25 574	0.158291
27	51	531 441	800 818	29 822	0.190099
33	63	658 503	712 815	37 069	0.223464
40	77	804 357	508 595	36 128	0.259571
50	96	1 000 000	328 842	32 822	0.304549

A.4 – SR-EMR

Table 28: Output data for Ti^{2+} cluster formation equal to assumed Ti^0 critical nuclei size as a function of reagent concentration

Ti^{2+} (ppm)	Number of iterations	Ti^{2+} cluster formation (hits)	Standard deviation
52	1 000 000	31 4760	0.553966
31	1 000 000	11 1028	0.330707
12	1 000 000	15 704	0.125042
8	1 000 000	6 751	0.082131
6	1 000 000	3 573	0.059718
5	1 000 000	2 394	0.048911
3	1 000 000	711	0.026655
2	1 000 000	213	0.014593

Table 29: Output data for Ti^{2+} cluster formation as a function of Ti^0 critical nuclei size = 2

Ti^{2+} (ppm)	Number of iterations	Ti^{2+} cluster formation (hits)	Standard deviation
52	1 000 000	2 637	0.051323
31	1 000 000	521	0.022819
12	1 000 000	33	0.005744
8	1 000 000	5	0.002236
6	1 000 000	0	0
5	1 000 000	0	0